Retrospective Cost Adaptive Control for Feedback and Feedforward Noise Control

by

Antai Xie

A dissertation submitted in partial fulfillment
of the requirements for the degree of
Doctor of Philosophy
(Aerospace Engineering)
in the University of Michigan
2017

Doctoral Committee:

       Professor Dennis S. Bernstein, Chair
       Professor Anouck Girard
       Professor Karl Grosh
       Professor Peter D. Washabaugh

No! Try not! Do, or do not. There is no try.

– Yoda

Antai Xie

antai@umich.edu

ORCID iD: 0000-0001-9570-8914

2017

I'd like to thank my Mother for her support in encouraging my academic development. At times I come to the realization that something you said when I was younger in hindsight turns out to be right after all. This can be definitely counted as one of those times.

I'd like to thank my advisor, Prof. Dennis S. Bernstein for this long journey. I learned many important lessons and skills not just in the field of academics, but also furthered my development as an individual. I will sorely miss our long research discussions, of which I've always felt our thinking at times conflict, but more often complement. I hope that I leave here with a fraction of your drive and perseverance.

Finally, I'd like give the tip of the hat to my friends/colleagues. I take comfort in the fact that everyone who graduates from this group has experienced at least some 2-3 hour meetings. It builds a sense of solidarity that I will not forget. It is my hope that our future careers cross paths.

TABLE OF CONTENTS

LIST OF FIGURES

ABSTRACT

This dissertation concerns the development of retrospective cost adaptive control (RCAC) and the application of RCAC to the active noise control (ANC) problem. We further the development of RCAC by presenting an alternative interpretation the retrospective performance variable. The retrospective performance decomposition is derived which separates the retrospective performance into the sum of a pseudo-performance term and a model-matching error term. We demonstrate an experimental application of RCAC by applying it to the broadband feedback road noise suppression problem in a vehicle. We show that RCAC is able to suppress the primary modes of the road noise at the performance microphone location. However, qualitative evaluation of the noise at the location of the driver was poor. This leads to the question, if you suppress the noise at the performance microphone, what is effect at the actual ear of the driver where you may not be able to place a sensor. The concept of spatial spillover is explored, where we develop an operator that relates relative suppression at the performance microphone to relative suppression at the evaluation microphone, which we denote as the spatial spillover function. The properties of the spatial spillover function are then validated numerically and experimentally. Finally, the framework of RCAC is extended to the feedforward control problem. Comparisons of RCAC feedforward control are made to linear-quadratic-Gaussian (LQG) control. It is shown that under certain conditions, RCAC is able to match the performance of LQG. Furthermore, we compare RCAC to the filtered-x/filtered-u least-mean-square (Fx/FuLMS) and the filtered-x/filtered-u recursive-least-square (Fx/FuRLS) algorithms and demon-

strate numerically that RCAC is able to achieve better asymptotic performance that
FuRLS. The RCAC feedforward control algorithm is demonstrated in an acoustic ex-
periment. We demonstrate experimentally that if the ideal feedforward controller is
implementable, the RCAC controller is able to recover the frequency response of the
ideal controller.

CHAPTER 1

Introduction

1.1 Active Noise Control

The problem of undesirable acoustic noise is prevalent in both commercial and indus-
trial applications. Traditional methods of noise control have largely been passive in the
form of enclosures, barriers, and insulating materials to reflect or absorb noise. Active
noise control (ANC) [1, 2] is the principle of canceling a sound wave with an anti-wave of
the same magnitude, 180° out of phase. The combined sum of the two sound waves leads
to the attenuation of both noises. The appeal of active noise control over traditional passive
methods is the ability to provide significant noise reduction with smaller, lighter, and at
times, cheaper solutions. Early methods involved model-based robust control design, but
with the advent of more powerful digital signal processing (DSP) hardware that can meet
real-time requirements, the switch to adaptive filtering/control methods has become the
norm. Some of the motivators for this switch from model-based to adaptive control can be
attributed to difficulty in modeling sound fields with multiple sources, the variability of the
system under environmental conditions such as temperature, and the non-stationary nature
of the noise in certain applications. This naturally leads to the need for control methods to
be adaptive. Some of the earliest such examples were active cancellation of harmonic noise
in a duct using adaptive filtering methods [3]. The use of adaptive control algorithms based
on adaptive filtering have extended the range of harmonic noise suppression applications,
the most recognizable being the filtered-x least-mean-squares (FxLMS) algorithm [4–6].

Some of the most successful current applications of active noise control include suppression of fan noise in heating, ventilation, and air conditioning (HVAC) systems, suppression of engine noise in a vehicle, and noise canceling headsets. In the field of Aerospace Engineering, active noise control has been applied to reduction of helicopter rotor noise using headsets, which was an early precursor to noise canceling headsets. Applications to noise reduction in an aircraft cabin has been explored in [7], however obtaining global suppression of the noise within the entire cabin remains a challenge as the increased size of the enclosure, relative to ground vehicles, increases the complexity of the acoustics.

Currently, the applications of ANC are still largely limited to low-frequency noise, relative to the range of human hearing. The challenge of extending the bandwidth of ANC comes from the increased complexity of higher order acoustic modes and the increased difficulty in implementation of algorithms at higher sampling rates. This is coupled to the fact that passive methods are shown to be more effective in most cases at high frequencies [5]. The other aspect limiting bandwidth is the ability to suppress noise at locations where a measurement is not directly available. Suppression of noise at a sensing location can potentially lead to amplification of noise at other locations of interest. We refer to this phenomenon as *spatial spillover*. Spatial spillover is tied, in part, to the size and complexity of acoustic space and the distribution of sensing and actuation, but also becomes more difficult to avoid at higher frequencies.

1.2   Spatial Spillover

Due to restrictions in the design of a system, a performance microphone may not always be placeable at all locations in where it is desirable to suppress noise. Thus, in the design phase, it is crucial to understand the relation between where the performance microphone is placed and evaluation locations where it is desirable to suppress noise [8]. This has led to the development alternative performance metrics beyond the sound pressure level (SPL).

In [9, 10], acoustic energy density at performance microphone locations is considered as an alternative performance metric that provides better global suppression.

In the present dissertation, we develop the notion of spatial spillover, which concerns the decrease in the noise amplitude at the location of the performance microphone z relative to its open-loop level as compared to the decrease in noise amplitude at the location of the evaluation microphone e relative to *its* open-loop level for a linear system. Consequently, spatial spillover is a measure of the relative effectiveness of the control at different locations. This notion is distinct from the fact, as shown in Figure 1.1, that the sum of two unit-amplitude sinusoidal waves of the same frequency may possess any amplitude between 0 and 2 depending on the relative phase shift of the waves. Consequently, a disturbance sinusoid and a control-speaker sinusoid may add destructively at one location and constructively at another location depending on the phase shift between the waves at these locations. This notion is sometimes used to estimate the bandwidth in which control is effective within an acoustic space. However, this phenomenon per se says nothing about
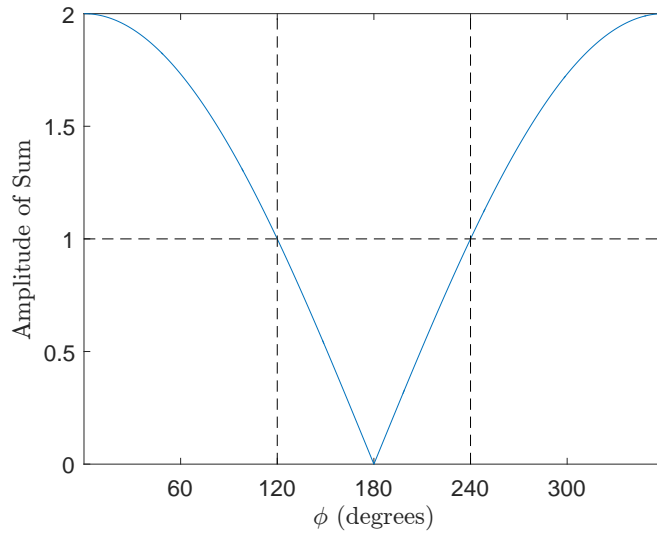
Figure 1.1: Amplitude of the sum of two unit-amplitude sinusoids with identical frequency ω and relative phase ϕ. For $\phi = 180$ deg, perfect cancellation occurs, and thus, the amplitude of the sum is zero. For $\phi = 180 \pm 60$ deg, the amplitude of the sum is 1. The plot is based on the fact that $\sin(\omega t) + \sin(\omega t + \phi) = 2\cos(\phi/2)\sin(\omega t + \phi/2)$.

the relationship between open- and closed-loop noise levels at a given location, and thus

is not relevant to spatial spillover as defined and analyzed in the present work. In this dissertation, we define a *spatial spillover function*, which relates the relative performance at the performance microphone z to the relative performance at an evaluation microphone e for both feedforward and feedback control. It turns out that the spatial spillover function has the same functional form for both feedforward and feedback control and, in addition, is independent of the controller in the case of scalar control. The contributions of the present work in this regard are the following:

- The derivation of the spatial spillover function for feedback and feedforward disturbance rejection in the case where z, e, and the disturbance w are scalars.

- Numerical validation and experimental measurement of the spatial spillover function for feedback and feedforward disturbance rejection.

Some of the spatial spillover results in this dissertation appear in [11].

1.3 Feedback and Feedforward Active Noise Control

In the context of ANC, algorithms can roughly be classified as either feedforward or feedback. Feedforward algorithms assume that a direct or indirect measurement of the disturbance is available. The assumption is that the disturbance measurement is not corrupted by the control speaker output, which means that the transfer function from the control input to the disturbance measurement is zero. Consequently, the only feedback in the system is the adaptation loop, which typically operates at a much slower rate than the time constant of the acoustics. The absence of a fast feedback loop means that these algorithms are less susceptible to instability. [2, 5]

In some applications, however, it is difficult to measure the disturbance either directly or indirectly. For example, in the case of interior noise in a ground vehicle which arises from the tire-road contact, current solutions for feedforward control rely on accelerometers

placed on the drivetrain as an indirect measurement of the noise. It can be challenging designing these systems since performance can be largely influenced by the degree of correlation between the accelerometer measurements and the actual acoustical noise, which, beyond placement of the sensors, is affected by the structural dynamics of the vehicle. In this situation, feedback control, which does not require an external measurement of the disturbance, can be a more appropriate architecture since feedback would rely only on internal microphones measurements in the control loop. However, feedback control is more challenging to implement due to its greater susceptibility to instability in the event of model errors.

Aside from these limitations, the two architectures differ in their performance relative to the disturbance spectrum. Both architectures perform well in the presence of narrowband (for example, tonal) disturbances [5, 12]. However, suppressing broadband disturbances is challenging for both methods. The achievable performance in broadband feedforward control is limited by two aspects. An overall limiting causality constraint exists in broadband feedforward control, where a delay in the transfer function from the control input to the performance microphone must be compensated for by a delay of at least equal length in the transfer function from the disturbance to the performance microphone. Furthermore, the existence of nonminimum phase (NMP) zeros in the transfer function from the control input to the performance microphone can limit the achievable performance [5]. Although feedback control can suppress broadband noise, feedback architectures are limited by the Bode integral constraint, which implies that reducing the magnitude of the frequency response is impossible at all frequencies [13–15]. For narrowband disturbances, this does not present a problem since the noise spectrum is confined to a limited bandwidth. However, for broadband disturbances, it is inevitable that, at least in some frequency range, the closed-loop noise level is amplified relative to the open-loop noise level. The challenge is thus to shape the closed-loop response so that *spectral spillover* has minimal effect on the closed-loop performance. In active noise control, this is especially challenging due to the

A-weighting effect of human hearing, which emphasizes the high-frequency range.

1.4 Retrospective Cost Adaptive Control

One of the focuses of this dissertation is the application of the retrospective cost adaptive control (RCAC) algorithm to feedforward and feedback broadband active noise control problems. RCAC was originally developed within the context of feedback active noise control experiments in an acoustic duct for both tonal and broadband disturbances [16]. Broadband feedback disturbance rejection using RCAC is further considered in [17–20]. In [21, 22], connections between broadband feedback disturbance rejection using RCAC and linear-quadratic-Gaussian (LQG) control, an H_2 optimal method, are considered. The contributions of the present work in this regard are the following:

- An experimental application of RCAC feedback active noise control applied to broadband road-noise disturbance rejection in a ground vehicle. Some of the results appear in [23].

- Extension of RCAC to broadband feedforward disturbance rejection with connections to LQG through numerical simulation and experimental results.

- Comparison of RCAC to the Filtered-x/Filtered-u least-mean-square (F-x/F-u LMS) and the Filtered-x/Filtered-u recursive-least-squares (F-x/F-u RLS) algorithms [4, 5, 24, 25].

We also extend the work in [20, 22] on the filter G_f for RCAC, which contains the necessary modeling information for the algorithm. In [20, 22], G_f is regarded as a target model for a specific closed-loop transfer function $\tilde{G}_{z\tilde{u}}$, which is called the intercalated transfer function. Part of the contribution is the derivation and interpretation of G_f and $\tilde{G}_{z\tilde{u}}$ in the context of feedforward disturbance rejection. The other major contribution of this dissertation is a new interpretation of the retrospective performance variable $\hat{z}(k, \hat{\theta})$ based

on the work in [20, 22]. In particular, we decompose $\hat{z}(k, \hat{\theta})$ to show that the retrospective performance variable is the sum of a performance-like term and a target model-matching error term.

1.5 Dissertation Outline

This dissertation is organized as follows.

Chapter 2 Summary

In Chapter 2, we derive the spatial spillover function for feedback and feedforward control in the case where z, e, and the disturbance w are scalar signals. We show that the spatial spillover function can be expressed as a ratio of transmissibility functions. For illustrative 2 degree of freedom (DOF) models, we compute the spatial spillover function in numerical simulations. The study is repeated experimentally in a broadband disturbance rejection acoustic experiment. In certain applications, obstructions that are difficult to model may be present in the acoustic space, for example, passengers in a vehicle. We thus introduce obstructions between the performance and evaluation microphones in order to determine the effect on the spatial spillover function.

Chapter 3 Summary

In Chapter 3, we present the framework for the standard problem and the equations of the RCAC algorithm.

Chapter 4 Summary

In Chapter 4, we present the interpretation of the target model G_{f} in the context of RCAC feedback control and derive the RCAC performance decomposition. What follows

is an experimental implementation of broadband feedback road noise suppression using RCAC. We incorporate the concepts of spatial spillover developed in Chapter 2 to the experiment and analyze suppression at evaluation microphone locations in the context of the spatial spillover function.

Chapter 5 Summary

In Chapter 5, we present the framework of the feedforward disturbance rejection problem and the ideal feedforward controller $\hat{G}_\mathrm{c}$. The equations of LQG and properties of high-authority LQG for feedforward disturbance rejection are reviewed. Next, the role of G_f and $\tilde{G}_{z\tilde{u}}$ are derived in the context of RCAC feedforward control. We show that RCAC is able to recover LQG controllers for various cases in a series of numerical examples. The controller update equations of RCAC are compared to the Fx/FuLMS and Fx/FuRLS algorithms. RCAC is then compared numerically to the FuRLS algorithm. Finally, we implement RCAC in a feedforward acoustic experiment.

In Chapter 6, we summarize the conclusions and contributions of this dissertation, and discuss future work.

CHAPTER 2

Spatial Spillover

In this chapter, we derive the spatial spillover function for feedforward control and numerically demonstrate its properties. The spatial spillover function is then derived for feedback control and numerically demonstrated. We show that the spatial spillover function has the same function form regardless of control architecture. An alternative formulation of the spatial spillover function involving the ratio of transmissibilities is then presented.

We then demonstrate the determination of the spatial spillover function for feedforward and feedback control in an acoustic experiment and examine the effect of obstructions within the acoustic space on the spatial spillover function.

2.1 Spatial Spillover Function for Feedforward Control

Consider the feedforward control problem shown in Figure 2.1, where $z \in \mathbb{R}$ is the performance variable, $e \in \mathbb{R}$ is the evaluation variable, $w \in \mathbb{R}$ is the disturbance, and $u \in \mathbb{R}^{l_u}$ is the control input. Note that z, e, and w are scalar signals and that u may be either a scalar or vector signal depending on whether $l_u = 1$ or $l_u > 1$, respectively. The dynamics and signals may be either continuous time or discrete time.
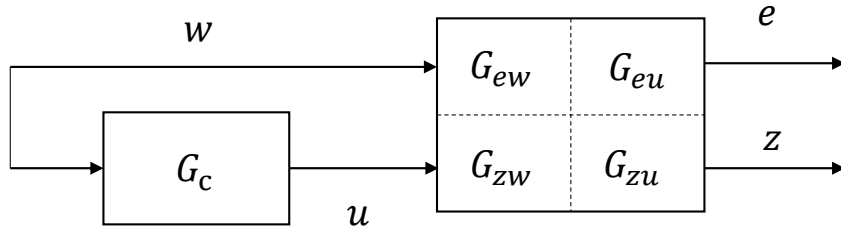
Figure 2.1: Feedforward control block diagram. The dynamics and signals may be either continuous time or discrete time.

It follows from Figure 2.1 that

$$z = G_{zu}u + G_{zw}w, \tag{2.1}$$

$$e = G_{eu}u + G_{ew}w, \tag{2.2}$$

where the feedforward control u is given by

$$u = G_{\mathrm{c}}w. \tag{2.3}$$

Therefore,

$$z = \widetilde{G}_{zw}w, \tag{2.4}$$

$$e = \widetilde{G}_{ew}w, \tag{2.5}$$

where

$$\widetilde{G}_{zw} \triangleq G_{zu}G_{\mathrm{c}} + G_{zw}, \tag{2.6}$$

$$\widetilde{G}_{ew} \triangleq G_{eu}G_{\mathrm{c}} + G_{ew}. \tag{2.7}$$

Define the *spatial spillover function* G_{ss} by

$$G_{ss} \triangleq \frac{\dfrac{\widetilde{G}_{ew}}{G_{ew}} - 1}{\dfrac{\widetilde{G}_{zw}}{G_{zw}} - 1}. \tag{2.8}$$

Note that, if $G_{zu}G_c = 0$, then $\widetilde{G}_{zw} = G_{zw}$, and thus the spatial spillover function is undefined. We therefore assume that $G_{zu}G_c \neq 0$. G_{ss} relates the performance of the controlled system relative to the uncontrolled system at e to the performance of the controlled system relative to the uncontrolled system at z. It follows from (2.6) and (2.7) that

$$\frac{\widetilde{G}_{zw}}{G_{zw}} - 1 = \frac{G_{zu}G_c}{G_{zw}}, \tag{2.9}$$

$$\frac{\widetilde{G}_{ew}}{G_{ew}} - 1 = \frac{G_{eu}G_c}{G_{ew}}, \tag{2.10}$$

and thus (2.8)–(2.10) implies that

$$G_{ss} = \frac{G_{eu}G_c G_{zw}}{G_{zu}G_c G_{ew}}. \tag{2.11}$$

In the case where u is scalar, that is, $l_u = 1$, it follows that

$$G_{ss} = \frac{G_{eu}G_{zw}}{G_{zu}G_{ew}}, \tag{2.12}$$

which is independent of G_c. Note that G_{ss} is a rational function of the Laplace or Z-transform variable. However, G_{ss} is not a transfer function since it may be improper and does not have input and output signals that can be specified in terms of z, e, w, and u.

11

2.2 Feedforward Control Numerical Examples

In this section, we demonstrate the spatial spillover function for feedforward control in numerical simulation. Feedforward controllers are designed to provide suppression at the z location in order to compute the spatial spillover function. Consider a discrete-time state-space representation of (2.1), (2.2) given by

$$x(k+1) = Ax(k) + Bu(k) + D_1 w(k), \tag{2.13}$$

$$z(k) = E_1 x(k), \tag{2.14}$$

$$e(k) = Cx(k), \tag{2.15}$$

where

$$G_{zw}(\mathbf{z}) = E_1(\mathbf{z}I - A)^{-1}D_1, \tag{2.16}$$

$$G_{zu}(\mathbf{z}) = E_1(\mathbf{z}I - A)^{-1}B, \tag{2.17}$$

$$G_{ew}(\mathbf{z}) = C(\mathbf{z}I - A)^{-1}D_1, \tag{2.18}$$

$$G_{eu}(\mathbf{z}) = C(\mathbf{z}I - A)^{-1}B, \tag{2.19}$$

and the state-space representation of the feedforward controller (2.3) given by

$$x_{\mathrm{c}}(k+1) = A_{\mathrm{c}}x_{\mathrm{c}}(k) + B_{\mathrm{c}}w(k), \tag{2.20}$$

$$u(k) = C_{\mathrm{c}}x_{\mathrm{c}}(k) + D_{\mathrm{c}}w(k), \tag{2.21}$$

where

$$G_{\mathrm{c}}(\mathbf{z}) = C_{\mathrm{c}}(\mathbf{z}I - A_{\mathrm{c}})^{-1}B_{\mathrm{c}} + D_{\mathrm{c}}, \tag{2.22}$$

$x_{\mathrm{c}} \in \mathbb{R}^{n_{\mathrm{c}}}$.

In the subsequent feedforward numerical examples, the discrete-time state-space systems are chosen arbitrarily as a 4th-order system with two modes. We assume that w is zero-mean Gaussian white noise with standard deviation 1. Feedforward controllers are designed to suppress the effect of w at z. No considerations are made in the controller design to suppress the effect of w at e. The details of the controller design are omitted since they are not relevant to the analysis.

In each example we compare the spatial spillover function for two different feedforward controller designs applied to the same system. The spatial spillover function is computed using (2.8) which is a function of G_{zw}, G_{ew}, $\widetilde{G}_{zw}$ given by (2.6), and $\widetilde{G}_{ew}$ given by (2.7). We demonstrate that, if $l_u = 1$, then (2.8) is independent of G_c, whereas if $l_u > 1$, then (2.8) is not independent of G_c.

Example 2.1: G_{ss} for feedforward control with scalar control u. Consider the 4th-order system

$$
A = \begin{bmatrix} 0.45 & 1 & 0 & 0 \\ -0.05 & 0.45 & -0.37 & -0.66 \\ 0 & 0 & 0.38 & 1 \\ 0 & 0 & -0.76 & 0.38 \end{bmatrix}, \qquad B = \begin{bmatrix} 0 \\ 1.01 \\ 0 \\ 0.76 \end{bmatrix}, \qquad D_1 = \begin{bmatrix} -1.53 \\ 0 \\ -1.11 \\ -1.04 \end{bmatrix},
$$

(2.23)

$$
E_1 = \begin{bmatrix} -0.15 & 0.99 & 0 & 0 \end{bmatrix}, \qquad\qquad C = \begin{bmatrix} 0.99 & 0.26 & -0.38 & 0.17 \end{bmatrix}. \qquad (2.24)
$$

Assuming that this discrete-time model arises from sampling a continuous-time system at the sample rate of 1 kHz, the corresponding continuous-time modal frequencies are $\omega_{n1} = 132$ Hz and $\omega_{n2} = 185$ Hz with damping ratios $\zeta_1 = 0.831$ and $\zeta_2 = 0.043$,

respectively. We apply two different feedforward controllers to this system, namely,

$$A_c = \begin{bmatrix} 0.52 & 0.74 & 0 \\ -0.74 & 0.52 & 0 \\ 0 & 0 & -0.30 \end{bmatrix}, \qquad B_c = \begin{bmatrix} -0.70 \\ -1.14 \\ 0.49 \end{bmatrix}, \qquad (2.25)$$

$$C_c = \begin{bmatrix} 0.59 & -0.23 & -0.17 \end{bmatrix}, \qquad D_c = -0.12 \qquad (2.26)$$

and

$$A_c = \begin{bmatrix} 0.62 & 0.67 & 0 & 0 \\ -0.67 & 0.62 & 0 & 0 \\ 0 & 0 & -0.54 & 0 \\ 0 & 0 & 0 & -0.01 \end{bmatrix}, \qquad B_c = \begin{bmatrix} 1.39 \\ 2.15 \\ -0.94 \\ 0.56 \end{bmatrix}, \qquad (2.27)$$

$$C_c = \begin{bmatrix} -0.56 & 0.18 & 0.15 & 0.21 \end{bmatrix}, \qquad D_c = -0.18. \qquad (2.28)$$

For both controllers, Figure 2.2 shows the frequency response of the controlled and uncon-trolled system at z and e as well as the frequency response of G_{ss}. Since u is scalar, G_{ss} is the same for both controllers.

Example 2.2: G_{ss} for feedforward control with vector control $u \in \mathbb{R}^2$. Consider the

4th-order system

$$
A = \begin{bmatrix} 0.66 & 1 & 0 & 0 \\ -0.46 & 0.66 & 0.38 & 0.59 \\ 0 & 0 & 0.90 & 1 \\ 0 & 0 & -0.09 & 0.90 \end{bmatrix}, \qquad B = \begin{bmatrix} 0 & 0 \\ 1.07 & 1 \\ 0 & 1 \\ 0.66 & 0 \end{bmatrix}, \qquad D_1 = \begin{bmatrix} -0.57 \\ -0.31 \\ 0.27 \\ 1.33 \end{bmatrix},
$$

$$
\tag{2.29}
$$

$$
E_1 = \begin{bmatrix} 0.53 & 0.93 & 0 & 0 \end{bmatrix}, \qquad\qquad C = \begin{bmatrix} 0.93 & 0.17 & -0.69 & -0.72 \end{bmatrix}. \tag{2.30}
$$

Assuming that this discrete-time model arises from sampling a continuous-time system at the sample rate of 1 kHz, the corresponding continuous-time modal frequencies are $\omega_{n1} = 52$ Hz and $\omega_{n2} = 127$ Hz with damping ratios $\zeta_1 = 0.162$ and $\zeta_2 = 0.069$, respectively. We apply two different feedforward controllers to this system, namely,

$$
A_c = \begin{bmatrix} -0.62 & 0 & 0 \\ 0 & 0.26 & 0.18 \\ 0 & -0.18 & 0.26 \end{bmatrix}, \qquad\qquad B_c = \begin{bmatrix} -1.02 \\ -0.47 \\ -3.18 \end{bmatrix}, \qquad \tag{2.31}
$$

$$
C_c = \begin{bmatrix} -1.26 & 0.05 & 0.61 \\ 0.20 & 1.14 & -0.13 \end{bmatrix}, \qquad\qquad D_c = \begin{bmatrix} 0.19 \\ 0.18 \end{bmatrix} \qquad \tag{2.32}
$$

15

and

$$A_{\mathrm{c}} = \begin{bmatrix} -0.95 & 0 & 0 & 0 \\ 0 & -0.51 & 0.64 & 0 \\ 0 & -0.64 & -0.51 & 0 \\ 0 & 0 & 0 & 0.33 \end{bmatrix}, \qquad B_{\mathrm{c}} = \begin{bmatrix} 4.22 \\ -1.16 \\ 3.16 \\ 0.86 \end{bmatrix}, \qquad (2.33)$$

$$C_{\mathrm{c}} = \begin{bmatrix} -0.75 & 0.74 & 0.20 & -1.89 \\ 0.14 & 0.28 & 0.19 & -1.77 \end{bmatrix}, \qquad D_{\mathrm{c}} = \begin{bmatrix} 0.29 \\ 0.27 \end{bmatrix}. \qquad (2.34)$$

For both controllers, Figure 2.3 shows the frequency response of the controlled and uncontrolled system at z and e as well as the frequency response of G_{ss}. Note that, since u is a vector, G_{ss} depends on G_{c}.

2.3 Spatial Spillover Function for Feedback Control

Consider the feedback control architecture shown in Figure 2.4, where $z \in \mathbb{R}$ is the performance variable, $e \in \mathbb{R}$ is the evaluation variable, $w \in \mathbb{R}$ is the disturbance, and $u \in \mathbb{R}^{l_u}$ is the control input. The system may be either continuous time or discrete time.

It follows from Figure 2.4 that

$$z = G_{zu}u + G_{zw}w, \qquad (2.35)$$

$$e = G_{eu}u + G_{ew}w, \qquad (2.36)$$

where the feedback control u is given by

$$u = G_{\mathrm{c}}z. \qquad (2.37)$$

16

Using (2.35) and (2.37) we obtain

$$z = \widetilde{G}_{zw} w, \tag{2.38}$$

where

$$\widetilde{G}_{zw} \triangleq \frac{G_{zw}}{1 - G_{zu} G_{\mathrm{c}}}. \tag{2.39}$$

In addition, it follows from (2.36), (2.37), and (2.38) that

$$e = \widetilde{G}_{ew} w, \tag{2.40}$$

where

$$\widetilde{G}_{ew} \triangleq G_{eu} G_{\mathrm{c}} \widetilde{G}_{zw} + G_{ew} = \frac{G_{eu} G_{\mathrm{c}} G_{zw}}{1 - G_{zu} G_{\mathrm{c}}} + G_{ew}. \tag{2.41}$$

For feedback control, we define the spatial spillover function G_{ss} by

$$G_{\mathrm{ss}} \triangleq \frac{\dfrac{\widetilde{G}_{ew}}{G_{ew}} - 1}{\dfrac{\widetilde{G}_{zw}}{G_{zw}} - 1}, \tag{2.42}$$

which is identical in form to G_{ss} defined by (2.8) for feedforward control. As in the case of feedforward control, we assume that $G_{zu} G_{\mathrm{c}} \neq 0$. However, $\widetilde{G}_{zw}$ and $\widetilde{G}_{ew}$ defined by (2.39) and (2.41) for feedback control are different from $\widetilde{G}_{zw}$ and $\widetilde{G}_{ew}$ defined by (2.6) and (2.7)

17

for feedforward control. It follows from (2.39) and (2.41) that

$$\frac{\widetilde{G}_{zw}}{G_{zw}} - 1 = \frac{G_{zu}G_{c}}{1 - G_{zu}G_{c}}, \tag{2.43}$$

$$\frac{\widetilde{G}_{ew}}{G_{ew}} - 1 = \frac{G_{eu}G_{c}G_{zw}}{G_{ew}(1 - G_{zu}G_{c})}. \tag{2.44}$$

Therefore, (2.42) implies that

$$G_{\text{ss}} = \frac{\dfrac{G_{eu}G_{c}G_{zw}}{G_{ew}(1 - G_{zu}G_{c})}}{\dfrac{G_{zu}G_{c}}{1 - G_{zu}G_{c}}} = \frac{G_{eu}G_{c}G_{zw}}{G_{zu}G_{c}G_{ew}}. \tag{2.45}$$

Note that (2.45) has the same form as G_{ss} given by (2.11) for feedforward control. In the case where u is scalar, it follows that

$$G_{\text{ss}} = \frac{G_{eu}G_{zw}}{G_{zu}G_{ew}}, \tag{2.46}$$

which is independent of G_{c} and coincides with (2.12) for feedforward control.

2.4   Feedback Control Numerical Examples

In this section, we demonstrate the spatial spillover function for feedback control in numerical simulation. Feedback controllers are designed to provide suppression at the z location in order to compute the spatial spillover function. Consider a discrete-time state-space representation of the system (2.35), (2.36) given by (2.13)–(2.19) and the state-space representation of the feedback controller (2.37) given by

$$x_{c}(k + 1) = A_{c}x_{c}(k) + B_{c}z(k), \tag{2.47}$$

$$u(k) = C_{c}x_{c}(k) + D_{c}z(k), \tag{2.48}$$

18

where

$$G_c(\mathbf{z}) = C_c(\mathbf{z}I - A_c)^{-1}B_c + D_c. \tag{2.49}$$

In the subsequent feedback numerical examples, we consider the same plants as in the feedforward numerical examples section. We assume that w is zero-mean Gaussian white noise with standard deviation 1. Feedback controllers are designed to suppress the effect of w at z. No considerations are made in the controller design to suppress the effect of w at e. The details of the controller design are omitted since they are not relevant to the analysis.

In each example we compare the spatial spillover function for two different feedback controller designs applied to the same system. The spatial spillover function is computed using (2.42) which is a function of G_{zw}, G_{ew}, $\widetilde{G}_{zw}$ given by (2.39), and $\widetilde{G}_{ew}$ given by (2.41). We demonstrate that, if $l_u = 1$, then (2.42) is independent of G_c, whereas if $l_u > 1$, then (2.42) is not independent of G_c.

Example 2.3: G_{ss} *for feedback control with scalar control u.* Consider the system (2.23), (2.24) with scalar control u. We apply two different feedback controllers to this system, namely,

$$A_c = \begin{bmatrix} -1.02 & 0 & 0 & 0 \\ 0 & 0.44 & 0.66 & 0 \\ 0 & -0.66 & 0.44 & 0 \\ 0 & 0 & 0 & 0.47 \end{bmatrix}, \qquad B_c = \begin{bmatrix} 0.49 \\ 0.42 \\ 1.08 \\ 1.12 \end{bmatrix}, \tag{2.50}$$

$$C_c = \begin{bmatrix} -0.97 & 0.17 & 0.02 & 0.10 \end{bmatrix}, \qquad D_c = 0 \tag{2.51}$$

and

$$A_c = \begin{bmatrix} -1.35 & 0 & 0 & 0 & 0 \\ 0 & 0.60 & 0.65 & 0 & 0 \\ 0 & -0.65 & 0.60 & 0 & 0 \\ 0 & 0 & 0 & 0.58 & 0 \\ 0 & 0 & 0 & 0 & -0.34 \end{bmatrix}, \qquad B_c = \begin{bmatrix} -0.87 \\ 1 \\ -1.72 \\ -1.46 \\ -0.54 \end{bmatrix}, \qquad (2.52)$$

$$C_c = \begin{bmatrix} 0.84 & -0.17 & -0.13 & -0.09 & -0.04 \end{bmatrix}, \qquad D_c = 0. \qquad (2.53)$$

For both controllers, Figure 2.5 shows the frequency response of the controlled and uncontrolled system at z and e as well as the frequency response of G_{ss}. Since u is scalar, G_{ss} is the same for both controllers.

Example 2.4: G_{ss} for feedback control with vector control u. Consider the system (2.29), (2.30), where $u \in \mathbb{R}^2$. We apply two different feedback controllers to this system, namely,

$$A_c = \begin{bmatrix} -1.35 & 0 & 0 \\ 0 & -0.01 & 0.34 \\ 0 & -0.34 & -0.01 \end{bmatrix}, \qquad B_c = \begin{bmatrix} -1.49 \\ 0.78 \\ -2.16 \end{bmatrix}, \qquad (2.54)$$

$$C_c = \begin{bmatrix} -0.62 & 0.61 & 0.47 \\ -0.58 & -0.56 & 0.20 \end{bmatrix}, \qquad D_c = \begin{bmatrix} 0 \\ 0 \end{bmatrix} \qquad (2.55)$$

and

$$A_c = \begin{bmatrix} -1.96 & 0 & 0 & 0 \\ 0 & 0.38 & 0.37 & 0 \\ 0 & -0.37 & 0.38 & 0 \\ 0 & 0 & 0 & 0.16 \end{bmatrix}, \qquad B_c = \begin{bmatrix} -1.98 \\ 4.27 \\ -4.60 \\ 4.26 \end{bmatrix}, \qquad (2.56)$$

$$C_c = \begin{bmatrix} -0.46 & 0.18 & -0.29 & -0.70 \\ -0.75 & 0.74 & -1.26 & 0.05 \end{bmatrix}, \qquad D_c = \begin{bmatrix} 0 \\ 0 \end{bmatrix}. \qquad (2.57)$$

For both controllers, Figure 2.6 shows the frequency response of the controlled and uncontrolled system at z and e as well as the frequency response of G_{ss}. Note that, since u is a vector, G_{ss} depends on G_c.

2.5 Spatial Spillover as a Ratio of Transmissibilities

Consider the case where z, e, w, and u are scalar signals and introduce the notation

$$G_{zw} = \frac{N_{zw}}{D_{zw}}, \quad G_{ew} = \frac{N_{ew}}{D_{ew}}, \quad G_{zu} = \frac{N_{zu}}{D_{zu}}, \quad G_{eu} = \frac{N_{eu}}{D_{eu}}. \qquad (2.58)$$

Assume that $D_{zw} = D_{ew}$ and $D_{zu} = D_{eu}$. The transmissibility [26–28] from z to e driven by w is given by

$$T_{ez,w} \triangleq \frac{G_{ew}}{G_{zw}} = \frac{\dfrac{N_{ew}}{D_{ew}}}{\dfrac{N_{zw}}{D_{zw}}} = \frac{N_{ew}}{N_{zw}}. \qquad (2.59)$$

Similarly, the transmissibility from z to e driven by u is given by

$$T_{ez,u} \triangleq \frac{G_{eu}}{G_{zu}} = \frac{N_{eu}}{N_{zu}}.$$ (2.60)

Therefore, it follows from (2.12) and (2.46) that

$$G_{ss} = \frac{G_{eu}G_{zw}}{G_{zu}G_{ew}} = \frac{N_{eu}N_{zw}}{N_{zu}N_{ew}} = \frac{\dfrac{N_{eu}}{N_{zu}}}{\dfrac{N_{ew}}{N_{zw}}} = \frac{T_{ez,u}}{T_{ez,w}}.$$ (2.61)

Hence G_{ss} can be expressed as the ratio of two transmissibility functions.

2.6   Experimental Results

2.6.1   Experimental Setup

We apply feedforward and feedback controllers to an acoustic experiment to investigate the spatial spillover function. Omni-directional microphones are used as sensors, and mid-bass woofers are used as the actuation. Real Time Workshop (RTW) and MAT-LAB/Simulink is used with a dSPACE DS1104 board to implement the designed controllers. Additional hardware used in implementation included speaker amplifiers, microphone amplifiers, and anti-aliasing filters. A diagram of the microphone and speaker placement is shown in Figure 2.7. The approximate dimensions of the acoustic space are 6 ft $\times$ 3 ft $\times$ 3 ft. We consider three microphone locations m_1, m_2, and m_3, and three speaker locations s_1, s_2, and s_3. In the subsequent experiments, one microphone is chosen as the performance microphone z, a separate microphone is chosen as the evaluation microphone e, one speaker is chosen to produce a disturbance w, and either one or both of the remaining speakers are chosen as the control speaker u. The frequency range of interest for this

study is from 50 Hz to 500 Hz, with all data sampled at 1 kHz. Each data set is run for 10,000 samples and multiple runs are repeated to check for consistency. In all experimental examples, the disturbance w is chosen as zero-mean Gaussian white noise.

2.6.2 Experimental Determination and Validation of the Spatial Spillover Function

In the subsequent feedforward control experiments, two methods for estimating the spatial spillover function G_{ss} are compared. We estimate G_{ss} using both (2.8) and (2.11). The Blackman-Tukey spectral analysis method [29] with a Hanning window is applied to input-output data in order to estimate the frequency response of various transfer functions in G_{ss}.

Determining G_{ss} using (2.8) requires estimates of G_{zw}, G_{ew}, $\widetilde{G}_{zw}$, and $\widetilde{G}_{ew}$. The frequency response of G_{zw} and G_{ew} are estimated by exciting the system with a known broadband input w and sampling the z microphone and e microphone outputs. The frequency response of $\widetilde{G}_{zw}$ and $\widetilde{G}_{ew}$ are estimated by applying the controller to the system with a known disturbance w and similarly obtaining measurements of the output signals z and e. Determining G_{ss} using (2.11) requires estimates of G_{zw}, G_{ew}, G_{zu}, and G_{eu}, and, in the case where u is a vector, depends on the design of G_{c}. The frequency response of G_{zw} and G_{ew} are estimated as described above. The frequency response of G_{zu} and G_{eu} are estimated by exciting the system with a known broadband input u and sampling the z microphone and e microphone outputs.

Note that G_{ss} estimated as (2.8) requires applying the controller to the system, whereas G_{ss} estimated as (2.11) does not. The goal of the experimental examples is to show that the estimated frequency response of (2.8) and (2.11) agree, despite the fact that one method requires applying the controller to the system. In practice, it may be more advantageous to estimate G_{ss} as (2.11) since the identification of G_{zu} and G_{eu} is of lower order and the expression is less complex than $\widetilde{G}_{zw}$ and $\widetilde{G}_{ew}$. Similar logic applies to the feedback case

between estimating G_{ss} as (2.42) and (2.45). The details of the controller design are again omitted since they are not relevant to the analysis of G_{ss}. We note that in all experimental examples, the matching between G_{ss} estimated using the two methods degrades as the Nyquist rate is approached. Furthermore, it was observed that if $\frac{\widetilde{G}_{ew}}{G_{ew}} \approx 1$, the matching between the two methods can be adversely effected.

2.6.3   Experimental Results Using Feedforward Control

Example 2.5: Comparison of G_{ss} for feedforward control with scalar control u. We choose m_2 as z, m_1 as e, s_1 as w, and s_2 as u. A feedforward controller is designed to suppress the effect of w at z. Figure 2.8 shows the frequency response of the controller, the controlled and uncontrolled system at z and e, and G_{ss} estimated using (2.8) and (2.11). The magnitude and phase of G_{ss} estimated using (2.8) and (2.11) are within 5 dB and 10 deg from 50 Hz to 380 Hz, and within 12 dB and 60 deg from 250 Hz to 500 Hz.

Example 2.6: Comparison of G_{ss} for feedforward control with vector control $u \in \mathbb{R}^2$. We choose m_2 as z, m_1 as e, s_1 as w, s_2 as u_1, and s_3 as u_2. A feedforward controller is designed to suppress to suppress the effect of w at z. Figure 2.9 shows the frequency response of the controller, the controlled and uncontrolled system at z and e, and G_{ss} estimated using (2.8) and (2.11). The magnitude and phase of G_{ss} estimated using (2.8) and (2.11) are within 5 dB and 10 deg from 50 Hz to 250 Hz, and within 12 dB and 60 deg from 250 Hz to 500 Hz.

2.6.4   Experimental Results Using Feedback Control

Example 2.7: Comparison of G_{ss} for feedback control with scalar control u. Consider the same choice of microphones and speakers as in Example 2.5. A feedback controller is designed to suppress the effect of w at z. Figure 2.10 shows the frequency response of the controller, the controlled and uncontrolled system at z and e, and G_{ss} estimated using (2.42) and (2.45). The magnitude and phase of G_{ss} estimated using (2.42) and (2.45) are

within 5 dB and 20 deg from 50 Hz to 250 Hz, and within 12 dB and 40 deg from 250 Hz to 500 Hz.

Example 2.8: Comparison of G_{ss} for feedback control with vector control $u \in \mathbb{R}^2$. Consider the same choice of microphones and speakers as in Example 2.6. A feedback controller is designed to suppress the effect of w at z. Figure 2.11 shows the frequency response of the controller, the controlled and uncontrolled system at z and e, and G_{ss} estimated using (2.42) and (2.45). The magnitude and phase of G_{ss} estimated using (2.42) and (2.45) are mismatched from 50 Hz to 100 Hz, and from 200 Hz to 250 Hz, where the difference between the two estimates exceeds 15 dB and 60 deg. At other frequencies, the magnitude and phase are within 5 dB and 20 deg. The large mismatch is partially due to the fact that $\widetilde{G}_{ew} \approx G_{ew}$ across those bands, and thus the numerator of (2.42) becomes approximately zero causing the numerical accuracy of the estimate to degrade.

2.6.5 Computing G_{ss} as a Ratio of Transmissibilities

Consider the case where u is a scalar. G_{ss} can be estimated using (2.61), which is a ratio of transmissibility functions. The advantage of this method is that estimating the frequency response of a transmissibility function does not explicitly require the input to be known, but only needs measurements of the ouptut. Hence, if a measurement of disturbance w is unavailable, an estimate of G_{ss} is still obtainable using only measurements of z and e. The disadvantage of estimating G_{ss} using (2.61) is that in order to estimate $T_{ez,u}$, the system must be excited only by u without the presence of w and vice versa when estimating $T_{ez,w}$. We compare G_{ss} estimated using (2.12) and (2.61), which are expected to agree.

Example 2.9: G_{ss} as a ratio of Transmissibilities. We choose m_1 as e, m_2 as z, s_1 as w, and s_3 as u. Figure 2.12 compares the frequency response of G_{ss} estimated using (2.12) and (2.61). The magnitude and phase of G_{ss} estimated as (2.12) and (2.61) are within 5 dB and 20 deg from 50 Hz to 450 Hz, and within 9 dB and 50 deg from 450 Hz to 500 Hz.

25

2.6.6 G_{ss} in the Presence of Obstructions

We examine G_{ss} in the presence of obstructions by comparing the estimate of G_{ss} between sensors with and without the presence of an obstruction. In the subsequent examples, G_{ss} estimated as (2.12), where we assume u is a scalar, using methods described above. Figure 2.13 shows a diagram of the two configurations considered in the acoustic space.

In each example, one microphone is chosen as z, one speaker is chosen as w, two e locations, denoted as e_1 and e_2, are chosen, and two separate locations for u are considered. The spatial spillover function is estimated for the pair z and e_1 and the pair z and e_2 for both choices of u. In certain cases, the presence of obstruction can significantly shift the magnitude and phase of the spatial spillover function relative to when the obstruction is not present.

Example 2.10: Comparison of G_{ss} with and without a height-wise obstruction. We choose m_2 as z, s_1 as w, and two e locations, with m_1 as e_1 and m_3 as e_2. We consider two choices of u, where for the first system we choose s_3 as u, and the second system we choose s_2 as u. Comparison of G_{ss} with and without a height-wise obstruction in the acoustic space for both choices of u is shown in Figure 2.14. Of the four cases considered in the example, a noticeable or significant shift in the magnitude and phase of G_{ss} is observed in three cases.

Example 2.11: Comparison of G_{ss} with and without a length-wise obstruction. We consider the same choices of speakers and microphones as in Example 2.10, and place a length-wise obstruction in the acoustic space. Comparison of G_{ss} with and without a length-wise obstruction in the acoustic space for both choices of u is shown in Figure 2.15. Of the four cases considered in the example, a noticeable or significant shift in the magnitude and phase of G_{ss} is observed in one case.

2.7　Conclusions

In this chapter, the spatial spillover function was validated in both numerical and experimental studies, and it was shown that the expression for G_{ss} is the same for both feedforward and feedback control. In the case where u is a scalar signal, the spatial spillover function is independent of the controller, and G_{ss} can be interpreted as a ratio of transmissibility functions. It was found that obstructions in the acoustic space may give rise to significant shifts in the magnitude and phase of G_{ss}.
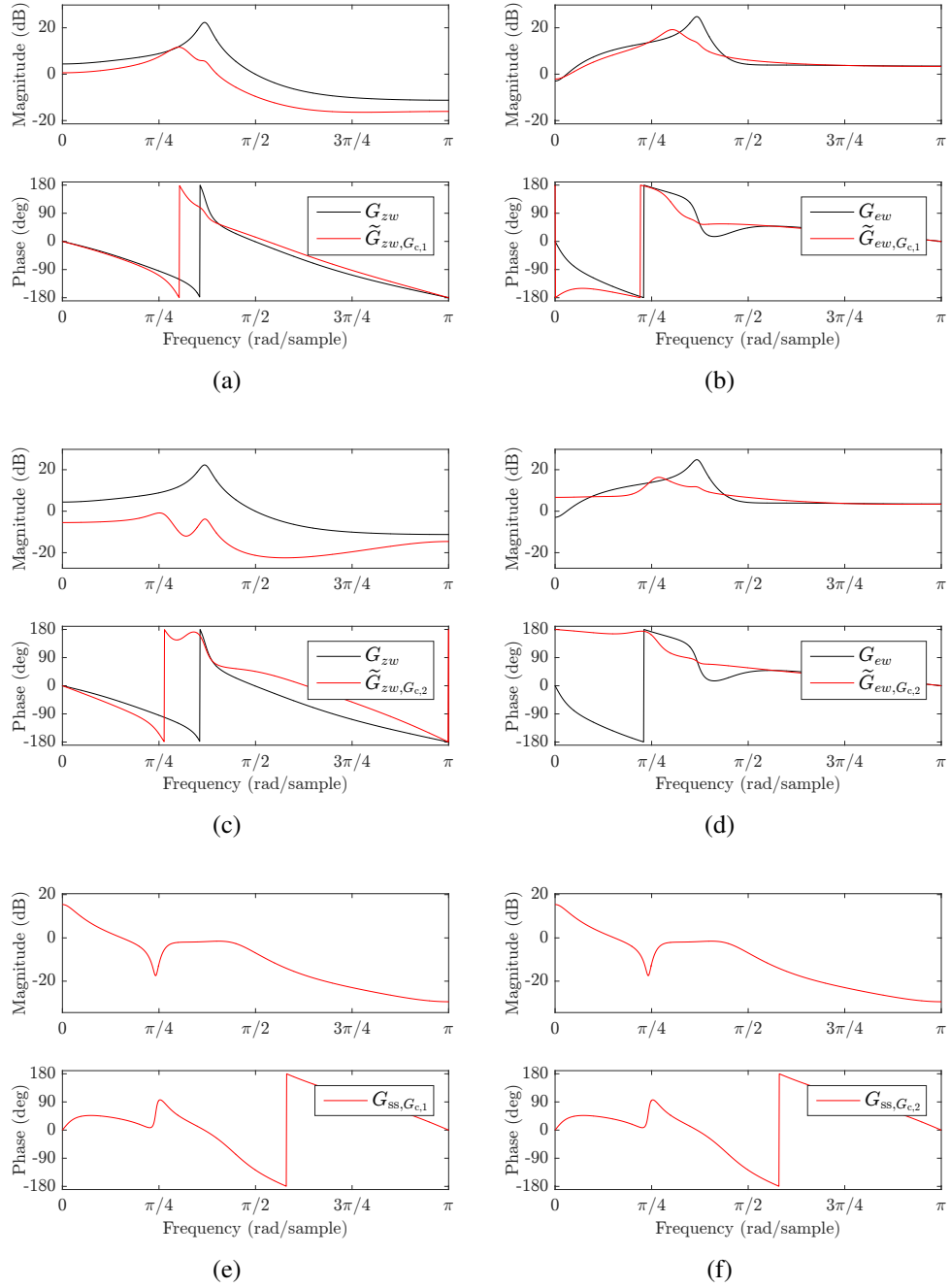
Figure 2.2: Example 2.1: Comparison of G_{ss} computed as (2.8) for feedforward control with scalar control u. (a) and (b) show the controlled and uncontrolled frequency response of the system (2.23), (2.24) using the controller (2.25), (2.26) denoted in the above legend as $G_{c,1}$; (c) and (d) show the controlled and uncontrolled frequency response of the system (2.23), (2.24) using the controller (2.27), (2.28) denoted in the above legend as $G_{c,2}$. Note that, since u is scalar, G_{ss} is independent of G_c, and thus (e), which shows the frequency response of G_{ss} for the controller (2.25), (2.26), is identical to (f), which shows the frequency response of G_{ss} for the controller (2.27), (2.28).

28
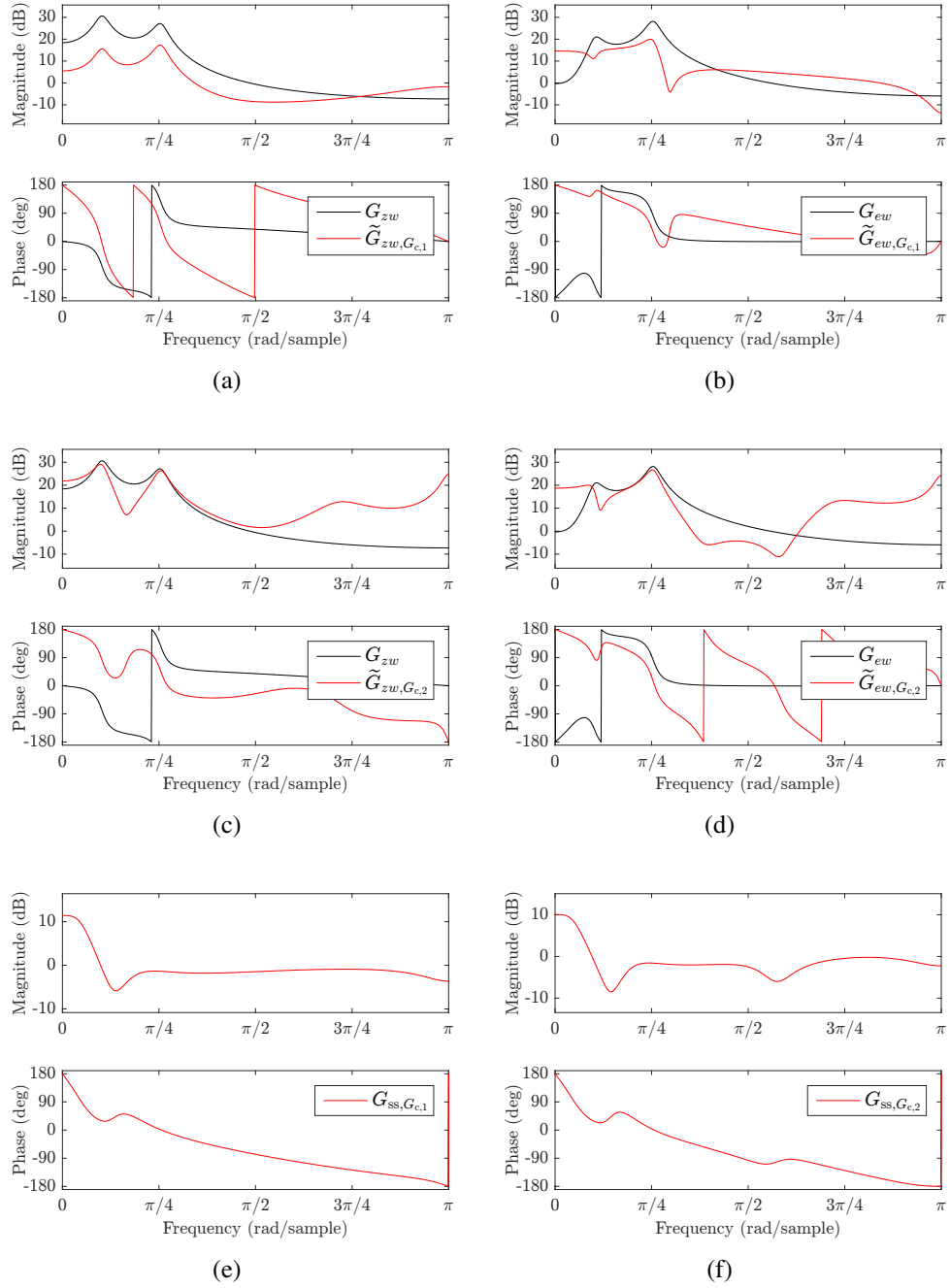
Figure 2.3: Example 2.2: Comparison of G_{ss} computed as (2.8) for feedforward control with vector control $u \in \mathbb{R}^2$. (a) and (b) show the controlled and uncontrolled frequency response of the system (2.29), (2.30) using the controller (2.31), (2.32) denoted in the above legend as $G_{c,1}$; (c) and (d) show the controlled and uncontrolled frequency response of the system (2.29), (2.30) using the controller (2.33), (2.34) denoted in the above legend as $G_{c,2}$. Note that, since u is a vector, G_{ss} depends on G_c, and thus (e), which shows the frequency response of G_{ss} for the controller (2.31), (2.32), differs from (f), which shows the frequency response of G_{ss} for the controller (2.33), (2.34).
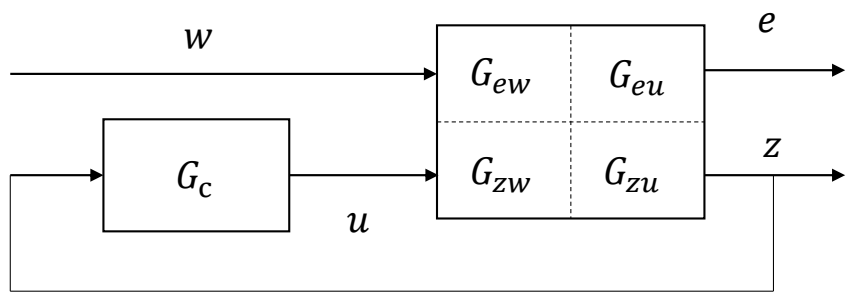
Figure 2.4: Feedback control block diagram. The dynamics and signals may be either continuous time or discrete time.
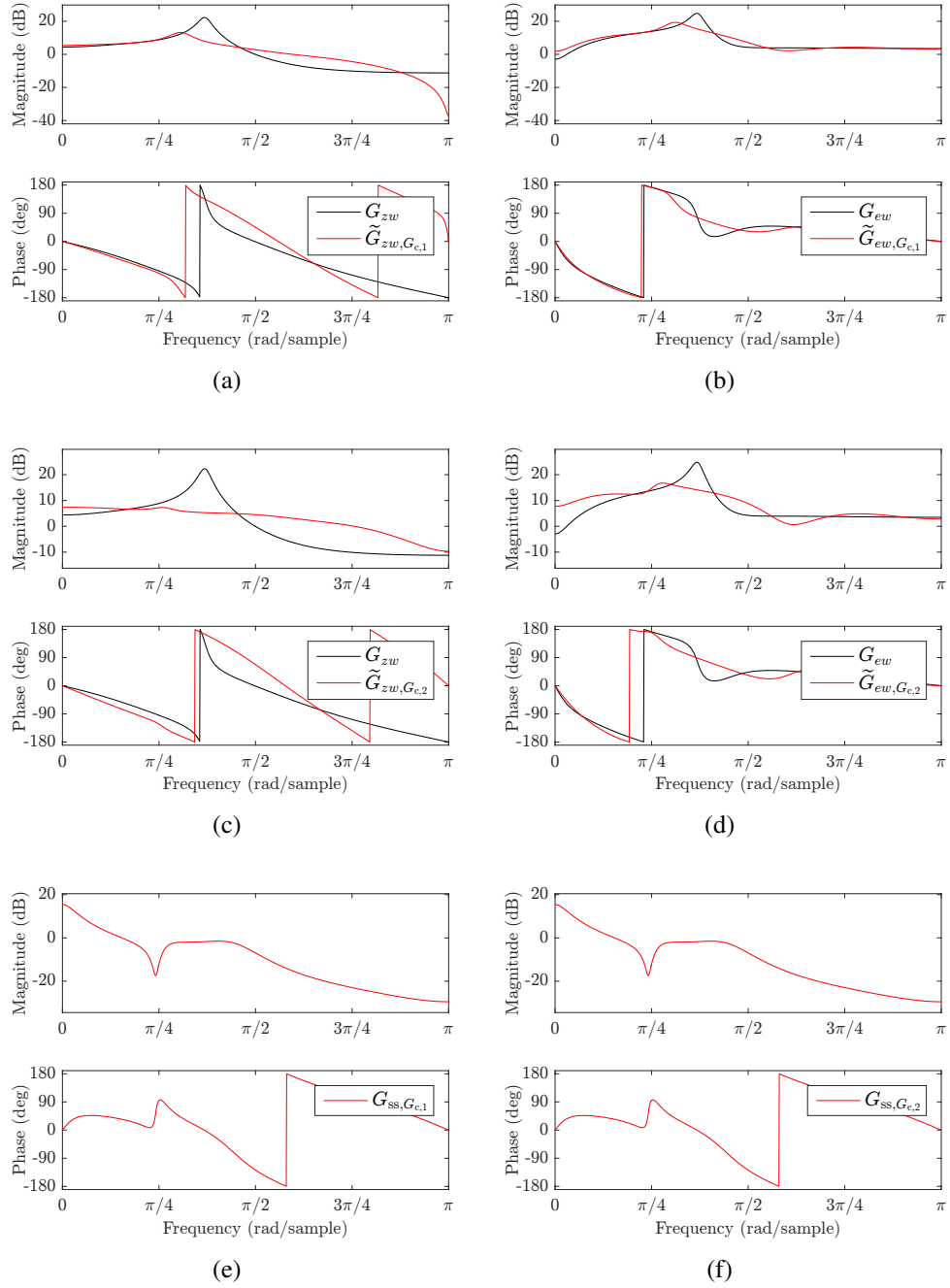
Figure 2.5: Example 2.3: Comparison of G_{ss} computed as (2.42) for feedback control with scalar control u. (a) and (b) show the controlled and uncontrolled frequency response of the system (2.23), (2.24) using the controller (2.50), (2.51) denoted in the above legend as $G_{c,1}$; (c) and (d) show the controlled and uncontrolled frequency response of the system (2.23), (2.24) using the controller (2.52), (2.53) denoted in the above legend as $G_{c,2}$. Note that, since u is scalar, G_{ss} is independent of G_c, and thus (e), which shows the frequency response of G_{ss} for the controller (2.50), (2.51), is identical to (f), which shows the frequency response of G_{ss} for the controller (2.52), (2.53).
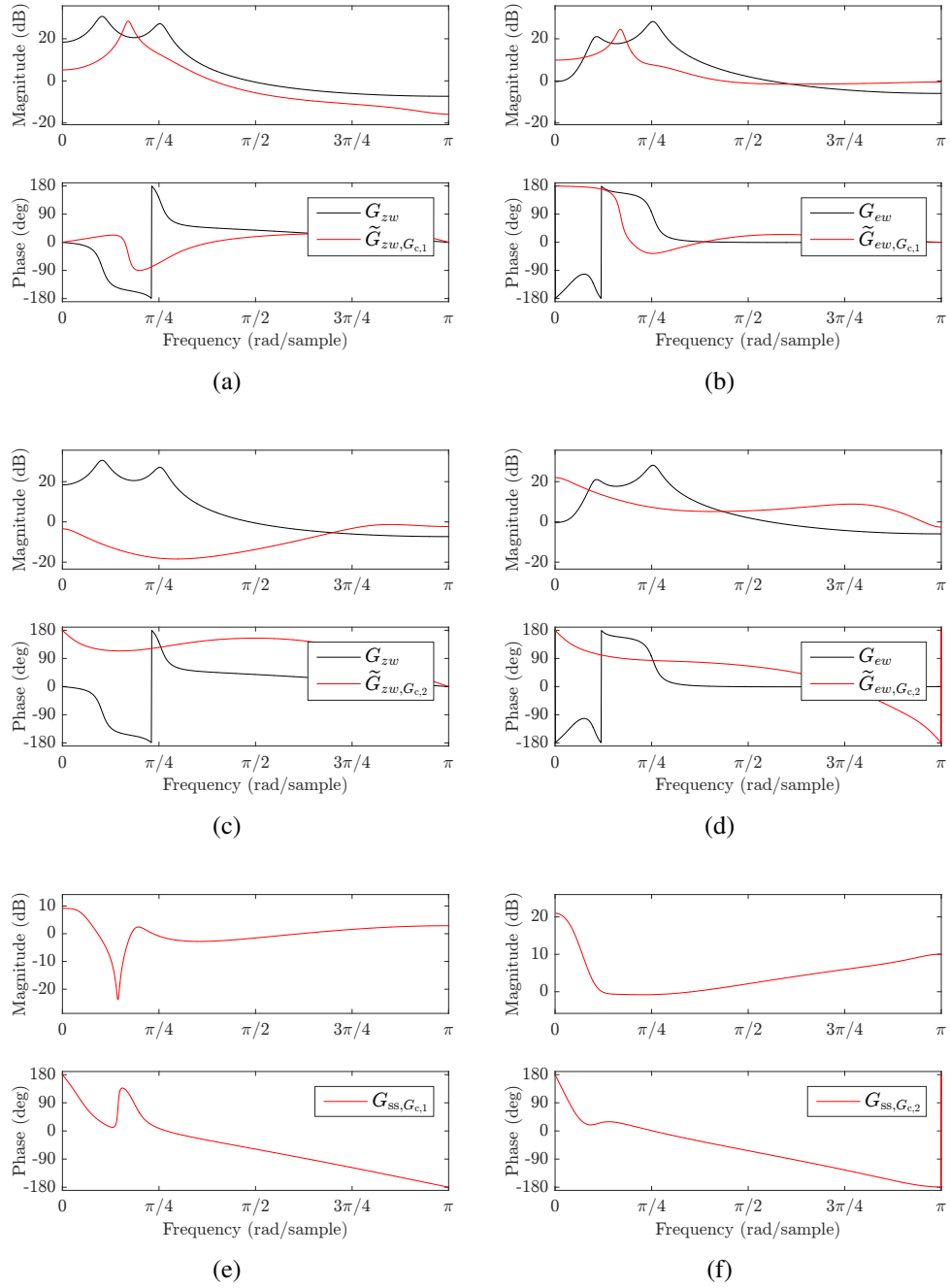
Figure 2.6: Example 2.4: G_{ss} for feedback control with vector control $u \in \mathbb{R}^2$. (a) and (b) show the controlled and uncontrolled frequency response of the system (2.29), (2.30) using the controller (2.54), (2.55) denoted in the above legend as $G_{\mathrm{c},1}$; (c) and (d) show the controlled and uncontrolled frequency response of the system (2.29), (2.30) using the controller (2.56), (2.57) denoted in the above legend as $G_{\mathrm{c},2}$. Note that, since u is a vector, G_{ss} depends on G_{c}, and thus (e), which shows the frequency response of G_{ss} for the controller (2.54), (2.55), differs from (f), which shows the frequency response of G_{ss} for the controller (2.56), (2.57).
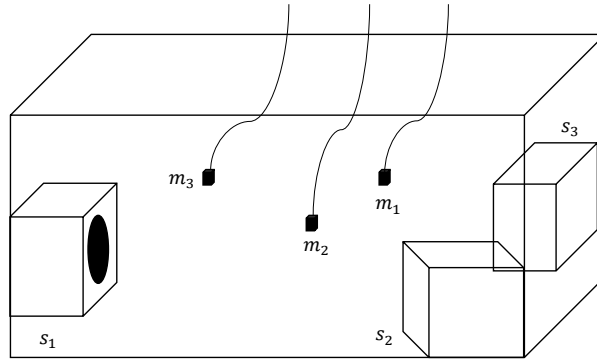
Figure 2.7: Sensor and actuator placement for the experimental evaluation of the spatial spillover function.

(a)

(b)

(c)

(d)
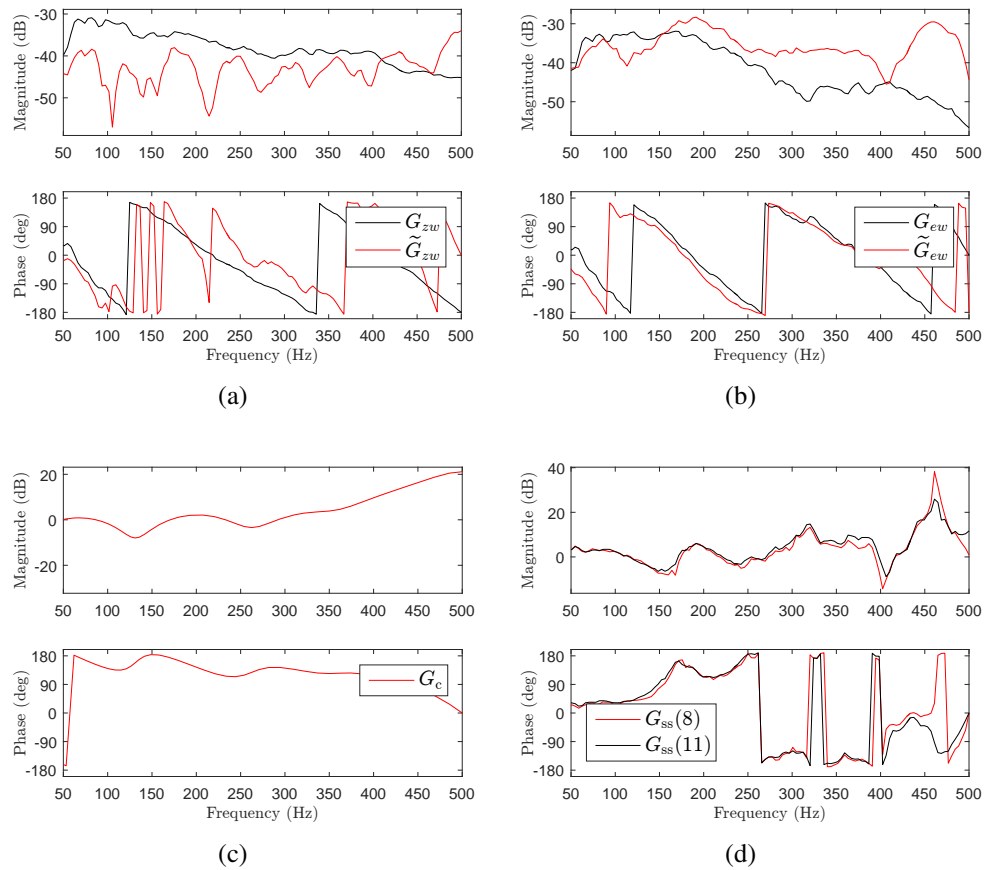
Figure 2.8: Example 2.5: Comparison of G_{ss} for feedforward control with scalar control u. (a) and (b) show the controlled and uncontrolled frequency response at z and e; (c) shows the frequency response of the controller. (d) compares G_{ss} estimated using (2.8) and (2.11).
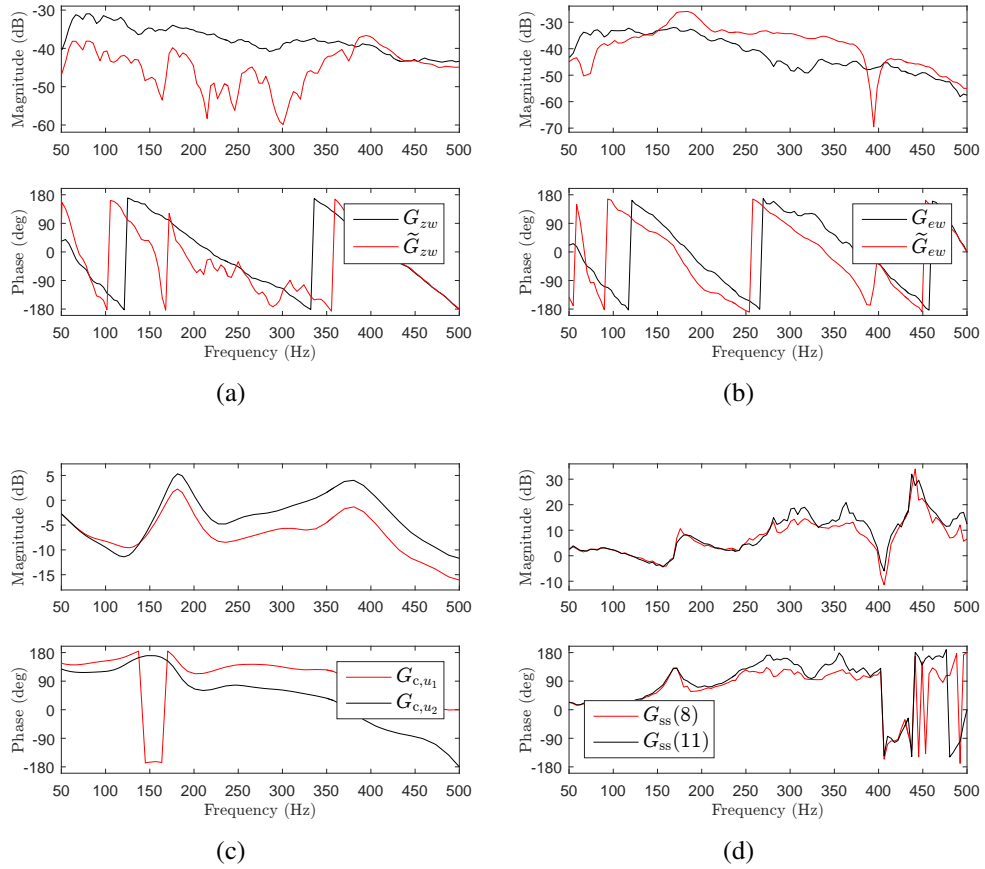
Figure 2.9: Example 2.6: Comparison of G_{ss} for feedforward control with vector control $u \in \mathbb{R}^2$. (a) and (b) show the controlled and uncontrolled frequency response at z and e; (c) shows the frequency response of both channels the controller. (d) compares G_{ss} estimated using (2.8) and (2.11).
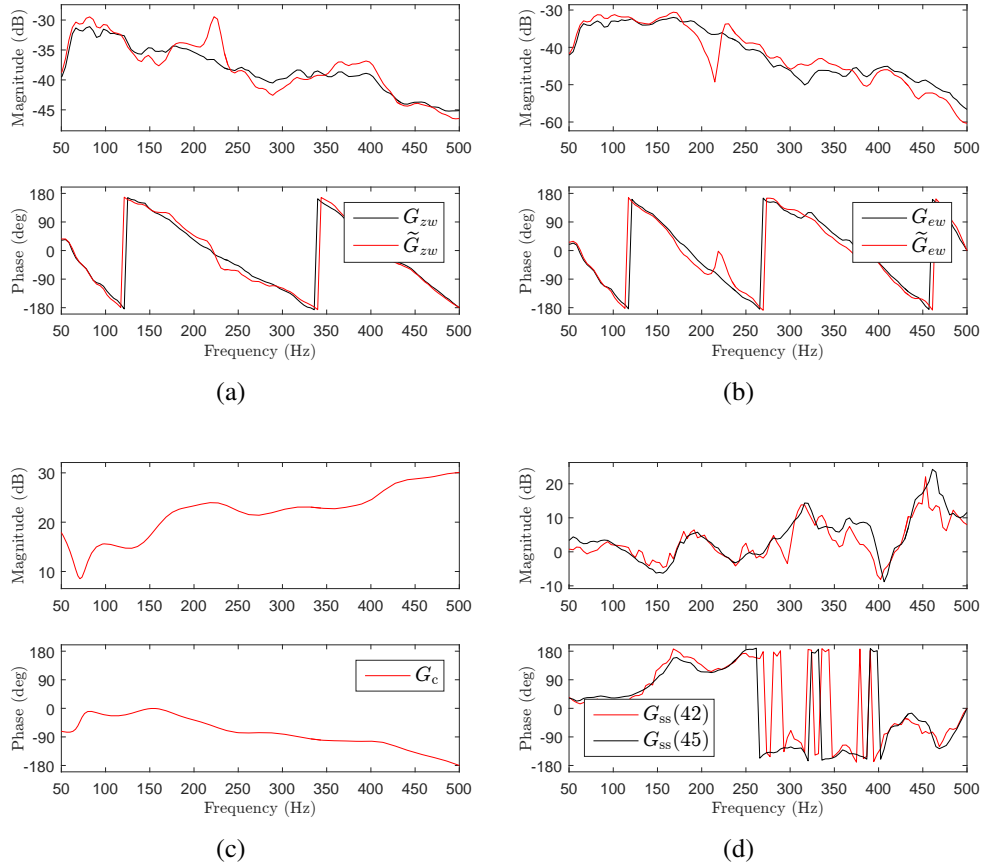
Figure 2.10: Example 2.7: Comparison of G_{ss} for feedback control with scalar control u. (a) and (b) show the controlled and uncontrolled frequency response at z and e; (c) shows the frequency response of the controller. (d) compares G_{ss} estimated using (2.42) and (2.45).
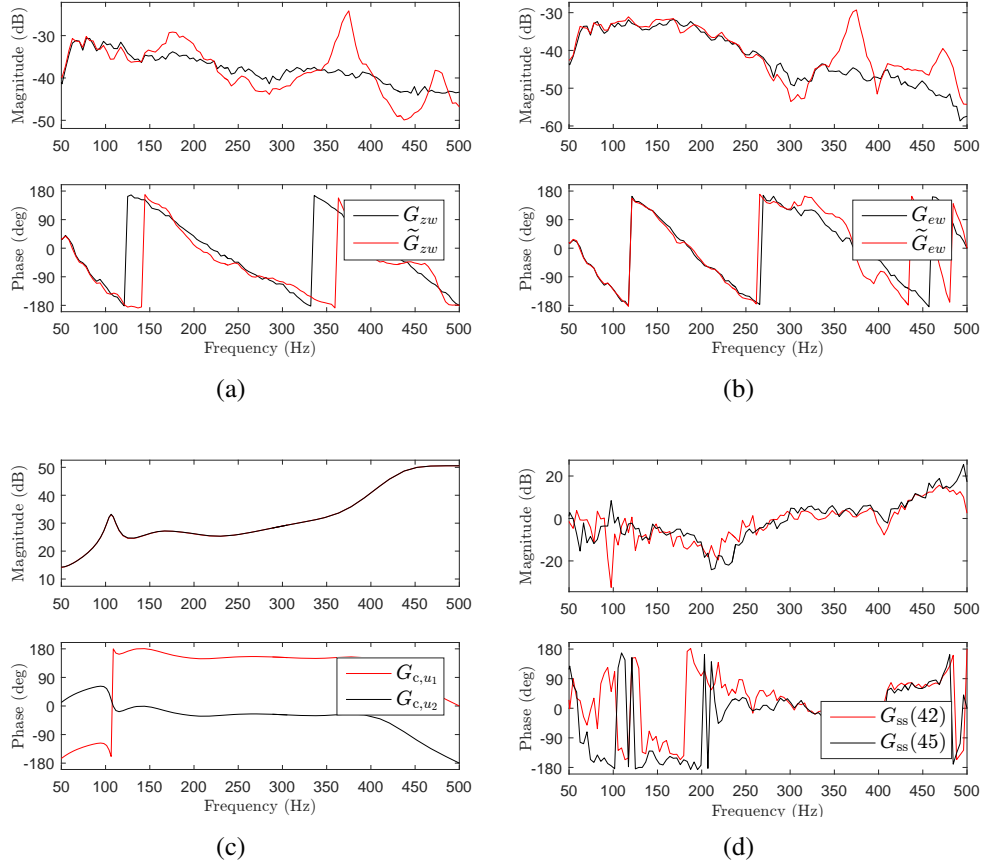
Figure 2.11: Example 2.8: Comparison of G_{ss} for feedback control with vector control $u \in \mathbb{R}^2$. (a) and (b) show the controlled and uncontrolled frequency response at z and e; (c) shows the frequency response of both channels the controller. (d) compares G_{ss} estimated using (2.42) and (2.45).
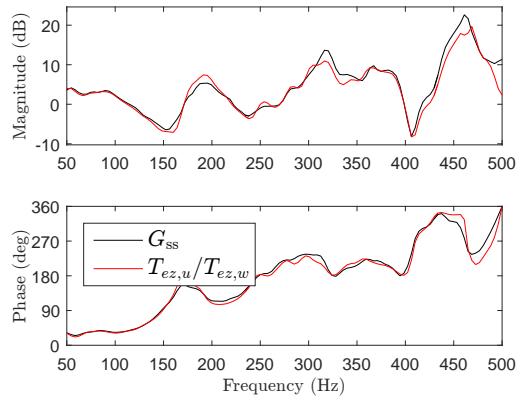
Figure 2.12: Example 2.9: Comparison of G_{ss} for scalar control u, estimated as (2.12), shown in black, and (2.61), shown in red.
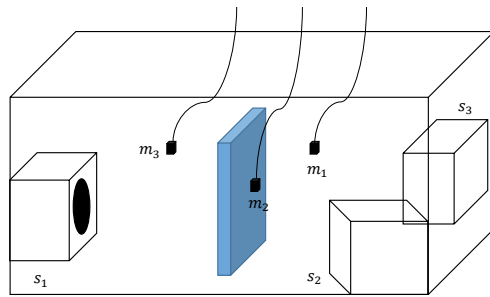
(a)
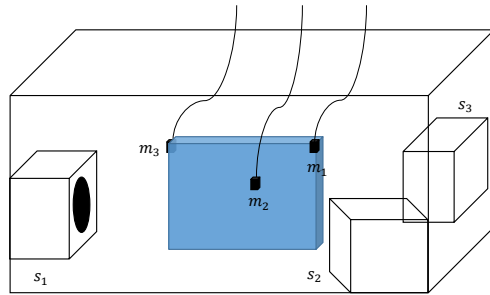
(b)

Figure 2.13: Diagram of two different obstructions tested in acoustic space for the experimental evaluation of the spatial spillover function. (a) shows a height-wise obstruction, and (b) shows a length-wise obstruction
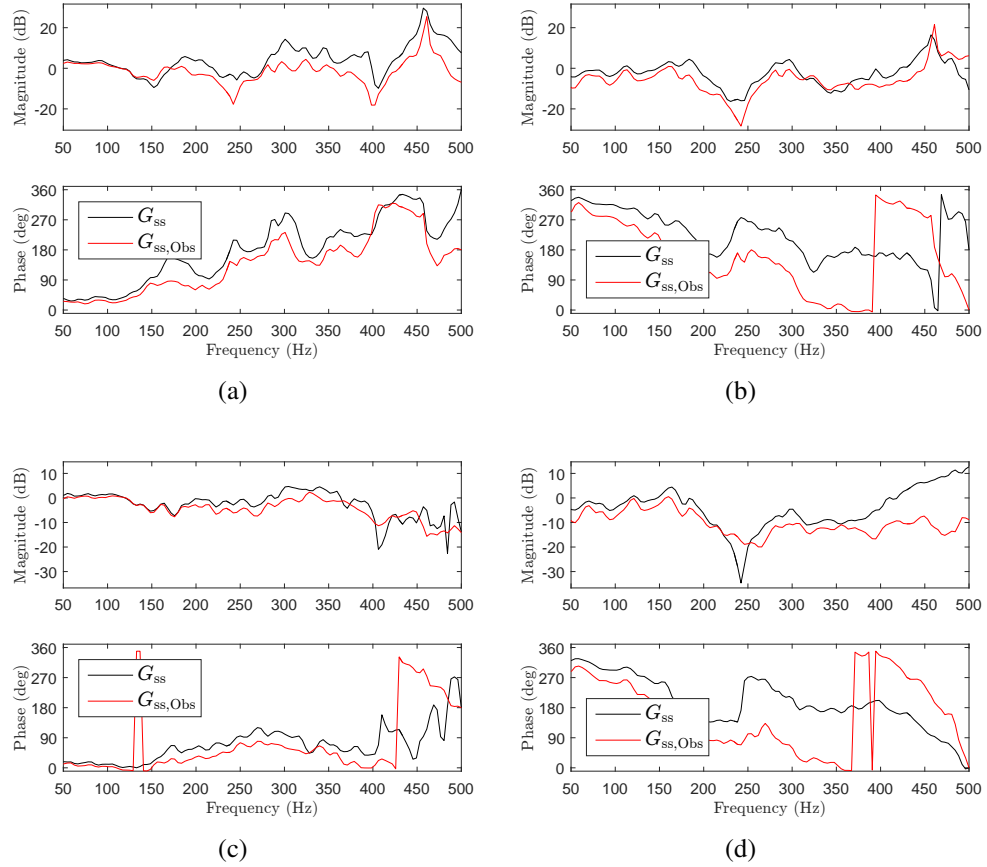
Figure 2.14: Example 2.10: Comparison of G_{ss} with and without a height-wise obstruction in the acoustic space. (a) shows G_{ss} for z and e_1 with s_3 as u, and (b) shows G_{ss} for z and e_2 with s_3 as u. Note that in (a), the magnitude and phase of G_{ss} noticeably shifts due to the obstruction. In (b), the magnitude of G_{ss} slightly shifts due to the obstruction while the phase of G_{ss} significantly shifts due to the obstruction. (c) shows G_{ss} for z and e_1 with s_1 as u, and (d) shows G_{ss} for z and e_2 with s_1 as u. Note that in (c), the magnitude and phase of G_{ss} slightly shifts due to the obstruction. In (d), the magnitude and phase of G_{ss} significantly shifts due to the obstruction.
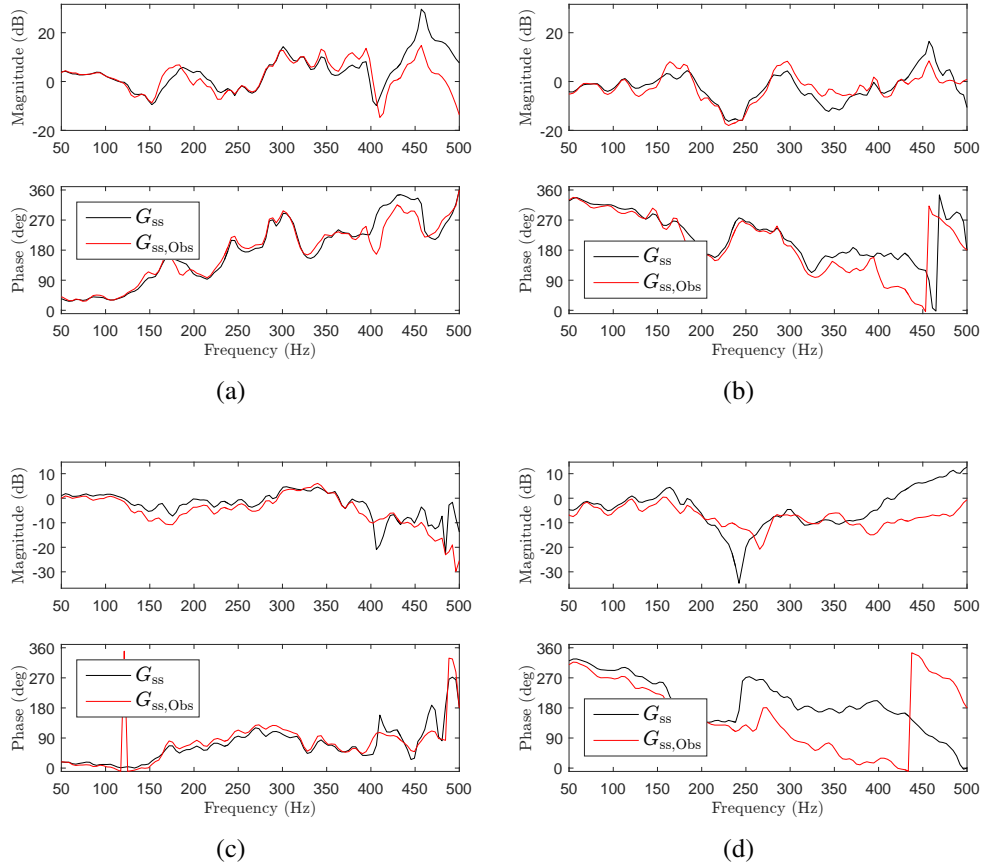
Figure 2.15: Example 2.11: Comparison of G_{ss} with and without a length-wise obstruction in the acoustic space. (a) shows G_{ss} for z and e_1 with s_3 as u, and (b) shows G_{ss} for z and e_2 with s_3 as u. Note that in both (a) and (b), the magnitude and phase of G_{ss} does not shift across the low and mid frequencies, but noticeably shifts at high frequencies due to the obstruction. (c) shows G_{ss} for z and e_1 with s_1 as u, and (d) shows G_{ss} for z and e_2 with s_1 as u. Note that in (c), the magnitude and phase of G_{ss} does not shift due to the obstruction. In (d), the magnitude and phase of G_{ss} significantly shifts due to the obstruction.

CHAPTER 3

Retrospective Cost Adaptive Control

In this chapter, we present the equations of the RCAC algorithm. We first introduce the discrete-time linear time-invariant standard problem. Then we state the equations of RCAC in its variations. Although both fixed-window and cumulative cost functions and gradient and recursive least square (RLS) based optimization versions of RCAC are presented, the examples in this dissertation use only the cumulative-cost RLS-based recursive controller update equations.

3.1   The Standard Problem

Consider the discrete-time, linear time-invariant standard problem with state-space representation

$$x(k+1) = Ax(k) + Bu(k) + D_1 w(k), \tag{3.1}$$

$$y(k) = Cx(k) + D_0 u(k) + D_2 w(k), \tag{3.2}$$

$$z(k) = E_1 x(k) + E_2 u(k) + E_0 w(k), \tag{3.3}$$

where $x(k) \in \mathbb{R}^n$ is the state, $y(k) \in \mathbb{R}^{l_y}$ is the measurement, $u(k) \in \mathbb{R}^{l_u}$ is the control input, $w(k) \in \mathbb{R}^{l_w}$ is the exogenous input, and $z(k) \in \mathbb{R}^{l_z}$ is the measured performance variable. The components of w can represent either a command signal r to be followed, a disturbance d to be rejected, or sensor noise v that corrupts the measurements. The plant

(3.1)-(3.3) may represent a continuous-time, linear time-invariant plant sampled at a fixed rate. Using the time-domain forward shift operator $\mathbf{q}$, (3.1)-(3.3) can be written as

$$z(k) = G_{zw}(\mathbf{q})w(k) + G_{zu}(\mathbf{q})u(k), \tag{3.4}$$

$$y(k) = G_{yw}(\mathbf{q})w(k) + G_{yu}(\mathbf{q})u(k), \tag{3.5}$$

where

$$G_{zw}(\mathbf{q}) \triangleq E_1(\mathbf{q}I - A)^{-1}D_1 + E_0, \quad G_{zu}(\mathbf{q}) \triangleq E_1(\mathbf{q}I - A)^{-1}B + E_2, \tag{3.6}$$

$$G_{yw}(\mathbf{q}) \triangleq C(\mathbf{q}I - A)^{-1}D_1 + D_2, \quad G_{yu}(\mathbf{q}) \triangleq C(\mathbf{q}I - A)^{-1}B + D_0. \tag{3.7}$$

Furthermore, consider the strictly proper discrete-time, linear time-invariant controller with state-space representation

$$x_{\mathrm{c}}(k + 1) = A_{\mathrm{c}}x_{\mathrm{c}}(k) + B_{\mathrm{c}}y(k), \tag{3.8}$$

$$u(k) = C_{\mathrm{c}}x_{\mathrm{c}}(k), \tag{3.9}$$

where $x_{\mathrm{c}}(k) \in \mathbb{R}^{n_{\mathrm{c}}}$ is the controller state. We can rewrite (3.8), (3.9) as

$$u(k) = G_{\mathrm{c}}(\mathbf{q})y(k), \tag{3.10}$$

where

$$G_{\mathrm{c}}(\mathbf{q}) \triangleq C_{\mathrm{c}}(\mathbf{q}I - A_{\mathrm{c}})^{-1}B_{\mathrm{c}} + D_{\mathrm{c}}. \tag{3.11}$$

The transfer function from w to z of the system (3.4), (3.5) with the controller (3.10) is given by

$$z(k) = \widetilde{G}_{zw}(\mathbf{q})w(k), \tag{3.12}$$

where

$$\widetilde{G}_{zw}(\mathbf{q}) \triangleq G_{zu}(\mathbf{q})G_{\mathrm{c}}(\mathbf{q})[I_{l_y} - G_{yu}(\mathbf{q})G_{\mathrm{c}}(\mathbf{q})]^{-1}G_{yw}(\mathbf{q}) + G_{zw}(\mathbf{q}). \tag{3.13}$$

In the case where $y, z, u,$ and w are scalar signals, the transfer functions (3.6), (3.7), and $G_{\mathrm{c}}(\mathbf{q})$ can be written as

$$G_{zw}(\mathbf{q}) = \frac{N_{zw}(\mathbf{q})}{D(\mathbf{q})}, \quad G_{zu}(\mathbf{q}) = \frac{N_{zu}(\mathbf{q})}{D(\mathbf{q})}, \quad G_{yw}(\mathbf{q}) = \frac{N_{yw}(\mathbf{q})}{D(\mathbf{q})}, \quad G_{\mathrm{c}}(\mathbf{q}) = \frac{N_{\mathrm{c}}(\mathbf{q})}{D_{\mathrm{c}}(\mathbf{q})}, \tag{3.14}$$

where it follows from (3.14) that (3.13) can be written as

$$\widetilde{G}_{zw}(\mathbf{q}) = \frac{N_{zw}(\mathbf{q})}{D(\mathbf{q})} + \frac{N_{zu}(\mathbf{q})N_{yw}(\mathbf{q})N_{\mathrm{c}}(\mathbf{q})}{D(\mathbf{q})[D(\mathbf{q})D_{\mathrm{c}}(\mathbf{q}) - N_{yu}(\mathbf{q})N_{\mathrm{c}}(\mathbf{q})]}. \tag{3.15}$$

Figure 3.1 shows a block diagram of the standard problem with the controller (3.10). Note that $\mathbf{q}$ is a time-domain operator that accounts for both the free response and the forced response. Hence, although (3.6), (3.7), and (3.11) are written as transfer functions, these expressions represent time-domain dynamics. For pole-zero analysis, $\mathbf{q}$ can be replaced by the Z-transform complex variable $\mathbf{z}$, in which case (3.4), (3.5), and (3.10) do not account for initial conditions.

42
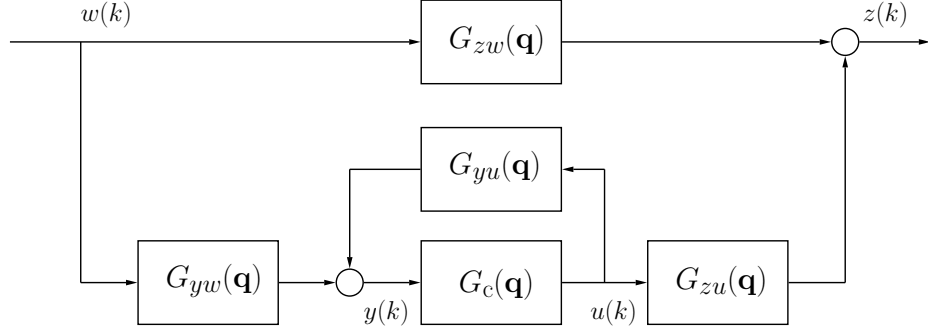
Figure 3.1: Block diagram of the standard problem (3.4), (3.5) with the controller G_c given by (3.10).

3.2 Retrospective Cost Adaptive Control Algorithm

We now review the equations of the RCAC algorithm [16, 18, 20, 22, 30]. For the adaptive standard problem shown in Figure 3.2 with the time-dependent adaptive controller $G_{c,k}$, z can be written as

$$z(k) = \widetilde{G}_{zw,k}(\mathbf{q})w(k), \tag{3.16}$$

where

$$\widetilde{G}_{zw,k}(\mathbf{q}) \triangleq G_{zu}(\mathbf{q})G_{c,k}(\mathbf{q})[I_{l_y} - G_{yu}(\mathbf{q})G_{c,k}(\mathbf{q})]^{-1}G_{yw}(\mathbf{q}) + G_{zw}(\mathbf{q}). \tag{3.17}$$
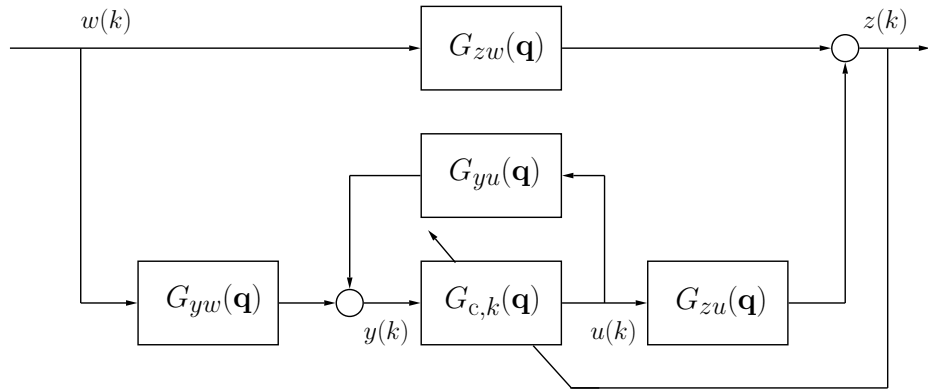
Figure 3.2: Block diagram of the discrete-time adaptive standard problem with controller $G_{c,k}$ in terms of the forward shift operator $\mathbf{q}$.

43

3.2.1 Controller Structure

Consider the linear, time-varying dynamic compensator

$$u(k) = \sum_{i=1}^{n_c} P_i(k)u(k-i) + \sum_{i=k_c}^{n_c} Q_i(k)y(k-i), \qquad (3.18)$$

where $P_i(k) \in \mathbb{R}^{l_u \times l_u}$ and $Q_i(k) \in \mathbb{R}^{l_u \times l_y}$ are time-dependent controller coefficient matrices, n_c is the controller order, and $k_c \geq 0$. For controller startup, we implement (3.18) as

$$u(k) = \begin{cases} 0, & k < k_w, \\ \Phi(k)\theta(k), & k \geq k_w, \end{cases} \qquad (3.19)$$

where the regressor matrix $\Phi(k)$ is defined by

$$\Phi(k) \triangleq \begin{bmatrix} u(k-1) \\ \vdots \\ u(k-n_c) \\ y(k-k_c) \\ \vdots \\ y(k-n_c) \end{bmatrix}^{\mathrm{T}} \otimes I_{l_u} \in \mathbb{R}^{l_u \times l_\theta}, \qquad (3.20)$$

$k_w \geq n_c$ is an initial waiting period during which $\Phi(k)$ is populated with data, and the controller coefficient vector $\theta(k)$ is defined by

$$\theta(k) \triangleq \mathrm{vec}\begin{bmatrix} P_1(k) & \cdots & P_{n_c}(k) & Q_{k_c}(k) & \cdots & Q_{n_c}(k) \end{bmatrix}^{\mathrm{T}} \in \mathbb{R}^{l_\theta}, \qquad (3.21)$$

$l_\theta \triangleq l_u^2 n_c + l_u l_y (n_c + 1 - k_c)$, "$\otimes$" is the Kronecker product, and "vec" is the column-stacking operator. Note that $k_c = 0$ allows an exactly proper controller, whereas $k_c \geq 1$ yields a

strictly proper controller of relative degree k_c. In terms of the forward-shift operator $\mathbf{q}$, the time-domain transfer function of (3.18) from y to u is given by

$$G_{c,k}(\mathbf{q}) = \left(I_{l_u}\mathbf{q}^{n_c} - P_1(k)\mathbf{q}^{n_c-1} - \cdots - P_{n_c}(k)\right)^{-1}\left(Q_{k_c}(k)\mathbf{q}^{n_c-k_c} + \cdots + Q_{n_c}(k)\right),$$
(3.22)

where the coefficients of $G_{c,k}$ are given by the components of θ. If y and u are scalar signals, then (3.22) can be written as

$$G_{c,k}(\mathbf{q}) = \frac{Q_{k_c}(k)\mathbf{q}^{n_c-k_c} + \cdots + Q_{n_c}(k)}{\mathbf{q}^{n_c} - P_1(k)\mathbf{q}^{n_c-1} - \cdots - P_{n_c}(k)}.$$
(3.23)

Note that (3.22) is an infinite-impulse-response (IIR) controller. A finite-impulse-response (FIR) controller structure can be enforced by removing $u(k-1), \ldots, u(k-n_c)$ from (3.18) yielding

$$u(k) = \sum_{i=k_c}^{n_c} Q_i(k)y(k-i),$$
(3.24)

where $\Phi(k)$, $\theta(k)$, and l_θ are redefined as

$$\Phi(k) \triangleq \begin{bmatrix} y(k-k_c) \\ \vdots \\ y(k-n_c) \end{bmatrix}^{\mathrm{T}} \otimes I_{l_u} \in \mathbb{R}^{l_u \times l_\theta}, \quad \theta(k) \triangleq \mathrm{vec}\begin{bmatrix} Q_{k_c}(k) & \cdots & Q_{n_c}(k) \end{bmatrix}^{\mathrm{T}} \in \mathbb{R}^{l_\theta},$$
(3.25)

and $l_\theta \triangleq l_u l_y(n_c + 1 - k_c)$. In this case, (3.22) specializes to

$$G_{c,k}(\mathbf{q}) = \frac{1}{\mathbf{q}^{n_c}}\left(Q_{k_c}(k)\mathbf{q}^{n_c-k_c} + \cdots + Q_{n_c}(k)\right).$$
(3.26)

45

3.2.2 Retrospective Performance Variable

The *retrospective performance variable* is defined by

$$\hat{z}(k, \hat{\theta}) \triangleq z(k) - G_{\mathrm{f}}(\mathbf{q})u(k) - G_{\mathrm{f}}(\mathbf{q})\Phi(k)\hat{\theta}, \tag{3.27}$$

where $\hat{\theta} \in \mathbb{R}^{l_\theta}$ and the $n_z \times n_u$ filter G_{f} has the form

$$G_{\mathrm{f}}(\mathbf{q}) \triangleq D_{\mathrm{f}}(\mathbf{q})^{-1} N_{\mathrm{f}}(\mathbf{q}), \tag{3.28}$$

where D_{f} is an $l_z \times l_z$ polynomial matrix with leading coefficient I_{l_z} and N_{f} is an $l_z \times l_u$ polynomial matrix. The filter G_{f} serves as the *target model* and is detailed in subsequent chapters. By defining the filtered regressor and filtered control $\Phi_{\mathrm{f}}(k) \in \mathbb{R}^{l_z \times l_\theta}$ and $u_{\mathrm{f}}(k) \in \mathbb{R}^{l_z}$ by

$$\Phi_{\mathrm{f}}(k) \triangleq G_{\mathrm{f}}(\mathbf{q})\Phi(k), \quad u_{\mathrm{f}}(k) \triangleq G_{\mathrm{f}}(\mathbf{q})u(k), \tag{3.29}$$

(3.27) can be written as

$$\hat{z}(k, \hat{\theta}) = z(k) - u_{\mathrm{f}}(k) - \Phi_{\mathrm{f}}(k)\hat{\theta}. \tag{3.30}$$

Note that implementation requires $k_w \geq \max(n_{\mathrm{c}}, n_{\mathrm{f}})$, where n_{f} is the McMillan degree of G_{f}.

3.2.3 RCAC Controller Update Law

In [16], the RCAC controller update is based on minimization of a sliding-window cost function using a recursive gradient-based update of the controller parameters. In [18], a modified sliding-window cost function is considered with a sliding-window batch-least-squares update law. More recently, an update law based on a cumulative cost function

using RLS is considered in [20, 22, 30].

3.2.4 Sliding-window Retrospective-Cost-Based Update Laws

In [16] a sliding-window retrospective cost is considered, given by

$$J_{\mathrm{O}}(k, \hat{\theta}) \triangleq \hat{Z}(k, \hat{\theta})^{\mathrm{T}} \hat{Z}(k, \hat{\theta}), \tag{3.31}$$

where

$$\hat{Z}(k, \hat{\theta}) \triangleq \begin{bmatrix} \hat{z}(k, \hat{\theta}) \\ \vdots \\ \hat{z}(k - p - 1, \hat{\theta}) \end{bmatrix} \tag{3.32}$$

and p is the window size. Defining

$$Z(k) \triangleq \begin{bmatrix} z(k) \\ \vdots \\ z(k - p - 1) \end{bmatrix}, \quad U_{\mathrm{f}}(k) \triangleq \begin{bmatrix} u_{\mathrm{f}}(k) \\ \vdots \\ u_{\mathrm{f}}(k - p - 1) \end{bmatrix}, \quad \tilde{\Phi}_{\mathrm{f}}(k) \triangleq \begin{bmatrix} \Phi_{\mathrm{f}}(k) \\ \vdots \\ \Phi_{\mathrm{f}}(k - p - 1) \end{bmatrix},$$

$$\tag{3.33}$$

it follows that (3.32) can be written as

$$\hat{Z}(k, \hat{\theta}) = Z(k) - [U_{\mathrm{f}}(k) - \tilde{\Phi}_{\mathrm{f}}(k)\hat{\theta}]. \tag{3.34}$$

The retrospective cost (3.31) is minimized using the gradient-based recursive controller update law

$$\theta(k + 1) = \theta(k) - \frac{\mu(k)}{2} \frac{\mathrm{d} J_{\mathrm{O}}}{\mathrm{d}\hat{\theta}}(k, \theta(k)), \tag{3.35}$$

where $\mu(k)$ is a time-varying step size. It follows from (3.31) and (3.35) that the recursive

47

controller coefficient update law is given by

$$\theta(k+1) = \theta(k) - \mu(k)\hat{Z}(k, \theta(k))^{\mathrm{T}}\tilde{\Phi}_{\mathrm{f}}(k). \tag{3.36}$$

The choice of $\mu(k)$ is discussed in [16].

In [18], the sliding-window retrospective cost (3.31) is extended to include additional weights for the control input $\Phi(k)\hat{\theta}$ and rate of change of the controller coefficients $\hat{\theta}-\theta(k)$, where

$$J_{\mathrm{W}}(k, \hat{\theta}) \triangleq \hat{Z}(k, \hat{\theta})^{\mathrm{T}}R_Z(k)\hat{Z}(k, \hat{\theta}) + 2\hat{Z}(k, \hat{\theta})^{\mathrm{T}}R_{Zu}(k)(\Phi(k)\hat{\theta})$$
$$+ (\Phi(k)\hat{\theta})^{\mathrm{T}}R_u(k)(\Phi(k)\hat{\theta})^{\mathrm{T}} + (\hat{\theta} - \theta(k))^{\mathrm{T}}R_{\Delta}(k)(\hat{\theta} - \theta(k)), \tag{3.37}$$

where $R_Z(k) \in \mathbb{R}^{pl_z \times pl_z}$, $R_u(k) \in \mathbb{R}^{l_u \times l_u}$, and $R_{Zu}(k) \in \mathbb{R}^{pl_z \times l_u}$ are such that the matrix

$$\begin{bmatrix} R_Z(k) & R_{Zu}(k) \\ R_{Zu}^{\mathrm{T}}(k) & R_u(k) \end{bmatrix} \tag{3.38}$$

is positive semidefinite, and $R_{\Delta}(k) \in \mathbb{R}^{l_\theta \times l_\theta}$ is positive semidefinite. The subsequent sliding-window batch-least-squares recursive update controller update law is obtained by taking $\frac{\mathrm{d}J_{\mathrm{W}}}{\mathrm{d}\hat{\theta}}$, setting the derivative equal to zero, and solving for $\hat{\theta}$.

3.2.5 Cumulative Retrospective-Cost-Based Update Law

In [20, 22, 30], a cumulative retrospective cost function is considered with weighting on the filtered control $\Phi_{\mathrm{f}}(k)\hat{\theta}$ of the form

$$
J_{\mathrm{C}}(k,\hat{\theta}) \triangleq \sum_{i=1}^{k} \lambda^{k-i}[\hat{z}^{\mathrm{T}}(i,\hat{\theta})R_z(i)\hat{z}(i,\hat{\theta}) + (\Phi_{\mathrm{f}}(i)\hat{\theta})^{\mathrm{T}}R_{u_{\mathrm{f}}}(i)\Phi_{\mathrm{f}}(i)\hat{\theta} + (\Phi(i)\hat{\theta})^{\mathrm{T}}R_u(i)\Phi(i)\hat{\theta}]
$$
$$
+ (\hat{\theta} - \theta(k-1))^{\mathrm{T}}R_\Delta(k)(\hat{\theta} - \theta(k-1)) + \lambda^k(\hat{\theta} - \theta(0))^{\mathrm{T}}R_\theta(\hat{\theta} - \theta(0)),
$$

$$(3.39)$$

where $\lambda \in (0,1]$ is the forgetting factor, $R_\theta \in \mathbb{R}^{l_\theta \times l_\theta}$ is positive definite, and, for all $k \geq 1$, $R_\Delta(k)$ is positive semidefinite, $R_z(k) \in \mathbb{R}^{l_z \times l_z}$ is positive definite, and $R_{u_{\mathrm{f}}}(k) \in \mathbb{R}^{l_z \times l_z}$ and $R_{u_{\mathrm{f}}}(k) \in \mathbb{R}^{l_u \times l_u}$ are positive semidefinite. For all $k \geq 0$, define the augmented weights

$$
R_{\mathrm{a}}(k) \triangleq \begin{bmatrix} R_z(k) + R_{u_{\mathrm{f}}}(k) & 0_{l_z \times l_u} \\ 0_{l_u \times l_z} & R_u(k) \end{bmatrix}, \quad R_{\mathrm{a}}'(k) \triangleq \begin{bmatrix} R_z(k) & 0_{l_z \times l_u} \\ 0_{l_u \times l_z} & R_u(k) \end{bmatrix}, \tag{3.40}
$$

$$
\Phi_{\mathrm{a}}(k) \triangleq \begin{bmatrix} \Phi_{\mathrm{f}}(k) \\ \Phi(k) \end{bmatrix}, \quad z_{\mathrm{a}}(k) \triangleq \begin{bmatrix} z(k) - u_{\mathrm{f}}(k) \\ 0_{l_u \times 1} \end{bmatrix}. \tag{3.41}
$$

Proposition: Let $P(0) = R_\theta^{-1}$, let $k \geq 1$, and let $\hat{\theta}^*$ denote the minimizer of (3.39). Then,

$$
\hat{\theta}^* = \theta(k) - P(k)\Phi_{\mathrm{a}}^{\mathrm{T}}(k)\Upsilon^{-1}(k)[\Phi_{\mathrm{a}}(k)\theta(k) + R_{\mathrm{a}}^{-1}(k)R_{\mathrm{a}}'(k)z_{\mathrm{a}}(k)]
$$
$$
+ P(k)R_\Delta(k)[\Phi_{\mathrm{a}}^{\mathrm{T}}(k)\Upsilon(k)^{-1}\Phi_{\mathrm{a}}(k)P(k) - I_{l_\theta}](\theta(k-1) - \theta(k)), \tag{3.42}
$$
$$
P(k+1) = \frac{1}{\lambda}P(k) - \frac{1}{\lambda}P(k)\Phi_{\mathrm{a}}^{\mathrm{T}}(k)\Upsilon^{-1}(k)\Phi_{\mathrm{a}}(k)P(k), \tag{3.43}
$$

where

$$
\Upsilon(k) \triangleq \lambda R_{\mathrm{a}}^{-1}(k) + \Phi_{\mathrm{a}}(k)P(k)\Phi_{\mathrm{a}}^{\mathrm{T}}(k). \tag{3.44}
$$

Defining $\theta(k+1) \stackrel{\triangle}{=} \hat{\theta}^*$, (3.42) yields the recursive controller coefficient update

$$\theta(k+1) = \theta(k) - P(k)\Phi_{\mathrm{a}}^{\mathrm{T}}(k)\Upsilon^{-1}(k)[\Phi_{\mathrm{a}}(k)\theta(k) + R_{\mathrm{a}}^{-1}(k)R_{\mathrm{a}}'(k)z_{\mathrm{a}}(k)]$$
$$+ P(k)R_{\Delta}(k)[\Phi_{\mathrm{a}}^{\mathrm{T}}(k)\Upsilon(k)^{-1}\Phi_{\mathrm{a}}(k)P(k) - I_{l_\theta}](\theta(k-1) - \theta(k)). \quad (3.45)$$

If $R_u = 0_{l_u \times l_u}$, $R_{u_{\mathrm{f}}} = 0_{l_z \times l_z}$, and $R_{\Delta} = 0_{l_\theta \times l_\theta}$, then (3.45) and (3.43) become

$$\theta(k+1) = \theta(k) - P(k)\Phi_{\mathrm{f}}^{\mathrm{T}}(k)\Upsilon^{-1}(k)[\Phi_{\mathrm{f}}(k)\theta(k) + z(k) - u_{\mathrm{f}}(k)], \quad (3.46)$$

$$P(k+1) = \frac{1}{\lambda}P(k) - \frac{1}{\lambda}P(k)\Phi_{\mathrm{f}}^{\mathrm{T}}(k)\Upsilon^{-1}(k)\Phi_{\mathrm{f}}(k)P(k), \quad (3.47)$$

where

$$\Upsilon(k) \stackrel{\triangle}{=} \lambda R_z^{-1}(k) + \Phi_{\mathrm{f}}(k)P(k)\Phi_{\mathrm{f}}^{\mathrm{T}}(k). \quad (3.48)$$

Note that, if $\lambda = 1$, then the covariance $P(k)$ decreases monotonically, and thus the rate of adaptation of RLS decreases. To maintain adaptation in cases where the plant or exogenous signals are changing, the covariance can be reset using suitable logic. Alternatively, choosing the forgetting factor $\lambda < 1$ prevents monotonic decrease of $P(k)$, but can lead to instability in the presence of noise and in the absence of persistency [31, 32].

Consider the covariance update equation (3.43) with the additional positive-semidefinite matrix $Q(k)\mathbb{R}^{l_\theta \times l_\theta}$ on the right-hand side of the form

$$P(k+1) = P(k) - P(k)\Phi_{\mathrm{f}}^{\mathrm{T}}(k+1)\Upsilon^{-1}(k)\Phi_{\mathrm{f}}(k)P(k) + Q(k), \quad (3.49)$$

where $\lambda = 1$ in (3.49). Note that (3.46) and (3.49) are the discrete-time Kalman predictor state-estimate update and error-covariance update equations [33], where the state-estimate is $\theta(k)$, the dynamics matrix is $A = I_{l_\theta}$, the output matrix is $C(k) = \Phi_{\mathrm{f}}(k)$, the prediction

50

error is $\hat{z}(k)$ given by (3.30), and process-noise covariance is $Q(k)$. Consequently, the controller update can be viewed as a state-estimation problem, where observability in (3.49) is determined by the time-varying system $(I_{l_\theta}, \Phi_{\mathrm{f}})$.

CHAPTER 4

Feedback Disturbance Rejection

In this chapter, we present the RCAC performance decomposition and discuss the necessary modeling information required in the target model G_{f} for feedback disturbance rejection.

Then RCAC is applied to the problem of broadband road noise suppression a vehicle using a feedback control architecture. We discuss how to experimentally obtain the necessary modeling information for G_{f}. Next we present a series of examples on the performance of RCAC for various microphone and speaker configurations.

We also examine the relation between suppression of noise at the performance microphone in relation to the suppression of noise at evaluation microphones placed at drivers' ears and attempt to correlate the behavior to the spatial spillover function presented in Chapter 2.

4.1 The Target Model G_{f} and the RCAC Performance Decomposition

The target model G_{f} is a key feature of RCAC. In [18], G_{f} is chosen to capture the relative degree, leading coefficient of the numerator, and NMP zeros of G_{zu}. In [19], G_{f} is viewed as a closed-loop transfer function involving an ideal feedback controller. In [20,22] G_{f} is interpreted as a target model for the closed-loop transfer function $\tilde{G}_{z\tilde{u}}$, known as

the intercalated transfer function defined by (4.3) below. In this section, we extend the work in [20, 22] to formulate the retrospective performance $\hat{z}(k, \theta)$ as a combination of the pseudo-performance and the model-matching error to obtain the RCAC performance decomposition.

Consider the minimizer $\hat{\theta}^*$ of the cumulative retrospective cost function (3.39) at step k, which is applied at step $k + 1$, yielding the recursive update (3.45). Evaluating the retrospective performance (3.27) at the minimizer $\hat{\theta}^* = \theta(k + 1)$ yields

$$\hat{z}(k, \theta(k + 1)) = z(k) - G_{\mathrm{f}}(\mathbf{q})u(k) - [G_{\mathrm{f}}(\mathbf{q})\Phi(k)]\theta(k + 1). \tag{4.1}$$

In (4.1), the notation $[G_{\mathrm{f}}(\mathbf{q})\Phi(k)]\theta(k+1)$ indicates that $G_{\mathrm{f}}(\mathbf{q})$ operates on $\Phi(k)$ but not on $\theta(k + 1)$. This restriction arises from the fact that, in the definition (3.27) of $\hat{z}(k, \hat{\theta})$, $\hat{\theta}$ is a constant that is not affected by $G_{\mathrm{f}}(\mathbf{q})$. Therefore, although the optimal value $\theta(k+1) = \hat{\theta}^*$ of $\hat{\theta}$ depends on k, $\theta(k + 1)$ in (4.1) is constant with respect to the operator $G_{\mathrm{f}}(\mathbf{q})$. For convenience in writing subsequent expressions, (4.1) is written as

$$\hat{z}(k, \theta(k + 1)) = z(k) - G_{\mathrm{f}}(\mathbf{q})[u(k) - \Phi(k)\theta(\overline{k + 1})], \tag{4.2}$$

where $\theta(\overline{k + 1})$ indicates that $\theta(k + 1)$ is constant with respect to $G_{\mathrm{f}}(\mathbf{q})$. By defining the *virtual external control perturbation* [22]

$$\tilde{u}(k, \hat{\theta}) \triangleq u(k) - \Phi(k)\hat{\theta}, \tag{4.3}$$

(4.2) can be written as

$$\hat{z}(k, \theta(k + 1)) = z(k) - G_{\mathrm{f}}(\mathbf{q})\tilde{u}(k, \theta(\overline{k + 1})). \tag{4.4}$$

Replacing $\hat{\theta}$ in (4.3) by $\theta(k+1)$ yields

$$u(k) = \tilde{u}(k, \theta(k+1)) + \Phi(k)\theta(k+1)$$

$$= \tilde{u}(k, \theta(k+1)) + \sum_{i=1}^{n_c} P_i(k+1)u(k-i) + \sum_{i=k_c}^{n_c} Q_i(k+1)y(k-i). \qquad (4.5)$$

It follows from (4.5) that

$$u(k) - \sum_{i=1}^{n_c} P_i(k+1)u(k-i) = \tilde{u}(k, \theta(k+1)) + \sum_{i=k_c}^{n_c} Q_i(k+1)y(k-i), \qquad (4.6)$$

and thus

$$\left(I_{l_u} - \sum_{i=1}^{n_c} P_i(k+1)\frac{1}{\mathbf{q}^i}\right)u(k) = \tilde{u}(k, \theta(k+1)) + \left(\sum_{i=k_c}^{n_c} Q_i(k+1)\frac{1}{\mathbf{q}^i}\right)y(k). \qquad (4.7)$$

Introducing the notation

$$\hat{\theta} \triangleq \mathrm{vec}\left[\hat{P}_1 \cdots \hat{P}_{n_c} \hat{Q}_{k_c} \cdots \hat{Q}_{n_c}\right]^{\mathrm{T}} \in \mathbb{R}^{l_\theta}, \qquad (4.8)$$

$$N_{c,\hat{\theta}}(\mathbf{q}) \triangleq \mathbf{q}^{n_c-k_c}\hat{Q}_{k_c} + \cdots + \hat{Q}_{n_c}, \qquad (4.9)$$

$$D_{c,\hat{\theta}}(\mathbf{q}) \triangleq \mathbf{q}^{n_c}I_{l_u} - \mathbf{q}^{n_c-1}\hat{P}_1 - \cdots - \hat{P}_{n_c}, \qquad (4.10)$$

(4.7) can be written as

$$u(k) = G_{p,\theta(k+1)}(\mathbf{q})\tilde{u}(k, \theta(\overline{k+1})) + G_{c,\theta(k+1)}(\mathbf{q})y(k), \qquad (4.11)$$

where

$$G_{c,\theta(k+1)}(\mathbf{q}) \triangleq D_{c,\theta(k+1)}^{-1}(\mathbf{q})N_{c,\theta(k+1)}(\mathbf{q}), \qquad (4.12)$$

$$G_{p,\theta(k+1)}(\mathbf{q}) \triangleq D_{c,\theta(k+1)}^{-1}(\mathbf{q})\mathbf{q}^{n_c}. \qquad (4.13)$$

54

It follows from (3.4), (3.5), and (4.11) that

$$z(k) = G_{zw}(\mathbf{q})w(k) + G_{zu}(\mathbf{q})G_{\mathrm{p},\theta(\overline{k+1})}(\mathbf{q})\tilde{u}(k, \theta(\overline{k+1})) + G_{zu}(\mathbf{q})G_{\mathrm{c},\theta(\overline{k+1})}(\mathbf{q})y(k),$$

(4.14)

$$y(k) = G_{yw}(\mathbf{q})w(k) + G_{yu}(\mathbf{q})G_{\mathrm{p},\theta(\overline{k+1})}(\mathbf{q})\tilde{u}(k, \theta(\overline{k+1})) + G_{yu}(\mathbf{q})G_{\mathrm{c},\theta(\overline{k+1})}(\mathbf{q})y(k).$$

(4.15)

Solving (4.15) for $y(k)$ and substituting $y(k)$ into (4.14) yields

$$z(k) = \tilde{G}_{zw,\theta(k+1)}(\mathbf{q})w(k) + \tilde{G}_{z\tilde{u},\theta(k+1)}(\mathbf{q})\tilde{u}(k, \theta(\overline{k+1})),$$

(4.16)

where

$$\tilde{G}_{zw,\theta(k+1)}(\mathbf{q}) \triangleq G_{zw}(\mathbf{q}) + G_{zu}(\mathbf{q})G_{\mathrm{c},\theta(\overline{k+1})}(\mathbf{q})(I_{ly} - G_{yu}(\mathbf{q})G_{\mathrm{c},\theta(\overline{k+1})}(\mathbf{q}))^{-1}G_{yw}(\mathbf{q}),$$

(4.17)

$$\tilde{G}_{z\tilde{u},\theta(k+1)}(\mathbf{q}) \triangleq [G_{zu}(\mathbf{q}) + G_{\mathrm{c},\theta(\overline{k+1})}(\mathbf{q})(I_{ly} - G_{yu}(\mathbf{q})G_{\mathrm{c},\theta(\overline{k+1})}(\mathbf{q}))^{-1}]G_{\mathrm{p},\theta(\overline{k+1})}(\mathbf{q}).$$

(4.18)

If y, z, u, and w are scalar signals, then, using the notation (3.14), (4.18) can be written as

$$\tilde{G}_{z\tilde{u},\theta(k+1)}(\mathbf{q}) = \frac{N_{zu}(\mathbf{q})\mathbf{q}^{n_{\mathrm{c}}}}{D(\mathbf{q})D_{\mathrm{c},\theta(k+1)}(\mathbf{q}) - N_{yu}(\mathbf{q})N_{\mathrm{c},\theta(k+1)}(\mathbf{q})}.$$

(4.19)

In [22], the retrospective performance $\hat{z}(k, \theta(k+1))$ given in (4.4) is seen as a residual fit between $z(k)$ and the output of $G_{\mathrm{f}}(\mathbf{q})\tilde{u}(k, \theta(\overline{k+1}))$. However it follows from (4.16) that the actual transfer function from $\tilde{u}(k, \theta(\overline{k+1}))$ to $z(k)$ is $\tilde{G}_{z\tilde{u},\theta(k+1)}(\mathbf{q})$. Hence it was viewed that RCAC chooses the controller coefficient vector $\theta(k+1)$ so as to optimally fit $\tilde{G}_{z\tilde{u},\theta(k+1)}$ to G_{f}. Using this argument, the modeling information required in G_{f} was derived based on $\tilde{G}_{z\tilde{u},\theta(k+1)}$.

In the present work, we present a different interpretation of the retrospective perfor-

mance $\hat{z}(k, \theta(k+1))$. While it is agreed that $G_{\mathrm{f}}(\mathbf{q})$ is a model for $\tilde{G}_{z\tilde{u},\theta(k+1)}$, the interpretation of the meaning of minimizing $\hat{z}(k, \theta(k+1))$ differs, leading to the RCAC performance decomposition.

4.1.1 RCAC Performance Decomposition

It follows that in substituting (4.16) into (4.4), the retrospective performance $\hat{z}(k, \theta(k+1))$ can be written as

$$\hat{z}(k, \theta(k+1)) = \tilde{G}_{zw,\theta(k+1)}(\mathbf{q})w(k) + [\tilde{G}_{z\tilde{u},\theta(k+1)}(\mathbf{q}) - G_{\mathrm{f}}(\mathbf{q})]\tilde{u}(k, \theta(\overline{k+1})). \quad (4.20)$$

Note that $\hat{z}(k, \theta(k+1))$ given by (4.20) consists of two terms. The first term, we define as the *pseudo-performance* $\hat{z}_{\mathrm{pp}}$, where

$$\hat{z}_{\mathrm{pp}}(k, \theta(k+1)) \triangleq \tilde{G}_{zw,\theta(k+1)}(\mathbf{q})w(k). \quad (4.21)$$

The pseudo-performance is the performance of the system assuming that the constant controller coefficient vector $\theta(k+1)$ had been used at step k. The second term, we define as the *model-matching error* $\hat{z}_{\mathrm{mm}}$, where

$$\hat{z}_{\mathrm{mm}}(k, \theta(k+1)) \triangleq [\widetilde{G}_{z\tilde{u},\theta(k+1)}(\mathbf{q}) - G_{\mathrm{f}}(\mathbf{q})]\tilde{u}(k, \theta(\overline{k+1})). \quad (4.22)$$

The model-matching error can be viewed as the residual between between the filter G_{f} and $\widetilde{G}_{z\tilde{u},\theta(k+1)}$ subject to the virtual external control perturbation $\tilde{u}(k, \theta(\overline{k+1}))$. We note the virtual external control perturbation is not an exogenous signal and persistency depends on $\theta(k+1)$. If $\theta(k)$ converges after step k_0, that is, $\theta(k+1) = \theta(k)$ for all $k > k_0$, then $\tilde{u}(k, \theta(k+1))$ is zero for all $k > k_0$. In this case, the model-matching term is zero, and

(4.20) reduces to

$$\hat{z}(k, \theta(k+1)) = \widetilde{G}_{zw,\theta(k+1)}(\mathbf{q})w(k) = \widetilde{G}_{zw}(\mathbf{q})w(k), \tag{4.23}$$

where, after convergence, $\hat{z}(k, \theta(k+1)) = z(k)$. It is not entirely clear that the transient response provides sufficient excitation such that $\widetilde{G}_{z\tilde{u},\theta(k+1)}(\mathbf{q}) - G_{\mathrm{f}}(\mathbf{q})$ is minimized. However it has been shown [22] numerically that under certain conditions, the frequency response of $\widetilde{G}_{z\tilde{u},\theta(k+1)}$ after convergence approximates the frequency response of G_{f}. We also validate this numerically for in Chapter 5 in the case of feedforward disturbance rejection.

The performance decomposition presents a new angle on the retrospective cost, where

$$\hat{z}(k, \theta(k+1)) = \hat{z}_{\mathrm{pp}}(k, \theta(k+1)) + \hat{z}_{\mathrm{mm}}(k, \theta(k+1)). \tag{4.24}$$

The retrospective performance can thus be viewed as the sum of a performance-like term and a model residual.

4.2 Modeling Information Required for G_{f}

In this section, we discuss the modeling information required for G_{f} motivated by the fact that RCAC is, in part, attempting to minimize the residual between G_{f} and $\widetilde{G}_{z\tilde{u},\theta(k+1)}$. For simplicity, we limit the discussion to the case where y, z, u, and w are scalar signals.

4.2.1 Relative degree

Since $\widetilde{G}_{z\tilde{u},\theta(k+1)}$ approximates G_{f}, it is advantageous to choose the relative degree of G_{f} to be equal to the relative degree of $\widetilde{G}_{z\tilde{u},\theta(k+1)}$. It follows from (4.19) that the relative degree of $\widetilde{G}_{z\tilde{u},\theta(k+1)}$ is equal to the relative degree of G_{zu}. We thus choose the relative degree of G_{f} to be equal to the relative degree of G_{zu}.

4.2.2 NMP zeros

In [19], the target model G_f is chosen such the NMP zeros of G_{zu} are modeled in the numerator of G_f. As can be seen from (4.19), a key feature of $\widetilde{G}_{z\tilde{u},\theta(k+1)}$ is the factor N_{zu} in its numerator and $D_{\text{c},\theta(k+1)}(\mathbf{q})$ in its denominator. Since RCAC adapts $G_{\text{c},\theta(k+1)}$ in order to minimize the residual between $\widetilde{G}_{z\tilde{u},\theta(k+1)}$ and G_f, RCAC may cancel NMP zeros in G_{zu} that are not included in the numerator of G_f in order to remove them from $\widetilde{G}_{z\tilde{u},\theta(k+1)}$ which leads to unstable pole-zero cancellation. This observation motivates the desire to capture all NMP zeros of G_{zu} in the numerator of G_f.

4.2.3 FIR Target Model

Let the numerator of G_{zu} be factored as

$$N_{zu}(\mathbf{q}) = H_{\text{d}_{zu}} N_{zu,\text{s}}(\mathbf{q}) N_{zu,\text{u}}(\mathbf{q}), \tag{4.25}$$

where $H_{\text{d}_{zu}}$ is the leading nonzero numerator coefficient of G_{zu}, or first nonzero Markov parameter, and the monic polynomials $N_{zu,\text{s}}$ and $N_{zu,\text{u}}$ represent the minimum-phase zeros and NMP zeros of G_{zu}, respectively. In the case where G_{zu} is minimum phase, we define the FIR target model

$$G_\text{f}(\mathbf{q}) \triangleq \frac{H_{\text{d}_{zu}}}{\mathbf{q}^{\text{d}_{zu}}}, \tag{4.26}$$

where d_{zu} is relative degree of G_{zu}. In the case where G_{zu} is NMP, we define the FIR target model

$$G_\text{f}(\mathbf{q}) \triangleq \frac{H_{\text{d}_{zu}} N_{zu,\text{u}}(\mathbf{q})}{\mathbf{q}^{\text{d}_{zu}+\deg(N_{zu,\text{u}})}}, \tag{4.27}$$

The target models (4.26) for when G_{zu} is minimum phase, and (4.27) for when G_{zu} is NMP, represent the modeling information required by RCAC for feedback control.

4.2.4 High-Authority LQG Target Model

In [21, 22], a target model which recovers the high-authority LQG performance is derived for feedback control in the case when the controller order is equal to the order of the plant, that is, $n_c = n$. We extend the analogies between RCAC and high-authority LQG to the broadband feedforward disturbance rejection problem in Chapter 5.

4.3 RCAC Feedback Active Noise Control Applied to Road Noise Suppression in a Vehicle

We present an experimental study done in collaboration with Ford Motor Company on the applications of RCAC to broadband road noise suppression in a vehicle using feedback control. Current applications of road noise suppression rely on feedforward control architectures which require accelerometer measurements placed on the vehicle suspension to provide an indirect measurement of the disturbance. One of the motivators of this project was to evaluate the effectiveness of an RCAC feedback control architecture in order to potentially eliminate the need for feedforward measurements. Aside from eliminating the cost of the accelerometers themselves, this would also significantly reduce engineering time required in their placement. In this section, we present our results and discuss the potential issues which arose due to spatial spillover.

4.3.1 Spectral Spillover and the Bode Integral Constraint

A fundamental limitation of feedback control that is not present in feedforward control is spectral spillover which is related to the Bode integral constraint [13–15]. Roughly speaking, whenever there is suppression in the closed-loop transfer function $\tilde{G}_{zw}$ relative the open-loop transfer function G_{zw} across a certain band, amplification will occur across other bands.

In implementing feedback active noise control, one of the challenges is to avoid concentration of the amplification to narrow bands, and instead spread the effect across the entire spectrum.

4.3.2 Experimental Setup

Real Time Workshop (RTW) in the MATLAB/Simulink environment with a dSPACE DS1005 Autobox was used to implement RCAC in the vehicle. A DS2004 I/O board and DS2102 I/O board were used for A/D and D/A conversions. Acoustic sensing was provided by omni-directional microphones with rated bandwidth from 50 Hz to 16 kHz. Acoustic actuation was provided by car audio speakers mounted on the vehicle doors. Additional hardware included microphone amplifiers and two low pass analog filters to avoid aliasing. A block diagram of the system components in the control loop is shown in Figure 4.1. All data was sampled at 1 kHz.
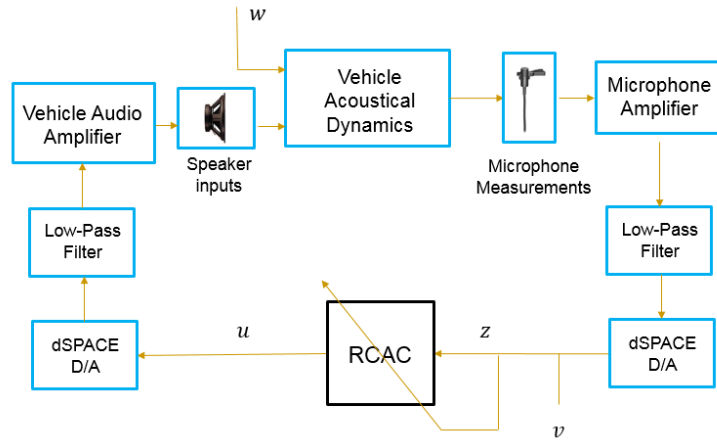
Figure 4.1: Block diagram of hardware components in the control loop.

We consider only SISO feedback control where the controlled plant is from a single speaker to a single microphone. Two evaluation microphones are placed on the driver seat headrest to evaluate qualitative cancellation for a person in the driver seat. We denote the left headrest as LH and the right headrest as RH. We consider five locations, p_1, p_2, p_3, RH,

and LH, to place the z microphone. Four door speakers are available as either the control speaker or to provide the disturbance. We denote these by front driver speaker FDS, front passenger speaker FPS, rear driver speaker RDS, and rear passenger speaker RPS. Figure 4.2 shows the approximate locations of the microphones and speakers in the vehicle.
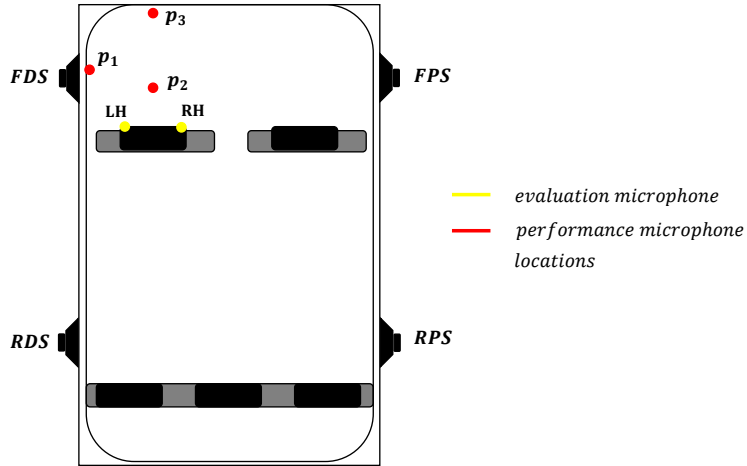
Figure 4.2: Vehicle microphone and speaker placement.

4.3.3 Experimentally Determining the Required Modeling Information

In this section, we discussion experimental constructing the FIR target model for NMP systems (4.27) for the vehicle.

4.3.3.1 Determining d_{zu} and $H_{d_{zu}}$

The relative degree and first nonzero Markov paramter of G_{zu} are obtained from the impulse response. The impulse response from front driver side speaker to p_1 is shown in Figure 4.3. '
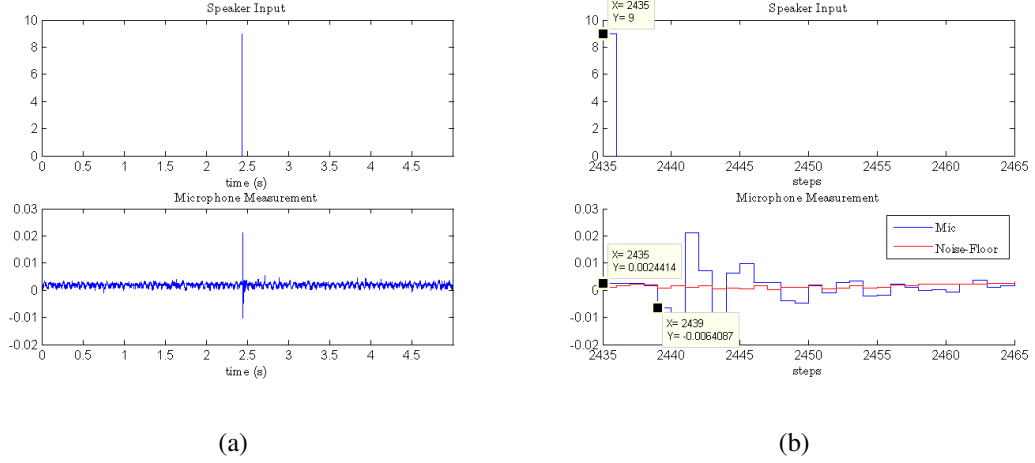
Figure 4.3: The impulse response from FDS to p_1 is shown in (a) and (b). The plots show the speaker input and the microphone response. In (b) we look at the first peak in the microphone response after the impulse is applied to obtain an estimate of d_{zu} and $H_{d_{zu}}$.

4.3.3.2 NMP zeros of G_{zu}

In order to experimentally determine the NMP zeros of G_{zu} in the vehicle, we tried estimating them using a Laurent expansion based on the Markov parameters [16,18]. It was found that this technique was unable to produce accurate estimates for the given amount of sensor noise. Hence, rather than attempting to identify the system using open-loop methods, we used RCAC to retroactively ID the NMP zeros of G_{zu}. The controller poles of RCAC will attempt to cancel any unmodeled NMP zeros of G_{zu}, however this will cause the system to diverge due to unstable pole-zero cancellation. We use this fact by allowing RCAC to perform unstable pole-zero cancellation and let the system to diverge. Afterward we check the controller for unstable poles and place them in G_f. The process is repeated till a stabilizing filter is obtained.

4.3.3.3 Known DC zeros

In acoustic applications, there is no DC response due the propagation of sound as waves. In discrete-time, a system which lacks at DC corresponds to a zero on the unit circle at 1.

These DC zeros are present in the transfer function of every microphone speaker pair. If the DC zero is not modeled in G_f, RCAC will attempt to cancel out the zero in G_{zu} by placing a controller pole at 1 and the controller builds a discrete time integrator. While the closed-loop system in this case can still be asymptotically stable in this case, we noted that, over time, the integrator in the controller was sensitive to electrical bias in the system and tended to cause output of the controller to diverge and hit actuator saturation. As the actuator is unable to respond to the saturation since there is no DC response, the control fails. Hence, in this case model the zeros at DC in G_f to avoid controller poles at DC. We noted two zeros are DC in the system, one due to the speaker, and one due to the microphone. The zeros at DC can also be obtained experimentally using retroactive ID with RCAC. An example of the retroactive ID method using RCAC is shown in Figure 4.4 which identifies the DC zeros and potential NMP zeroes.

(a)   (b)
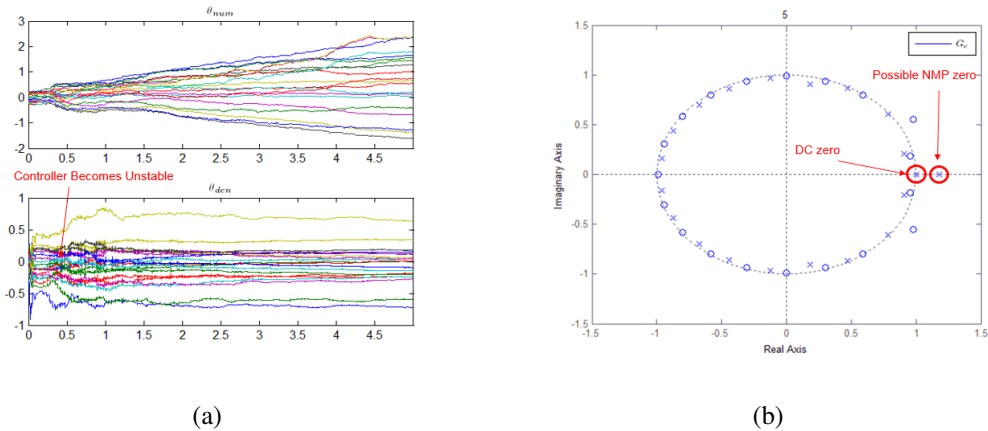
Figure 4.4: Retroactive ID of NMP zeros in G_{zu}. Controller gains are shown in (a), where the top plot shows the numerator gains and the bottom plot shows the denominator gains. The pole-zero map of the controller at $t = 5$ is shown in (b). Although not shown, the system in this example was noted to begin diverging at around $t = 1$. In (b) we note the possible locations of NMP and DC zeros in the system based on the pole-zero map of the controller.

4.3.4 Static Test

In this section, we present a series of static examples in the vehicle for a single speaker to a single performance microphone as the control-loop. Two evaluation microphones are placed on either side of the driver headrest to check the qualitative performance. All frequency domain data is sampled at 1kHz with 1 Hz resolution and is A-weighted [34] to better account for the qualitative perception of noise. The disturbance profile that we considered was measured from the vehicle driving over a Glen Eagle type surface. The profile has two distinct modes that we would like to suppress centered around 140 Hz and 200 Hz. We place the z microphone at p_1, p_2 and p_3 and check the closed-loop performance at the evaluation microphones.

Example 4.1: Closed-loop performance of RCAC with the z microphone placed at p_1, FPS as the control speaker, and RPS as the disturbance speaker. Figure 4.5 shows the closed-loop power spectral density of the performance and evaluation microphones.

Example 4.2: Closed-loop performance of RCAC with the z microphone placed at p_2, FPS as the control speaker, and RPS as the disturbance speaker. Figure 4.6 shows the closed-loop power spectral density of the performance and evaluation microphones.

4.3.5 Static Test with Spatial Spillover

Note that in both Example 4.1 and 4.2, RCAC is able to suppress the peak modes of interest at the performance microphone. However, the suppression at the evaluation microphones varied, and in some cases showed large amplification relative to open-loop noise levels. The notion of spatial spillover presented in Chapter 2 was motivated by this work. In this study, we estimate the spatial spillover function and attempt to correlate the suppression relative to the open-loop between the performance microphone z and the evaluation microphones LH, and RH in terms of the spatial spillover function. An effort was made to qualitatively accesses relative suppression in terms of the magnitude and phase of the spatial spillover function which is outlined in Table 4.1. We admit that the observations
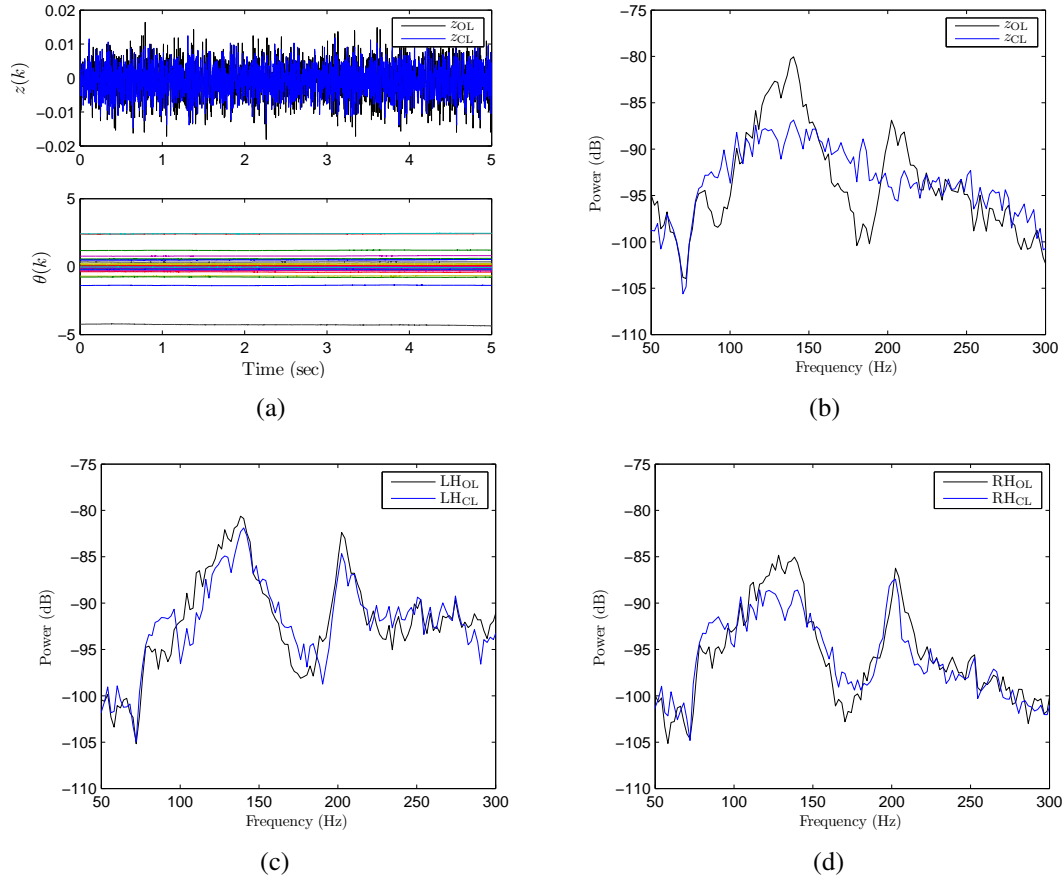
Figure 4.5: Example 4.1: Closed-loop performance of RCAC with the z microphone placed at p_1, FPS as the control speaker, and RPS as the disturbance speaker. At z, the peak in the open-loop response centered at 140 Hz is suppressed from 115 Hz to 155 Hz in closed loop, with 6.8 dB power suppression at the center frequency 140 Hz. The peak in the open-loop response centered at 200 Hz is suppressed from 195 Hz to 220 Hz in closed loop, with 5.1 dB power suppression at the center frequency 200 Hz. At LH, suppression of the open-loop response centered at both peaks is minimal. At RH, the peak in the open-loop response centered at 140 Hz is suppressed from 115 Hz to 145 Hz in closed loop, with 3.9 dB power suppression at the center frequency 140 Hz. Suppression of the peak centered at 200 Hz is minimal.

are mostly qualitative and subjective, and some examples fall slightly outside the predicted trends, however in a large number of cases, the results do agree with the Table 4.1.

Example 4.3: Spatial spillover at the evaluation microphones with the z microphone colocated with LH, FPS as the control speaker, and RPS as the disturbance speaker. Figure 4.7 shows the closed-loop power spectral density of the performance and evaluation microphones, as well as G_{ss} between z and the evaluation microphones.
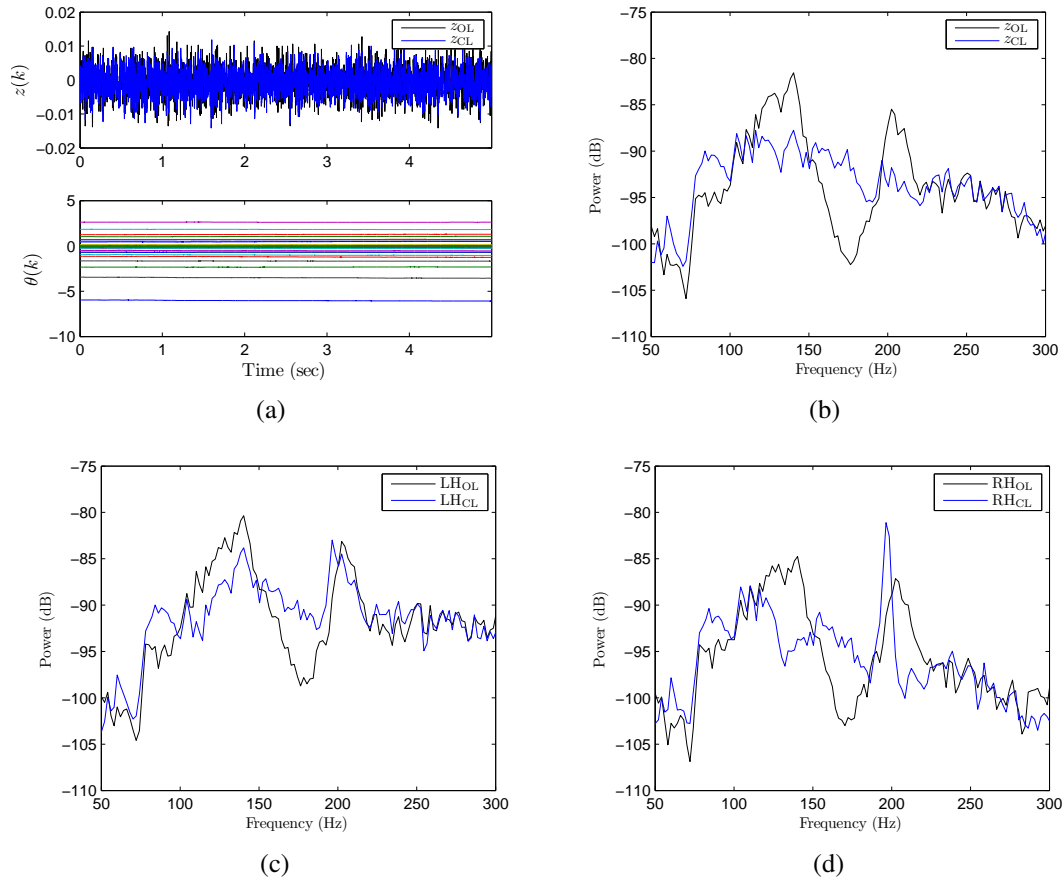
Figure 4.6: Example 4.2: Closed-loop performance of RCAC with the z microphone placed at p_2, FPS as the control speaker, and RPS as the disturbance speaker. At z, the peak in the open-loop response centered at 140 Hz is suppressed from 110 Hz to 150 Hz in closed loop, with 6.2 dB power suppression at the center frequency 140 Hz. The peak in the open-loop response centered at 200 Hz is suppressed from 195 Hz to 220 Hz in closed loop, with 6.3 dB power suppression at the center frequency 200 Hz. Spectral spillover primarily occurs from 150 Hz to 195 Hz. At LH, the peak in the open-loop response centered at 140 Hz is suppressed from 105 Hz to 150 Hz in closed loop, with 3.5 dB power suppression at the center frequency 140 Hz. Suppression of the peak centered at 200 Hz is minimal. At RH, the peak in the open-loop response centered at 140 Hz is suppressed from 115 Hz to 150 Hz in closed loop, with 9.1 dB power suppression at the center frequency 140 Hz. The peak in the open-loop response centered at 200 Hz is suppressed from 200 Hz to 220 Hz in closed loop, with 7.1 dB power suppression at the center frequency 200 Hz. However, there is sharp amplification at 196 Hz.

Example 4.4: Spatial spillover at the evaluation microphones with the z microphone colocated with RH, FPS as the control speaker, and RPS as the disturbance speaker. Figure 4.8 shows the closed-loop power spectral density of the performance and evaluation

Table 4.1: Observations on the performance and spatial spillover of the evaluation microphone relative to the z microphone.

	$\left\lvert\frac{G_{eu}}{G_{zu}}\right\rvert > 2\left\lvert\frac{G_{ew}}{G_{zw}}\right\rvert$	$\left\lvert\frac{G_{eu}}{G_{zu}}\right\rvert \approx \left\lvert\frac{G_{ew}}{G_{zw}}\right\rvert$	$2\left\lvert\frac{G_{eu}}{G_{zu}}\right\rvert < \left\lvert\frac{G_{ew}}{G_{zw}}\right\rvert$
$\lvert\angle G_{\mathrm{ss}}\rvert < 10°$	1. Good suppression	2. Good suppression	3. Fair suppression
$10° < \lvert\angle G_{\mathrm{ss}}\rvert < 30°$	4. Good suppression	5. Fair suppression	6. Limited suppression
$30° < \lvert\angle G_{\mathrm{ss}}\rvert < 60°$	7. Fair suppression	8. Limited suppression	9. Limited suppression
$60° < \lvert\angle G_{\mathrm{ss}}\rvert$	10. Minimal Spillover	11. Some Spillover	12. Large Spillover

microphones, as well as G_{ss} between z and the evaluation microphones.

Example 4.5: Spillover at the evaluation microphones for Example 4.4. Figure 4.9 shows G_{ss} between z and the evaluation microphones for Example

Example 4.6: Spatial spillover at the evaluation microphones with the z microphone placed at p_3, FPS *as the control speaker, and* RPS *as the disturbance speaker.* Figure 4.10 shows the closed-loop power spectral density of the performance and evaluation microphones, as well as G_{ss} between z and the evaluation microphones.
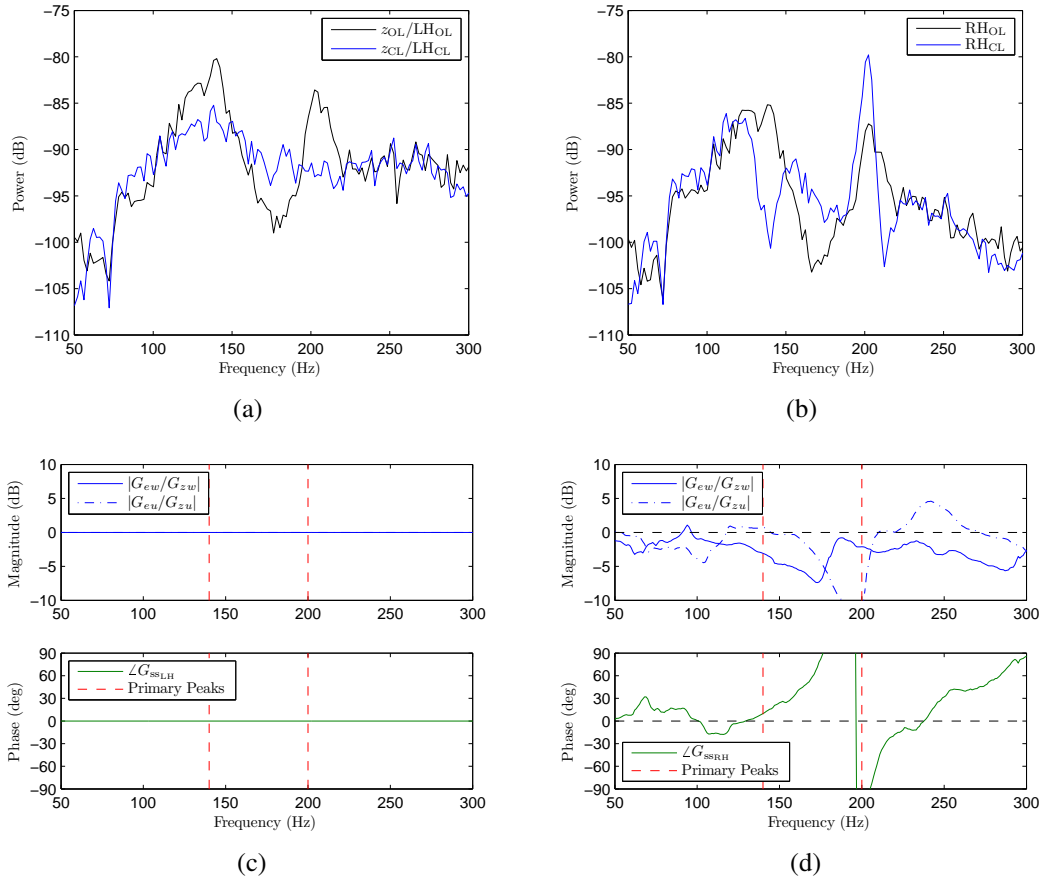
Figure 4.7: Example 4.3: Spatial spillover at the evaluation microphones with the z microphone colocated with LH, FPS as the control speaker, and RPS as the disturbance speaker. At z/LH, both the peak at 140 Hz and 200 Hz are suppressed. At RH, for the peak at 140 Hz, cases 2 and 5 apply, resulting in good suppression in this range as expected. For the peak at 200 Hz, case 12 applies, resulting in sharp amplification in this range as expected.
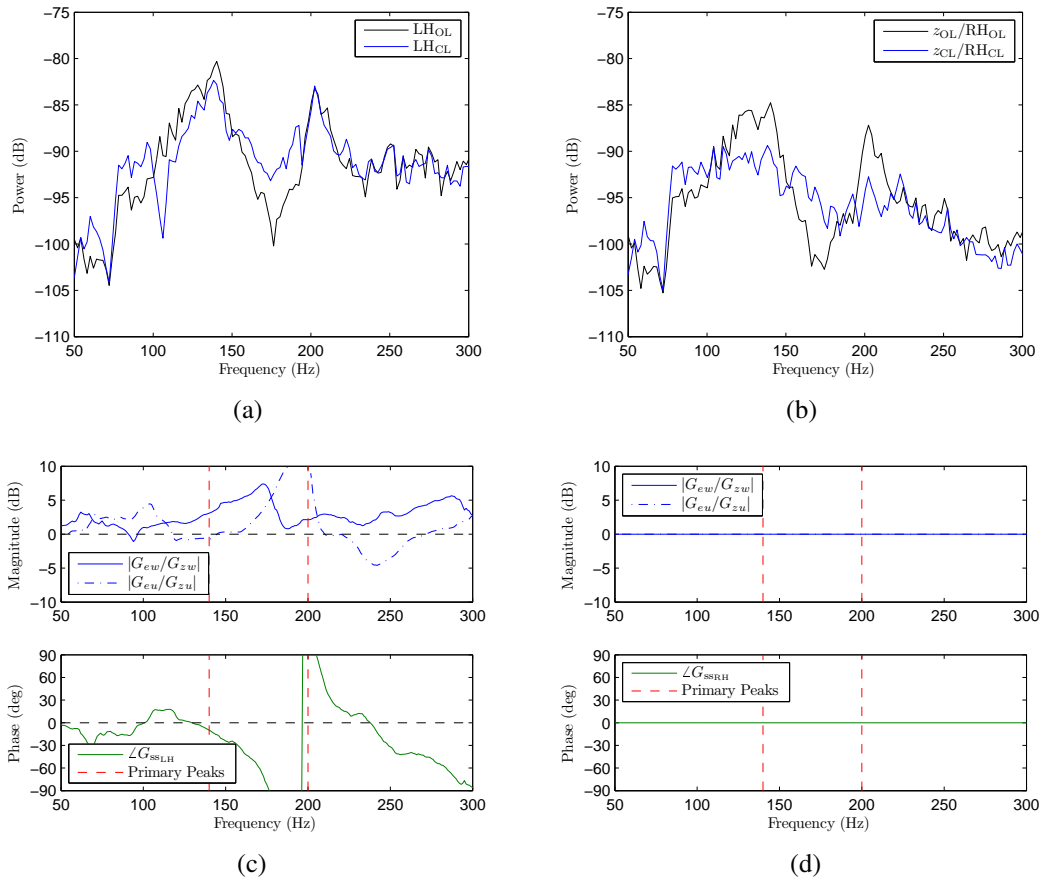
Figure 4.8: Example 4.4: Spatial spillover at the evaluation microphones with the z micro-phone colocated with RH, FPS as the control speaker, and RPS as the disturbance speaker. At the z/RH microphone, both the peak at 140 Hz and 200 Hz are suppressed. At LH, for the peak at 140 Hz case 5 applies, resulting in some suppression as expected. For the peak at 200 Hz, case 10 applies, and resulting in very little to no spatial spillover in this range as expected.
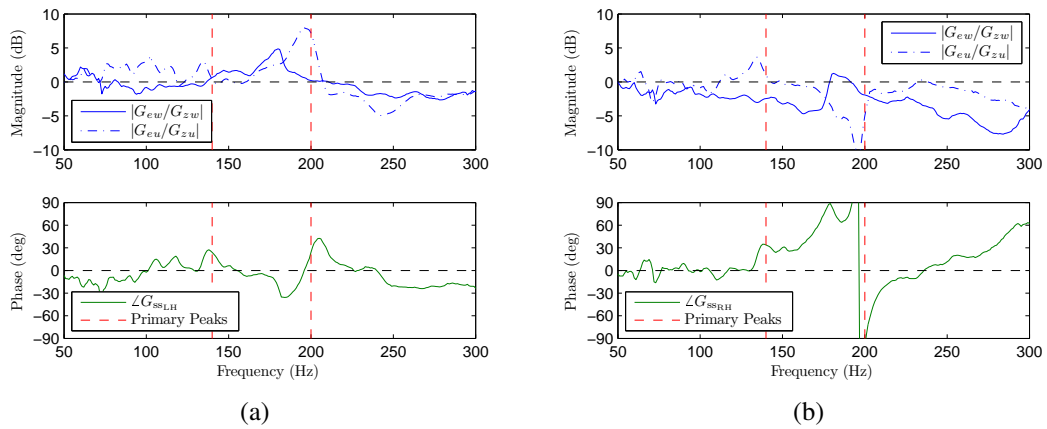
Figure 4.9: Example 4.5: Spatial spillover at the evaluation microphones for Example 2. At LH, for the peak at 140 Hz, cases 2 and 5 apply, resulting in suppression in this range in Example 2 as expected. For the peak at 200 Hz, case 7 applies and we expect to see fair suppression in this range, however, the actual suppression in Example 2 is limited. At RH, for the peak at 140 Hz, cases 2 and 5 apply resulting in suppression in this range as expected. For the peak at 200 Hz, case 12 applies, resulting in sharp amplification as expected.
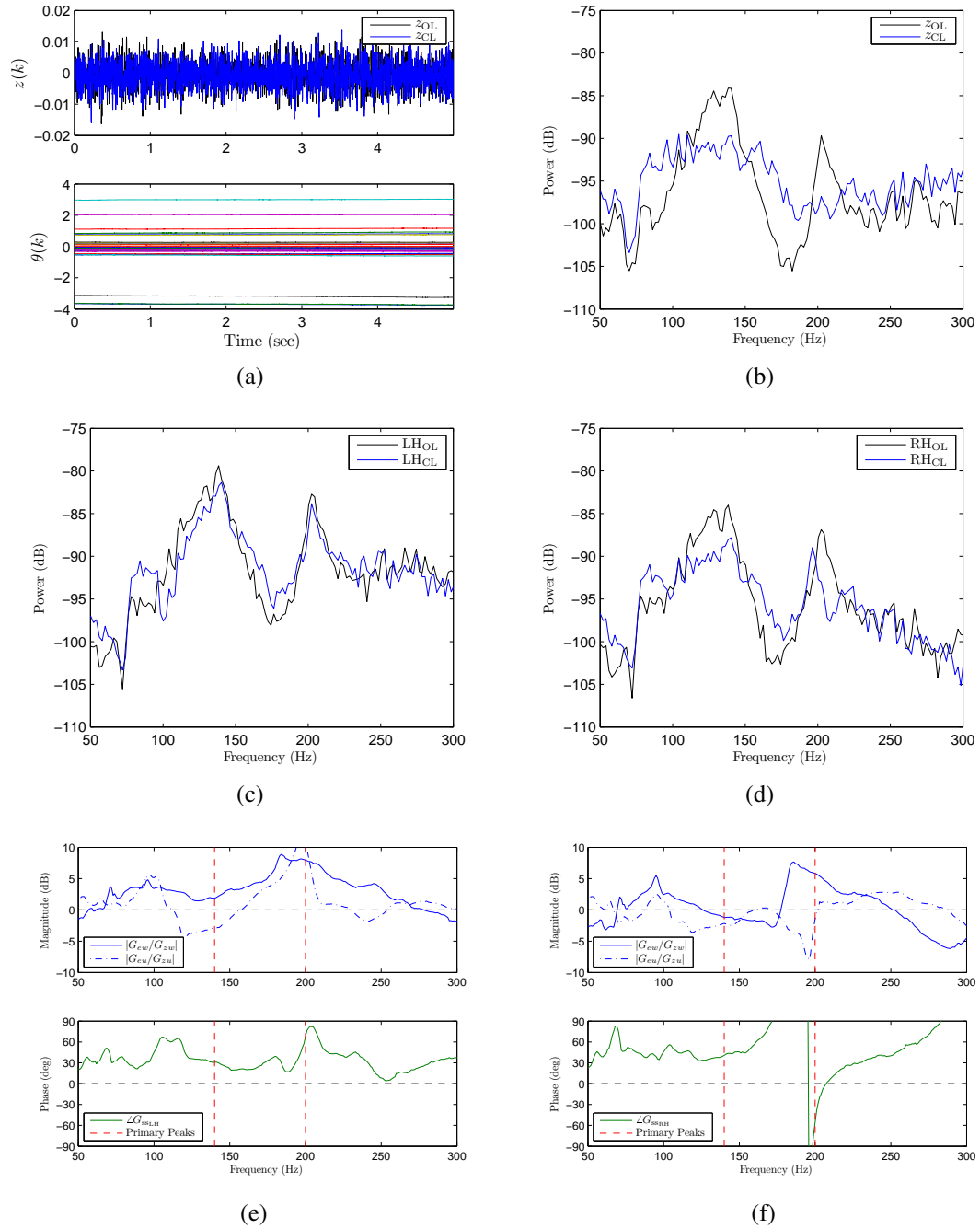
Figure 4.10: Example 4.6: Spatial spillover at the evaluation microphones with the z microphone placed at p_3, FPS as the control speaker, and RPS as the disturbance speaker. At z, both the peak at 140 Hz and 200 Hz are suppressed. At LH, for the peak at 140 Hz, cases 6 and 9 apply, resulting in limited suppression as expected. For the peak at 200 Hz, cases 8 and 11 apply. We expect to see limited suppression with some spatial spillover, but none was observed. At RH, for the peak at 140 Hz, case 8 applies, and we expect to see limited suppression, but the actual suppression is fair. For the peak at 200 Hz, cases 11 and 12 apply, and we expect to see large spillover, but limited spillover is observed.

4.4 Conclusions

In this chapter, we derive the performance decomposition for the retrospective performance $\hat{z}(k, \theta(k+1))$, where we show that RCAC seeks to minimize the sum of a pseudo-performance term and a model-matching error term. An experimental study on the application of feedback active noise control for suppression of broadband road noise is presented. For all locations of the performance microphone, RCAC suppressed the noise at the primary disturbance peaks, however additional evaluation microphones placed at the ear locations of the driver showed that suppression at the performance microphone does not always lead to suppression at the driver ear locations and can sometimes lead to amplification. We analyze this behavior between the performance microphone and the evaluation microphone in the context of spatial spillover and show that it is possible to predict qualitative trends based on the magnitude and phase of the spatial spillover function.

CHAPTER 5

Feedforward Disturbance Rejection

In this section, we apply RCAC to the feedforward disturbance rejection problem. Although the equations for the feedforward control problem were discussed in Chapter 2, no distinction is made between continous time and discrete time.

We first present a more rigorous set of equations for the discrete-time feedforward disturbance rejection problem. The concept of an ideal feedforward controller and conditions in which the ideal feedfoward controller can be implemented is then discussed. Next, we present the equations of discrete-time LQG for feedforward disturbance rejection, and consider the solution to the high-authority LQG problem as an alternative in cases when the ideal controller is cannot be implemented.

The necessary modeling information required in the target model G_f for feedforward disturbance rejection is discussed, followed by the definition of a choice of G_f that can recover the high-authority LQG performance in the case of $n_\mathrm{c} = n$. Numerical examples demonstrating the relation between RCAC and high-authority LQG are then presented.

Next, we show the relation between RCAC and the variations of the FxLMS algorithm, followed by a numerical study comparing performance and convergence between RCAC and Filtered-u RLS.

Finally, we leverage the acoustic experiment used for the spatial spillover experimental study in Chapter 2 to test RCAC feedforward control.

5.1 Feedforward Control Problems

5.1.1 Feedforward Disturbance Rejection

Consider the discrete-time *feedforward disturbance rejection problem*, a specialization of the standard problem where we make the assumption that that the measurement y is unaffected by the control u, or equivalently $G_{yu}(\mathbf{q}) = 0$. Hence,

$$y(k) = G_{yw}(\mathbf{q})w(k). \tag{5.1}$$

It follows from (3.4), (3.10), and (5.1) that

$$\widetilde{G}_{zw}(\mathbf{q}) = G_{zu}(\mathbf{q})G_{\mathrm{c}}(\mathbf{q})G_{yw}(\mathbf{q}) + G_{zw}(\mathbf{q}). \tag{5.2}$$

Note that, unlike feedback control, the controller G_{c} in (2.6) cannot stabilize $\widetilde{G}_{zw}$, and thus, if either G_{zu}, G_{yw}, or G_{zw} is not asymptotically stable, then (2.6) is not asymptotically stable. We therefore assume for this problem that G_{zu}, G_{yw}, and G_{zw} are asymptotically stable. Furthermore, if G_{c} is unstable, then $\widetilde{G}_{zw}$ is unstable, and thus all controllers implemented for the feedforward disturbance rejection problem must be asymptotically stable. Figure 5.1 shows a block diagram of the feedforward disturbance rejection problem as a special case of Figure 3.1. In the case where $y, z, u,$ and w are scalar signals, (2.6) can be
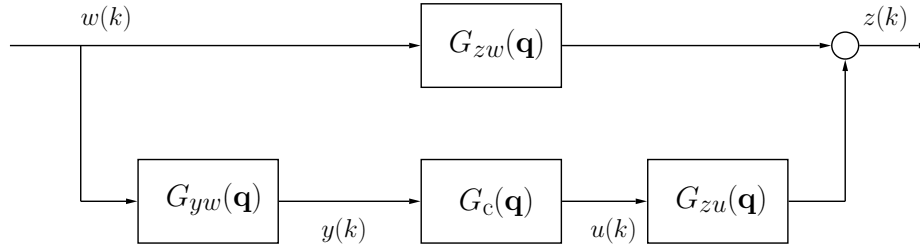
Figure 5.1: Block diagram of the discrete-time feedforward disturbance rejection problem with controller G_{c}.

written as

$$G_{zw}(\mathbf{q}) = \frac{N_{zu}(\mathbf{q})N_{\mathrm{c}}(\mathbf{q})N_{yw}(\mathbf{q}) + N_{yw}(\mathbf{q})}{D(\mathbf{q})D_{\mathrm{c}}(\mathbf{q})}. \tag{5.3}$$

5.1.2 Direct Feedforward Disturbance Rejection

We denote the *direct feedforward disturbance rejection problem* as a specialization of the feedforward disturbance rejection problem with $G_{yw}(\mathbf{q}) = I_{l_w}$. In this case, we assume that the disturbance is measured directly and without delay. Hence,

$$y(k) = w(k). \tag{5.4}$$

It follows from (3.4), (3.10), and (5.4) that

$$\widetilde{G}_{zw}(\mathbf{q}) = G_{zu}(\mathbf{q})G_{\mathrm{c}}(\mathbf{q}) + G_{zw}(\mathbf{q}). \tag{5.5}$$

Since it is difficult in practice to measure the disturbance exactly and without delay, this problem can be viewed as an idealization. This idealization provides the framework in [5] for the FxLMS feedforward control problem.

5.2 Ideal Controller for Feedforward Disturbance Rejection

In this section, we review the equations of the ideal controller for the feedforward disturbance rejection problem [2, 5]. For simplicity we assume that y, z, u, and w are scalar signals.

Denote the *ideal feedforward controller* $\hat{G}_{\mathrm{c}}$ as the controller that exactly suppresses the disturbance for all time, that is, $z(k) = 0$ for all k. Equivalently, the ideal controller

satisfies $\widetilde{G}_{zw}(\mathbf{q}) = 0$. By setting $\widetilde{G}_{zw}(\mathbf{q}) = 0$, it follows from (2.6) that

$$\hat{G}_{\mathrm{c}}(\mathbf{q}) \triangleq -\frac{G_{zw}(\mathbf{q})}{G_{zu}(\mathbf{q})G_{yw}(\mathbf{q})}. \tag{5.6}$$

Using the notation (3.14), (5.6) can be written as

$$\hat{G}_{\mathrm{c}}(\mathbf{q}) = \frac{\hat{N}_{\mathrm{c}}(\mathbf{q})}{\hat{D}_{\mathrm{c}}(\mathbf{q})} = -\frac{N_{zw}(\mathbf{q})D(\mathbf{q})}{N_{zu}(\mathbf{q})N_{yw}(\mathbf{q})}. \tag{5.7}$$

Note that $\hat{G}_{\mathrm{c}}$ is a ratio involving the numerators and denominators of G_{zu}, G_{zw}, and G_{yw}, and thus may be strictly proper, exactly proper, or improper. In particular, $\hat{G}_{\mathrm{c}}$ is strictly proper if and only if $\mathrm{d}_{zu} + \mathrm{d}_{yw} < \mathrm{d}_{zw}$, where d_{zu}, d_{yw}, and d_{zw} denote the relative degrees of G_{zu}, G_{yw} and G_{zw}, respectively. Because of communication and computational delays, exactly proper controllers are difficult to implement in practice and thus are not considered in this dissertation. In addition, $\hat{G}_{\mathrm{c}}$ may be unstable depending on the zeros of G_{zu} and G_{yw}; in particular, $\hat{G}_{\mathrm{c}}$ is asymptotically stable if and only if G_{zu} and G_{yw} are both minimum phase.

The ideal controller $\hat{G}_{\mathrm{c}}$ is *implementable* if it is both strictly proper and asymptotically stable. In the case of direct feedforward disturbance rejection, it follows from (5.5) that

$$\hat{G}_{\mathrm{c}}(\mathbf{q}) = -\frac{G_{zw}(\mathbf{q})}{G_{zu}(\mathbf{q})} = -\frac{\dfrac{N_{zw}(\mathbf{q})}{D(\mathbf{q})}}{\dfrac{N_{zu}(\mathbf{q})}{D(\mathbf{q})}} = -\frac{N_{zw}(\mathbf{q})}{N_{zu}(\mathbf{q})}. \tag{5.8}$$

The ideal direct feedforward controller (5.8) is implementable if and only if $\mathrm{d}_{zu} < \mathrm{d}_{zw}$ and G_{zu} is minimum phase.

5.3 Discrete-Time LQG Control for Broadband Feedforward Disturbance Rejection

We now review the equations of the discrete-time LQG controller for the standard problem [35, p. 878], where w is zero-mean Gaussian white noise; the analogous continuous-time case is considered in [36, 37]. The LQG feedforward controller provides a baseline for assessing the asymptotic performance of RCAC considered in later sections.

Consider the nth-order strictly proper dynamic compensator (3.8), (3.9) applied to the standard problem (3.1)–(3.3). The dynamics of the controlled system can be written as

$$\widetilde{x}(k+1) = \widetilde{A}\widetilde{x}(k) + \widetilde{D}w(k), \tag{5.9}$$

$$z(k) = \widetilde{E}\widetilde{x}, \tag{5.10}$$

where

$$\widetilde{x}(k) \triangleq \begin{bmatrix} x(k) \\ x_{\mathrm{c}}(k) \end{bmatrix}, \quad \widetilde{A} \triangleq \begin{bmatrix} A & BC_{\mathrm{c}} \\ B_{\mathrm{c}}C & A_{\mathrm{c}} + B_{\mathrm{c}}D_0 C_{\mathrm{c}} \end{bmatrix}, \tag{5.11}$$

$$\widetilde{D} \triangleq \begin{bmatrix} D_1 \\ B_{\mathrm{c}}D_2 \end{bmatrix}, \quad \widetilde{E} \triangleq \begin{bmatrix} E_1 & E_2 C_{\mathrm{c}} \end{bmatrix}. \tag{5.12}$$

Define

$$R_1 \triangleq E_1^{\mathrm{T}} E_1 \in \mathbb{R}^{n \times n}, \qquad R_{12} \triangleq E_1^{\mathrm{T}} E_2 \in \mathbb{R}^{n \times l_u}, \qquad R_2 \triangleq E_2^{\mathrm{T}} E_2 \in \mathbb{R}^{l_u \times l_u}, \tag{5.13}$$

$$V_1 \triangleq D_1 D_1^{\mathrm{T}} \in \mathbb{R}^{n \times n}, \qquad V_{12} \triangleq D_1 D_2^{\mathrm{T}} \in \mathbb{R}^{n \times l_y}, \qquad V_2 \triangleq D_2 D_2^{\mathrm{T}} \in \mathbb{R}^{l_y \times l_y}, \tag{5.14}$$

$$\hat{A}_{\mathrm{R}} \triangleq A - BR_2^{-1}R_{12}^{\mathrm{T}}, \quad \hat{R}_1 \triangleq R_1 - R_{12}R_2^{-1}R_{12}^{\mathrm{T}}, \tag{5.15}$$

$$\hat{A}_{\mathrm{E}} \triangleq A - V_{12}V_2^{-1}C, \quad \hat{V}_1 \triangleq V_1 - V_{12}V_2^{-1}V_{12}^{\mathrm{T}}, \tag{5.16}$$

and assume that the following conditions are satisfied:

i) (A, B) is stabilizable.

ii) $(\hat{A}_{\mathrm{R}}, \hat{R}_1)$ has no unobservable eigenvalues on the unit circle.

iii) (A, C) is detectable.

iv) $(\hat{A}_{\mathrm{E}}, \hat{V}_1)$ has no uncontrollable eigenvalues on the unit circle.

Then the strictly proper controller

$$A_{\mathrm{c}} = A + BC_{\mathrm{c}} - B_{\mathrm{c}}C - B_{\mathrm{c}}D_0 C_{\mathrm{c}}, \tag{5.17}$$

$$B_{\mathrm{c}} = (AQC^{\mathrm{T}} + V_{12})(V_2 + CQC^{\mathrm{T}})^{-1}, \tag{5.18}$$

$$C_{\mathrm{c}} = -(R_2 + B^{\mathrm{T}}PB)^{-1}(R_{12}^{\mathrm{T}} + B^{\mathrm{T}}PA) \tag{5.19}$$

asymptotically stabilizes the system (5.9), (5.10) and minimizes the LQG cost function

$$J(A_{\mathrm{c}}, B_{\mathrm{c}}, C_{\mathrm{c}}) \triangleq \lim_{k \to \infty} \mathbb{E}\left[\frac{1}{k}\sum_{i=0}^{k} z^{\mathrm{T}}(i)z(i)\right] = \lim_{k \to \infty} \mathbb{E}[z^{\mathrm{T}}(k)z(k)]. \tag{5.20}$$

The matrices $P \in \mathbb{R}^{n \times n}$ and $Q \in \mathbb{R}^{n \times n}$ in (5.17)–(5.19) are the unique positive-semidefinite solutions of the discrete-time algebraic Riccati equations

$$P = \hat{A}_{\mathrm{R}}^{\mathrm{T}}P\hat{A}_{\mathrm{R}} - \hat{A}_{\mathrm{R}}^{\mathrm{T}}PB(R_2 + B^{\mathrm{T}}PB)^{-1}B^{\mathrm{T}}P\hat{A}_{\mathrm{R}} + \hat{R}_1, \tag{5.21}$$

$$Q = \hat{A}_{\mathrm{E}}Q\hat{A}_{\mathrm{E}}^{\mathrm{T}} - \hat{A}_{\mathrm{E}}QC^{\mathrm{T}}(V_2 + CQC^{\mathrm{T}})^{-1}CQ\hat{A}_{\mathrm{E}}^{\mathrm{T}} + \hat{V}_1. \tag{5.22}$$

With the controller (5.17)–(5.19), the poles of the controlled system (5.9), (5.10) are the eigenvalues of $\widetilde{A}$, which, due to separation, are given by

$$\mathrm{mspec}(\widetilde{A}) = \mathrm{mspec}(A + BC_{\mathrm{c}}) \cup \mathrm{mspec}(A - B_{\mathrm{c}}C), \tag{5.23}$$

where "mspec" denotes the set of eigenvalues including multiplicity.

5.3.1 Specializion of LQG to Feedforward Disturbance Rejection

Assuming $G_{yu}(\mathbf{q}) = 0_{l_y \times l_u}$ as in the feedforward disturbance rejection problem, it follows that G_{yu} given by (3.7) implies that there exists a state space basis for $(3.1) - (3.3)$ such that A, B, C, D_0 have the form

$$
A = \begin{bmatrix} A_{11} & 0_{n_z \times n_y} \\ 0_{n_y \times n_z} & A_{22} \end{bmatrix}, \quad B = \begin{bmatrix} B_z \\ 0_{n_y \times l_u} \end{bmatrix}, \quad C = \begin{bmatrix} 0_{l_y \times n_z} & C_y \end{bmatrix}, \quad D_0 = 0_{l_y \times l_u},
$$

(5.24)

where $A_{11} \in \mathbb{R}^{n_z \times n_z}$, $A_{22} \in \mathbb{R}^{n_y \times n_y}$, $B_z \in \mathbb{R}^{n_z \times l_u}$, and $C_y \in \mathbb{R}^{l_y \times n_y}$. Note that $n_z + n_y = n$.

Assume that $R_{12} = 0_{n \times l_y}$ and $V_{12} = 0_{n \times l_u}$. Partitioning $P = \begin{bmatrix} P_{11} & P_{12} \\ P_{12}^{\mathrm{T}} & P_{22} \end{bmatrix}$, where $P_{11} \in \mathbb{R}^{n_z \times n_z}$, $P_{12} \in \mathbb{R}^{n_z \times n_y}$, and $P_{22} \in \mathbb{R}^{n_y \times n_y}$, (5.19) and (5.24) imply

$$
C_{\mathrm{c}} = -(R_2 + B_z^{\mathrm{T}} P_{11} B_z)^{-1} \begin{bmatrix} B_z^{\mathrm{T}} P_{11} A_{11} & B_z^{\mathrm{T}} P_{12} A_{22} \end{bmatrix}.
$$

(5.25)

Note that C_{c} depends only on P_{11} and P_{12}, which satisfy

$$
P_{11} = A_{11}^{\mathrm{T}} P_{11} A_{11} + A_{11}^{\mathrm{T}} P_{11} B_z (R_2 + B_z^{\mathrm{T}} P_{11} B_z)^{-1} B_z^{\mathrm{T}} P_{11} A_{11} + R_{1,11},
$$

(5.26)

$$
P_{12} = A_{11}^{\mathrm{T}} P_{12} A_{22} + A_{11}^{\mathrm{T}} P_{11} B_z (R_2 + B_z^{\mathrm{T}} P_{11} B_z)^{-1} B_z^{\mathrm{T}} P_{12} A_{22} + R_{1,12},
$$

(5.27)

where $R_1 = \begin{bmatrix} R_{1,11} & R_{1,12} \\ R_{1,12}^{\mathrm{T}} & R_{1,22} \end{bmatrix}$. Hence C_{c} is completely described by the reduced solution (5.25)–(5.27). Likewise, partitioning $Q = \begin{bmatrix} Q_{11} & Q_{12} \\ Q_{12}^{\mathrm{T}} & Q_{22} \end{bmatrix}$, where $Q_{11} \in \mathbb{R}^{n_z \times n_z}$, $Q_{12} \in$

$\mathbb{R}^{n_z \times n_y}$, and $Q_{22} \in \mathbb{R}^{n_y \times n_y}$, (5.18) and (5.24) imply

$$B_c = \begin{bmatrix} A_{11} Q_{12} C_y^T \\ A_{22} Q_{22} C_y^T \end{bmatrix} (V_2 + C_y Q_{22} C_y^T)^{-1}, \tag{5.28}$$

where Q_{12} and Q_{22} satisfy

$$Q_{12} = A_{11} Q_{12} A_{22}^T + A_{11} Q_{12} C_y^T (V_2 + C_y Q_{22} C_y^T)^{-1} C_y Q_{22} A_{22}^T + V_{1,12}, \tag{5.29}$$

$$Q_{22} = A_{11} Q_{12} A_{22}^T + A_{22} Q_{22} C_y^T (V_2 + C_y Q_{22} C_y^T)^{-1} C_y Q_{22} A_{22}^T + V_{1,22}, \tag{5.30}$$

and $V_1 = \begin{bmatrix} V_{1,11} & V_{1,12} \\ V_{1,12}^T & V_{1,22} \end{bmatrix}$.

Introducing the notation

$$B_c = \begin{bmatrix} B_{c1} \\ B_{c2} \end{bmatrix}, \qquad C_c = \begin{bmatrix} C_{c1} & C_{c2} \end{bmatrix}, \tag{5.31}$$

it follows from (5.23) that the eigenvalues of $\widetilde{A}$ are given by

$$\mathrm{mspec}(\widetilde{A}) = \mathrm{mspec}\left(\begin{bmatrix} A_{11} + B_z C_{c1} & B_z C_{c2} \\ 0_{n_y \times n_z} & A_{22} \end{bmatrix} \right) \cup \mathrm{mspec}\left(\begin{bmatrix} A_{11} & -B_{c1} C_y \\ 0_{n_y \times n_z} & A_{22} - B_{c2} C_y \end{bmatrix} \right)$$

$$\tag{5.32}$$

$$= \mathrm{mspec}\,(A) \cup \mathrm{mspec}(A_{11} + B_z C_{c1}) \cup \mathrm{mspec}(A_{22} - B_{c2} C_y). \tag{5.33}$$

Hence (5.33) and (5.17) imply that

$$\mathrm{mspec}(\widetilde{A}) = \mathrm{mspec}\,(A) \cup \mathrm{mspec}\,(A_c). \tag{5.34}$$

Note that the eigenvalues of $\widetilde{A}$ do not depend on C_{c2} and B_{c1}. If $R_{12} = 0_{n \times l_y}$ and $V_{12} =$

$0_{n \times l_u}$ so that C_c and B_c are given by (5.25) and (5.28), then the eigenvalues of $\widetilde{A}$ are fully described by $A_{11}, A_{22}, B_z, C_y, P_{11}$, and Q_{22} and the LQG weightings.

5.3.2 Specializion of LQG to Direct Feedforward Disturbance Rejection

For direct feedforward disturbance rejection, $y(k) = w(k)$ and

$$C = 0_{l_y \times n}, \quad D_2 = I_{l_w}, \quad D_0 = 0_{l_y \times l_u}. \tag{5.35}$$

Using (5.35), the controller (5.17)–(5.19) can be written as

$$A_c = A + BC_c, \tag{5.36}$$

$$B_c = V_{12}V_2^{-1} = D_1, \tag{5.37}$$

$$C_c = -(R_2 + B^{\mathrm{T}}PB)^{-1}(R_{12}^T + B^{\mathrm{T}}PA). \tag{5.38}$$

Note that B_c is given directly by D_1 and thus does not require the solution of a Riccati equation.

5.4 Analysis of the High-Authority LQG Feedforward Controller

We now consider the LQG feedforward controller in the case where y, z, u, and w are scalar signals and the LQG weights satisfy

$$R_2 = E_2^{\mathrm{T}}E_2 = 0, \quad V_2 = D_2D_2^{\mathrm{T}} = 0. \tag{5.39}$$

The weights (5.39) indicate the high-authority discrete-time LQG control problem. Properties of the high-authority LQG controller for continuous-time systems are given in [37, pp. 281-289]; analogous properties in discrete-time are considered in [21]. It follows from (5.39) that G_{zu} and G_{yw} are strictly proper.

Defining the characteristic polynomial $\widetilde{D}_{zw}$ of the closed-loop system (5.9)–(5.12) by

$$\widetilde{D}_{zw}(\mathbf{z}) \triangleq \det(\mathbf{z}I - \widetilde{A}), \tag{5.40}$$

it follows from (5.23) that (5.40) can be factored as

$$\widetilde{D}_{zw}(\mathbf{z}) = \widetilde{D}_{zw,\mathrm{LQR}}(\mathbf{z})\widetilde{D}_{zw,\mathrm{LQE}}(\mathbf{z}), \tag{5.41}$$

where

$$\widetilde{D}_{zw,\mathrm{LQR}} \triangleq \det(\mathbf{z}I - (A + BC_\mathrm{c})), \quad \widetilde{D}_{zw,\mathrm{LQE}} \triangleq \det(\mathbf{z}I - (A - B_\mathrm{c}C)). \tag{5.42}$$

The poles of the closed-loop system are given by the roots of $\widetilde{D}_{zw,\mathrm{LQR}}$ (the linear-quadratic regulator) and $\widetilde{D}_{zw,\mathrm{LQE}}$ (the linear-quadratic estimator). In order to analyze $\widetilde{D}_{zw,\mathrm{LQR}}$ and $\widetilde{D}_{zw,\mathrm{LQE}}$, we factor N_{zu} defined by (3.14) as

$$N_{zu}(\mathbf{z}) = H_{\mathrm{d}_{zu}} N_{zu,\mathrm{s}}(\mathbf{z}) N_{zu,\mathrm{u}}(\mathbf{z}), \tag{5.43}$$

where $H_{\mathrm{d}_{zu}}$ is the leading nonzero numerator coefficient of G_{zu} and the roots of the monic polynomials $N_{zu,\mathrm{s}}$ and $N_{zu,\mathrm{u}}$ are the minimum-phase (open-unit-disk) zeros and NMP zeros of G_{zu}, respectively.

If $R_2 = 0$, then the high-authority LQR design places the roots of $\widetilde{D}_{zw,\mathrm{LQR}}$ at

$$\widetilde{D}_{zw,\mathrm{LQR}} = \mathbf{z}^{\mathrm{d}_{zu}} N_{zu,\mathrm{s}}(\mathbf{z}) N_{zu,\mathrm{u}}(\mathbf{z}^{-1}), \tag{5.44}$$

where the roots of $N_{zu,\mathrm{u}}(\mathbf{z}^{-1})$ are the reciprocals of the NMP zeros of G_{zu}. Similarly, if $V_2 = 0$, then the high-authority LQE design places the roots of $\widetilde{D}_{zw,\mathrm{LQE}}$ at

$$\widetilde{D}_{zw,\mathrm{LQE}}(\mathbf{z}) = \mathbf{z}^{\mathrm{d}_{yw}} N_{zw,\mathrm{s}}(\mathbf{z}) N_{yw,\mathrm{u}}(\mathbf{z}^{-1}), \tag{5.45}$$

where the roots of $N_{yw,\mathrm{u}}(\mathbf{z}^{-1})$ are the reciprocals of the NMP zeros of G_{yw}. It follows that if $R_2 = 0$ and $V_2 = 0$, then

$$\widetilde{D}_{zw}(\mathbf{z}) = \mathbf{z}^{\mathrm{d}_{zu}} N_{zu,\mathrm{s}}(\mathbf{z}) N_{zu,\mathrm{u}}(\mathbf{z}^{-1}) \mathbf{z}^{\mathrm{d}_{yw}} N_{zw,\mathrm{s}}(\mathbf{z}) N_{yw,\mathrm{u}}(\mathbf{z}^{-1}). \tag{5.46}$$

5.4.1 High-Authority LQG Controller for Feedforward Disturbance Rejection

In the case of feedforward disturbance rejection, it follows from (5.34) that (5.40) can be factored as

$$\widetilde{D}_{zw}(\mathbf{z}) = D_{\mathrm{c}}(\mathbf{z}) D(\mathbf{z}), \tag{5.47}$$

where

$$D_{\mathrm{c}}(\mathbf{z}) \triangleq \det(\mathbf{z}I - A_{\mathrm{c}}), \quad D(\mathbf{z}) \triangleq \det(\mathbf{z}I - A). \tag{5.48}$$

Furthermore, it follows from (5.24) that (5.48) can be factored as

$$D(\mathbf{z}) = D_z(\mathbf{z}) D_y(\mathbf{z}), \tag{5.49}$$

where

$$D_z(\mathbf{z}) \triangleq \det(\mathbf{z}I_{n_z \times n_z} - A_{11}), \quad D_y(\mathbf{z}) \triangleq \det(\mathbf{z}I_{n_y \times n_y} - A_{22}). \tag{5.50}$$

83

Proposition 1: Consider the feedforward disturbance rejection problem, where y, z, u, and w are scalar signals. Then there exist polynomials $\overline{N}_{zu}$ and $\overline{N}_{yw}$ such that the numerators of G_{zu} and G_{yw} can be expressed as

$$N_{zu}(\mathbf{z}) = \overline{N}_{zu}(\mathbf{z})D_y(\mathbf{z}), \quad N_{yw}(\mathbf{z}) = \overline{N}_{yw}(\mathbf{z})D_z(\mathbf{z}). \tag{5.51}$$

Lemma 1: Let $A \in \mathbb{R}^{l\times l}$, $B \in \mathbb{R}^{l\times m}$, $C \in \mathbb{R}^{m\times l}$, and $D \in \mathbb{R}^{m\times m}$. If A is nonsingular, then

$$\det\left(\begin{bmatrix} A & B \\ C & D \end{bmatrix}\right) = \det(A)\det(D - CA^{-1}B). \tag{5.52}$$

If, $m = 1$, then

$$\det\left(\begin{bmatrix} A & B \\ C & D \end{bmatrix}\right) = (D + 1)\det(A) - \det(A + BC). \tag{5.53}$$

Proof of Proposition 1: Consider the Rosenbrock system matrix (RSM) for G_{zu}, where

$$\mathrm{RSM}(\mathbf{z}) = \begin{bmatrix} \mathbf{z}I - A & B \\ E_1 & E_2 \end{bmatrix}. \tag{5.54}$$

Since (5.54) is square, the zeros of G_{zu} can be obtained from the characteristic polynomial of the RSM. Using Lemma 1, the characteristic polynomial of (5.54) can be written as

$$N_{zu}(\mathbf{z}) = \det(\mathrm{RSM}(\mathbf{z})) = (E_2 + 1)\det(\mathbf{z}I - A) + \det(\mathbf{z}I - A + BE_1). \tag{5.55}$$

Introduce the notation

$$E_1 = \begin{bmatrix} E_{1z} & E_{1y} \end{bmatrix}, \tag{5.56}$$

where $E_{1z} \in \mathbb{R}^{l_u \times n_z}$, and $E_{1y} \in \mathbb{R}^{l_u \times n_y}$. Using (5.24) and (5.56), (5.55) can be written as

$$
N_{zu}(\mathbf{z}) = (E_2 + 1)\det \left(\begin{bmatrix} \mathbf{z}I_{n_z \times n_z} - A_{11} & A_{12} \\ 0_{n_y \times n_z} & \mathbf{z}I_{n_y \times n_y} - A_{22} \end{bmatrix} \right) +
$$

$$
\det \left(\begin{bmatrix} \mathbf{z}I_{n_z \times n_z} - A_{11} + B_z E_{1z} & A_{12} + B_z E_{2z} \\ 0_{n_y \times n_z} & \mathbf{z}I_{n_y \times n_y} - A_{22} \end{bmatrix} \right). \tag{5.57}
$$

Exploiting the structure of upper block triangular matrices, (5.57) is equivalent to

$$
N_{zu}(\mathbf{z}) = (E_2 + 1)D_z(\mathbf{z})D_y(\mathbf{z}) + \det(\mathbf{z}I_{n_z \times n_z} - A_{11} + B_z E_{1z})D_y(\mathbf{z}). \tag{5.58}
$$

It follows that (5.58) can be written as

$$
N_{zu}(\mathbf{z}) = \overline{N}_{zu}(\mathbf{z})D_y(\mathbf{z}), \tag{5.59}
$$

where

$$
\overline{N}_{zu}(\mathbf{z}) = (E_2 + 1)D_z(\mathbf{z}) + \det(\mathbf{z}I_{n_z \times n_z} - A_{11} + B_z E_{1z}). \tag{5.60}
$$

Introduce the notation

$$
D_1 = \begin{bmatrix} D_{1z} \\ D_{1y} \end{bmatrix}, \tag{5.61}
$$

where $D_{1z} \in \mathbb{R}^{n_z \times l_y}, D_{1y} \in \mathbb{R}^{n_y \times l_y}$. Following the same arguments, it can be seen that $N_{yw}(\mathbf{z})$ can be written as

$$
N_{yw}(\mathbf{z}) = \overline{N}_{yw}(\mathbf{z})D_z(\mathbf{z}), \tag{5.62}
$$

where

$$\overline{N}_{yw}(\mathbf{z}) = (D_2 + 1)D_z(\mathbf{z}) + \det(\mathbf{z}I_{n_z \times n_z} - A_{22} + D_{1y}C_y). \tag{5.63}$$

Proposition 1 shows that the numerator and denominator of G_{zu} given by (3.6) are not coprime. It also shows that the numerator and denominator of G_{yw} given by (3.7) in the case of feedforward disturbance rejection are not coprime. Furthermore, it follows from Proposition 1 that

$$G_{zu}(\mathbf{z}) = \frac{N_{zu}(\mathbf{z})}{D(\mathbf{z})} = \frac{\overline{N}_{zu}(\mathbf{z})}{D_z(\mathbf{z})}, \qquad G_{yw}(\mathbf{z}) = \frac{N_{yw}(\mathbf{z})}{D(\mathbf{z})} = \frac{\overline{N}_{yw}(\mathbf{z})}{D_y(\mathbf{z})}. \tag{5.64}$$

Since, for the feedforward disturbance rejection problem, the roots of D are assumed to be contained in the open unit disk, it follows from (5.51) that

$$N_{zu,\mathrm{u}}(\mathbf{z}) = \overline{N}_{zu,\mathrm{u}}(\mathbf{z}), \quad N_{yw,\mathrm{u}}(\mathbf{z}) = \overline{N}_{yw,\mathrm{u}}(\mathbf{z}), \tag{5.65}$$

that is, all NMP zeros of G_{zu} and G_{yw} are roots of $\overline{N}_{zu}$ and $\overline{N}_{yw}$, respectively. It follows from (5.46)–(5.65) that

$$D_\mathrm{c}(\mathbf{z})D(\mathbf{z}) = \mathbf{z}^{\mathrm{d}_{zu}}\overline{N}_{zu,\mathrm{s}}(\mathbf{z})\overline{N}_{zu,\mathrm{u}}(\mathbf{z}^{-1})D_y(\mathbf{z})\mathbf{z}^{\mathrm{d}_{yw}}\overline{N}_{zw,\mathrm{s}}(\mathbf{z})\overline{N}_{yw,\mathrm{u}}(\mathbf{z}^{-1})D_z(\mathbf{z}), \tag{5.66}$$

$$D_\mathrm{c}(\mathbf{z}) = \mathbf{z}^{\mathrm{d}_{zu}}\overline{N}_{zu,\mathrm{s}}(\mathbf{z})\overline{N}_{zu,\mathrm{u}}(\mathbf{z}^{-1})\mathbf{z}^{\mathrm{d}_{yw}}\overline{N}_{zw,\mathrm{s}}(\mathbf{z})\overline{N}_{yw,\mathrm{u}}(\mathbf{z}^{-1}), \tag{5.67}$$

where (5.67) give the denominator of the high-authority LQG controller.

The denominator of the high-authority LQG controller given by (5.67) indicates the locations of the controller poles in the case where the ideal feedforward controller (5.6) is unstable. In particular, if either G_{zu} or G_{yw} is NMP and thus the ideal controller is unstable, then the high-authority LQG design places the poles of the controller at the reciprocals of the unstable poles of the ideal controller. Note that, if the ideal controller has at least one

unstable pole, then it is not implementable. However, the LQG design is implementable in all cases.

5.4.2 High-Authority LQG Controller for Direct Feedforward Disturbance Rejection

For direct feedforward disturbance rejection, the LQE gain (5.37) does not involve the solution of the Riccati equation (5.22). In this case, the high-authority LQG problem corresponds to $R_2 = 0$ with $B_c = D_1$. It follows from (5.67) that the denominator of the high-authority LQG controller is given by

$$D_c(\mathbf{z}) = \mathbf{z}^{d_{zu}} \overline{N}_{zu,s}(\mathbf{z}) \overline{N}_{zu,u}(\mathbf{z}^{-1}).$$ (5.68)

5.5 Modeling Information Required to Construct the Target Model G_f in Feedforward Disturbance Rejection

The derivation of the retrospective performance decomposition (4.20) in Section 4.1 was largely independent of whether the control architecture is feedback or feedforward. We specialize the equations in Section 4.1 to the feedforward control problem below.

Consider (4.14), where $y(k)$ for feedforward control is given by (5.1). Substituting (5.1) into (4.14) yields

$$z(k) = \tilde{G}_{zw,\theta(k+1)}(\mathbf{q})w(k) + \tilde{G}_{z\tilde{u},\theta(k+1)}(\mathbf{q})\tilde{u}(k,\theta(\overline{k+1})),$$ (5.69)

where

$$\tilde{G}_{zw,\theta(k+1)}(\mathbf{q}) \triangleq G_{zw}(\mathbf{q}) + G_{zu}(\mathbf{q})G_{\mathrm{c},\theta(\overline{k+1})}(\mathbf{q})G_{yw}(\mathbf{q}), \tag{5.70}$$

$$\tilde{G}_{z\tilde{u},\theta(k+1)}(\mathbf{q}) \triangleq G_{zu}(\mathbf{q})G_{\mathrm{p},\theta(\overline{k+1})}(\mathbf{q}). \tag{5.71}$$

If $y, z, u,$ and w are scalar signals, then (4.18) can be written as

$$\tilde{G}_{z\tilde{u},\theta(k+1)}(\mathbf{q}) = \frac{N_{zu}(\mathbf{q})\mathbf{q}^{n_{\mathrm{c}}}}{D(\mathbf{q})D_{\mathrm{c},\theta(k+1)}(\mathbf{q})}. \tag{5.72}$$

Furthermore, using (5.49) and (5.51), (5.72) becomes

$$\tilde{G}_{z\tilde{u},\theta(k+1)}(\mathbf{q}) = \frac{\overline{N}_{zu}(\mathbf{q})\mathbf{q}^{n_{\mathrm{c}}}}{D_z(\mathbf{q})D_{\mathrm{c},\theta(k+1)}(\mathbf{q})}. \tag{5.73}$$

5.6 Constructing the Target Model G_{f}

We consider modeling information required for G_{f} in the feedforward disturbance rejection problem. Note that as the functional form of the performance decomposition (4.20) has not changed, we still view G_{f} as a target model for $\tilde{G}_{z\tilde{u},\theta(k+1)}$.

5.6.1 Relative degree

We again choose the relative degree of G_{f} to be equal to the relative degree of $\widetilde{G}_{z\tilde{u},\theta(k+1)}$. It follows from (5.72) that the relative degree of $\widetilde{G}_{z\tilde{u},\theta(k+1)}$ is still equal to the relative degree of G_{zu}. We thus choose the relative degree of G_{f} to be equal to the relative degree of G_{zu}.

5.6.2 NMP zeros

We note that the numerator of $\tilde{G}_{z\tilde{u},\theta(k+1)}$ for feedback (4.19) and feedforward (5.72) are the same. Hence the risk of RCAC canceling NMP zeros in G_{zu} that are not included

in the numerator of G_f in order to remove them from $\widetilde{G}_{z\tilde{u},\theta(k+1)}$ remains. This observation motivates the desire to again capture all NMP zeros of G_{zu} in the numerator of G_f.

5.6.3   FIR Target Model

Despite having different formulations, on the issue of relative degree and NMP zeros, $\widetilde{G}_{z\tilde{u},\theta(k+1)}$ for feedback and feedforward agree. Hence, in terms of the required modeling information, the FIR target models (4.26) for when G_{zu} is minimum phase, and (4.27) for when G_{zu} is NMP, also represent the modeling information required by RCAC for feedforward control.

5.6.4   Optimal Target Model G_f^*

The *optimal target model* G_f^* is the target model that recovers the high-authority LQG performance, assuming the conditions for high-authority LQG are satisfied. Consider $G_{z\tilde{u},\theta(k+1)}$ given by (5.73) and a target model G_f chosen as

$$G_\mathrm{f}(\mathbf{q}) = \frac{H_{\mathrm{d}_{zu}} \overline{N}_{zu}(\mathbf{z}) \mathbf{q}^{\overline{n}_\mathrm{c}}}{D_z(\mathbf{q}) D_{\mathrm{c,LQG}}(\mathbf{q})}, \tag{5.74}$$

where $D_{\mathrm{c,LQG}}$ is given by (5.67). It follows that in minimizing the model-matching error between (5.73) and (5.74), RCAC places the roots of $D_{\mathrm{c},\theta(k+1)}(\mathbf{q})$ at $D_{\mathrm{c,LQG}}$. Hence, if G_{zu} is minimum phase, then

$$G_\mathrm{f}^*(\mathbf{q}) = \frac{H_{\mathrm{d}_{zu}} \mathbf{q}^{n + \deg(\overline{N}_{\mathrm{yw}}) - \mathrm{d}_{\mathrm{zu}}}}{D_z(\mathbf{q}) \overline{N}_{yw,\mathrm{s}}(\mathbf{q}) \overline{N}_{yw,\mathrm{u}}(\mathbf{q}^{-1})}, \tag{5.75}$$

whereas, if G_{zu} is NMP, then

$$G_\mathrm{f}^*(\mathbf{q}) = \frac{H_{\mathrm{d}_{zu}} \overline{N}_{zu,\mathrm{u}}(\mathbf{q}) \mathbf{q}^{n + \deg(\overline{N}_{\mathrm{yw}}) - (\mathrm{d}_{\mathrm{zu}} + \deg(\overline{N}_{\mathrm{zu,u}}))}}{D_z(\mathbf{q}) \overline{N}_{zu,\mathrm{u}}(\mathbf{q}^{-1}) \overline{N}_{yw,\mathrm{s}}(\mathbf{q}) \overline{N}_{yw,\mathrm{u}}(\mathbf{q}^{-1})}. \tag{5.76}$$

For direct feedforward disturbance rejection, (5.75) reduces to

$$G_{\mathrm{f}}^*(\mathbf{q}) = \frac{H_{\mathrm{d}_{zu}}\mathbf{q}^{n-\mathrm{d}_{zu}}}{D_z(\mathbf{q})}, \tag{5.77}$$

and (5.76) reduces to

$$G_{\mathrm{f}}^*(\mathbf{q}) = \frac{H_{\mathrm{d}_{zu}}\overline{N}_{zu,\mathrm{u}}(\mathbf{q})\mathbf{q}^{n-(\mathrm{d}_{zu}+\deg(\overline{\mathrm{N}}_{\mathrm{zu,u}}))}}{D_z(\mathbf{q})\overline{N}_{zu,\mathrm{u}}(\mathbf{q}^{-1})}. \tag{5.78}$$

5.6.5   Choice of G_{f} for $n_{\mathrm{c,RCAC}} > n$

For sufficiently high controller order, it is possible for the RCAC controller to approximate the frequency response of the high-authority LQG feedforward controller in steady state without using the ideal filter G_{f}^* as long as the required modeling information is satisfied. In the subsequent numerical examples, we demonstrate that, for $n_{\mathrm{c,RCAC}} > n$, RCAC is able to approximate the frequency response of the high-authority LQG feedforward controller using only the FIR target model (4.26) in the case where G_{zu} is minimum phase and the FIR target model (4.27) in the case where G_{zu} is NMP.

5.6.6   Target model G_{f} for FIR Controller Structures

Consider the case where the controller structure is restricted to be FIR. In this case, $D_{\mathrm{c},\theta(k+1)} = \mathbf{q}^{n_{\mathrm{c}}}$ for all k, and thus (5.73) reduces to

$$\widetilde{G}_{z\tilde{u},\theta(k+1)}(\mathbf{q}) = \frac{\overline{N}_{zu}(\mathbf{q})}{D_z(\mathbf{q})}. \tag{5.79}$$

Since $\widetilde{G}_{z\tilde{u},\theta(k+1)}(\mathbf{q})$ does not depend on $\theta(k+1)$, it follows that the residual between G_{f} and $\widetilde{G}_{z\tilde{u}}$ is constant. Therefore, to minimize the retrospective performance (4.20), it is

advantageous to choose

$$G_{\mathrm{f}}^*(\mathbf{q}) = G_{zu}(\mathbf{q}) = \frac{\overline{N}_{zu}(\mathbf{q})}{D_z(\mathbf{q})}. \tag{5.80}$$

Note that, since G_{zu} is assumed to be asymptotically stable, the filter (5.80) can be represented as a Laurent expansion based on the Markov parameters of G_{zu}. In particular, for each complex number $\mathbf{z}$ whose absolute value is greater than the spectral radius of A, it follows that G_{zu} has the Laurent expansion

$$G_{zu}(\mathbf{z}) = E_1(\mathbf{z}I - A)^{-1}B = \sum_{i=d_{zu}}^{\infty} \frac{H_i}{\mathbf{z}^i}, \tag{5.81}$$

where $H_0 \triangleq E_2$ and, for all $i \geq 1$, the ith Markov parameter of G_{zu} is given by

$$H_i \triangleq E_1 A^{i-1} B. \tag{5.82}$$

The frequency response of G_{zu} can be approximated using the truncated Laurent expansion

$$G_{zu}(\mathbf{z}) \approx \sum_{i=d_{zu}}^{\overline{n}} \frac{H_i}{\mathbf{z}^i}. \tag{5.83}$$

5.7 RCAC and High-authority LQG Numerical Examples

Example 5.1: RCAC with an IIR controller, where G_{zu} is minimum phase, $\hat{G}_c$ is implementable, and G_f is the optimal target model (5.75). *Consider*

$$G_{zw}(\mathbf{z}) = \frac{\mathbf{z} - 0.2}{(\mathbf{z}^2 - 1.62\mathbf{z} + 0.81)(\mathbf{z}^2 - 0.72\mathbf{z} + 0.81)}, \quad G_{yw}(\mathbf{z}) = \frac{\mathbf{z} - 0.9}{\mathbf{z}^2 - 1.71\mathbf{z} + 0.81},$$

(5.84)

$$G_{zu}(\mathbf{z}) = \frac{(\mathbf{z} - 0.7)(\mathbf{z}^2 - 1.26\mathbf{z} + 0.81)}{(\mathbf{z}^2 - 1.62\mathbf{z} + 0.81)(\mathbf{z}^2 - 0.72\mathbf{z} + 0.81)}, \quad G_{yu}(\mathbf{z}) = 0. \tag{5.85}$$

Figure 5.2 shows the pole-zero map of the plant and the ideal controller $\hat{G}_c$ given by (5.6) for (5.84) and (5.85). Note that $\hat{G}_c$ is strictly proper and asymptotically stable, and thus is implementable. We apply RCAC with an IIR controller of order $n_c = n = 6$. The optimal target model (5.75) is given by

$$G_f(\mathbf{z}) = \frac{\mathbf{z}^4}{(\mathbf{z} - 0.9)(\mathbf{z}^2 - 1.62\mathbf{z} + 0.81)(\mathbf{z}^2 - 0.72\mathbf{z} + 0.81)}. \tag{5.86}$$

Figure 5.3 shows the performance of RCAC, compares the frequency responses of the ideal controller $\hat{G}_c$, the high-authority LQG controller $G_{c,\mathrm{LQG}}$, and the final RCAC controller $G_{c,500}$, and compares the frequency response of the target model G_f with the frequency response of the transfer function $\widetilde{G}_{z\tilde{u},500}$. By selecting the optimal target model, RCAC approximates the high-authority LQG controller with $n_c = n$. ◇

Figure 5.2: The pole-zero maps of (5.84) and (5.85) are shown in (a). The pole-zero map of the ideal controller $\hat{G}_\mathrm{c}$ given by (5.6) is shown in (b). The ideal controller is strictly proper and asymptotically stable, and thus is implementable.

Figure 5.3: Example 5.1: RCAC with an IIR controller applied to (5.84) and (5.85) with $n_c = n = 6$ with the target model G_f given by (5.86). The performance and control input are shown in (a), where z_u denotes the uncontrolled performance and z denotes the performance with RCAC. The controller gains and the pseudo-performance and model-matching error of the retrospective performance decomposition (4.20) are shown in (b). (c) compares the frequency responses of the final RCAC controller $G_{c,500}$, $G_{c,LQG}$, and $\hat{G}_c$. Note that the frequency response of $G_{c,500}$ approximates the frequency response of $\hat{G}_c$. (d) compares the frequency response of G_f with the frequency response of $\widetilde{G}_{z\tilde{u},500}$. Note that the frequency response of $\widetilde{G}_{z\tilde{u},500}$ approximates the frequency response of G_f.

94

Example 5.2: RCAC with an IIR controller, where G_{zu} is minimum phase, $\hat{G}_c$ is not implementable, and G_f is the FIR target model (4.26). Consider

$$G_{zw}(\mathbf{z}) = \frac{\mathbf{z}^2 - 0.7\mathbf{z} + 0.49}{(\mathbf{z}^2 - 1.62\mathbf{z} + 0.81)(\mathbf{z}^2 - 0.72\mathbf{z} + 0.81)}, \quad G_{yw}(\mathbf{z}) = \frac{\mathbf{z} - 1.2}{\mathbf{z}^2 - 1.71\mathbf{z} + 0.81},$$

(5.87)

$$G_{zu}(\mathbf{z}) = \frac{\mathbf{z}^2 - 1.26\mathbf{z} + 0.81}{(\mathbf{z}^2 - 1.62\mathbf{z} + 0.81)(\mathbf{z}^2 - 0.72\mathbf{z} + 0.81)}, \quad G_{yu}(\mathbf{z}) = 0. \qquad (5.88)$$

Figure 5.4 shows the pole-zero map of the plant and the ideal controller $\hat{G}_c$ given by (5.6) for (5.87) and (5.88). Note that $\hat{G}_c$ is strictly proper, but, since G_{yw} is NMP, it is unstable, and thus is not implementable. We apply RCAC with an IIR controller of order $n_c = 16$. The FIR target model (4.26) is given by

$$G_f(\mathbf{z}) = \frac{1}{\mathbf{z}^2}. \qquad (5.89)$$

Figure 5.5 shows the performance of RCAC, compares the frequency responses of the ideal controller $\hat{G}_c$, the high-authority LQG controller $G_{c,\mathrm{LQG}}$, and the final RCAC controller $G_{c,2000}$, and compares the frequency response of the target model G_f with the frequency response of the transfer function $\widetilde{G}_{z\tilde{u},2000}$. For a sufficiently high controller order, RCAC approximates the high-authority LQG controller using the nominal modeling information given by the FIR target model (4.26).   ◇
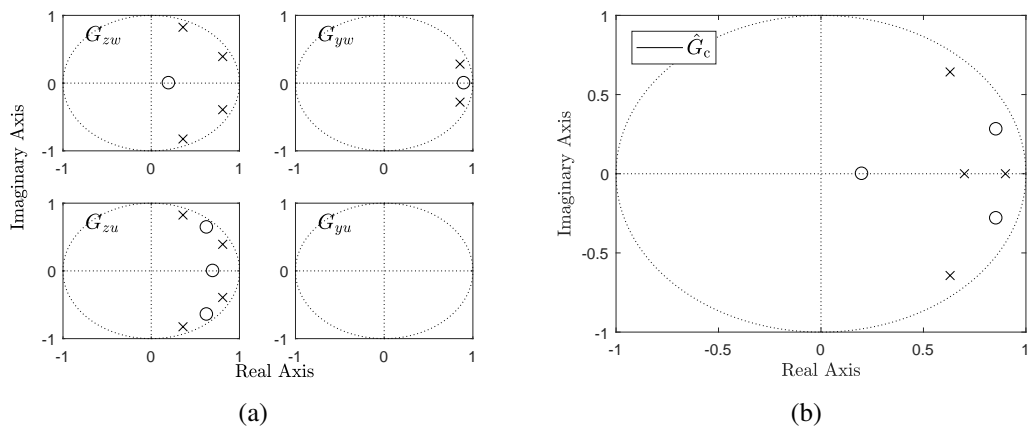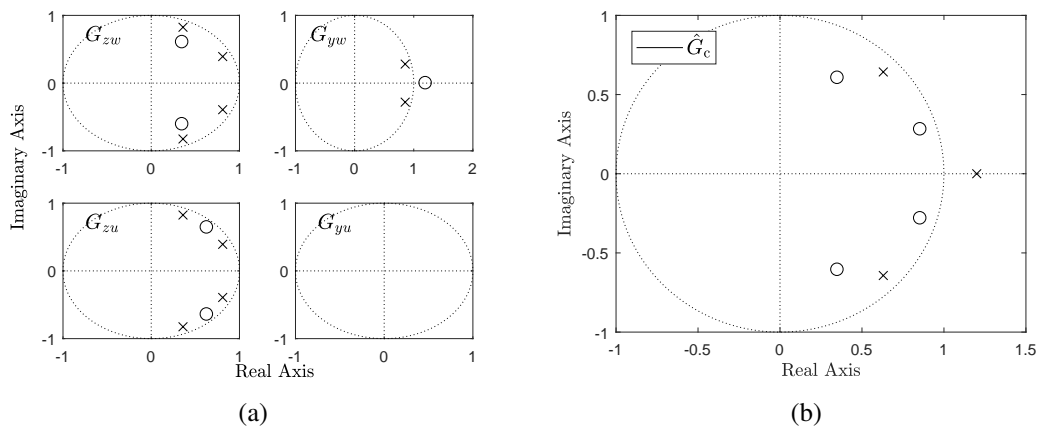
Figure 5.4: The pole-zero maps of (5.87) and (5.88) are shown in (a). The pole-zero map of the ideal controller $\hat{G}_\mathrm{c}$ is shown in (b). The ideal controller is strictly proper but unstable, and thus is not implementable.
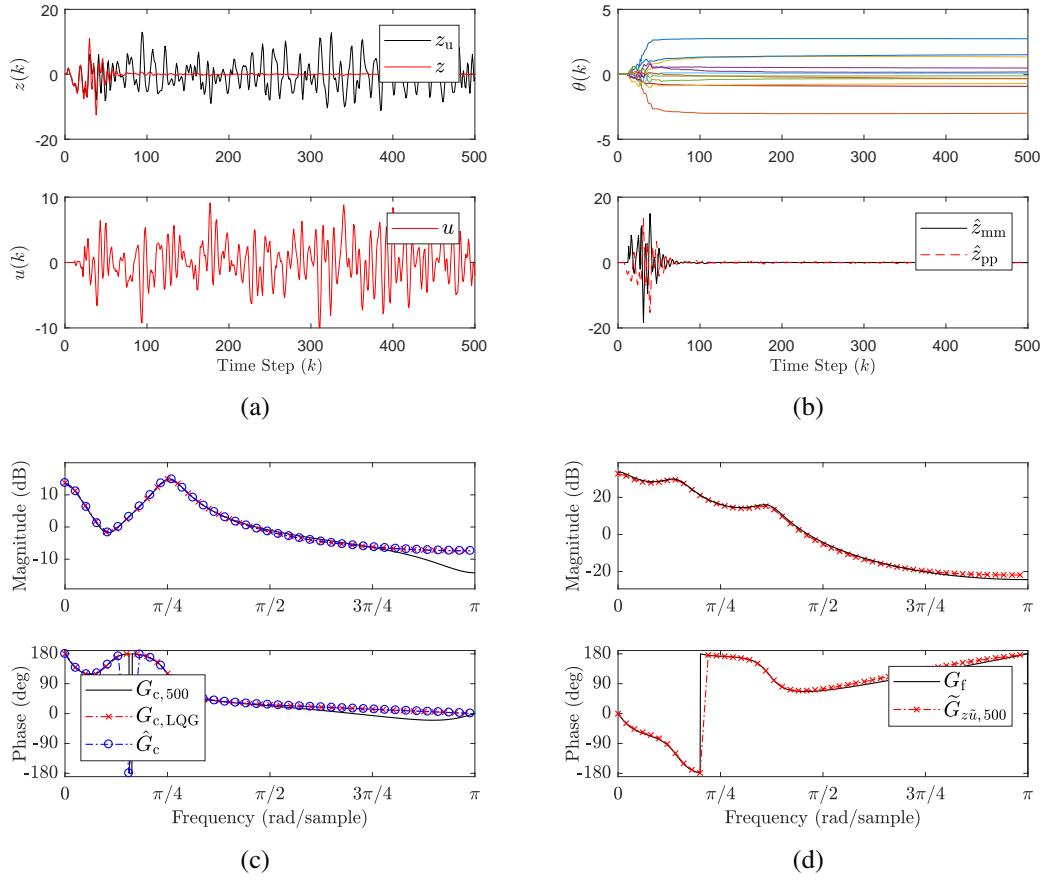
Figure 5.5: Example 5.2: RCAC with an IIR controller applied to (5.87) and (5.88) with $n_c = 16$ and the target model G_f given by (5.89). The performance and control input are shown in (a), where z_u denotes the uncontrolled performance and z denotes the performance with RCAC. The controller gains and the pseudo-performance and model-matching error of the performance decomposition (4.20) are shown in (b). (c) compares the frequency responses of the final RCAC controller $G_{c,2000}$, $G_{c,LQG}$, and $\hat{G}_c$. Note that the frequency response of $G_{c,2000}$ approximates the frequency response of $G_{c,LQG}$. (d) compares the frequency response of G_f with the frequency response of $\widetilde{G}_{z\tilde{u},2000}$. Note that the frequency response of $\widetilde{G}_{z\tilde{u},2000}$ approximates the frequency response of G_f.

RCAC with an IIR controller, where G_{zu} is NMP, $\hat{G}_c$ is not implementable, and the target models (4.26) and (4.27) are compared. Consider

$$G_{zw}(\mathbf{z}) = \frac{\mathbf{z} - 0.2}{(\mathbf{z}^2 - 1.62\mathbf{z} + 0.81)(\mathbf{z}^2 - 0.72\mathbf{z} + 0.81)}, \quad G_{yw}(\mathbf{z}) = \frac{\mathbf{z} - 0.9}{\mathbf{z}^2 - 1.71\mathbf{z} + 0.81},$$
(5.90)

$$G_{zu}(\mathbf{z}) = \frac{(\mathbf{z} - 0.7)(\mathbf{z}^2 - 1.54\mathbf{z} + 1.21)}{(\mathbf{z}^2 - 1.62\mathbf{z} + 0.81)(\mathbf{z}^2 - 0.72\mathbf{z} + 0.81)}, \quad G_{yu}(\mathbf{z}) = 0.$$
(5.91)

Figure 5.6 shows the pole-zero map of the plant and the ideal controller $\hat{G}_c$ given by (5.6) for (5.90) and (5.91). Note that $\hat{G}_c$ is not strictly proper and, since G_{zu} is NMP, is unstable; hence $\hat{G}_c$ is not implementable. We apply RCAC with an IIR controller of order $n_c = 16$. The FIR target model (4.26) is given by

$$G_f(\mathbf{z}) = \frac{1}{\mathbf{z}},$$
(5.92)

which does not include the NMP zero of G_{zu}. Figure 5.7 shows the performance of RCAC using the target model (5.92), the pole-zero map of the RCAC controller $G_{c,350}$, and compares the frequency response of the target model G_f with the frequency response of the transfer function $\widetilde{G}_{z\tilde{u}}$. Note that, since the NMP zeros of G_{zu} are not included in G_f, RCAC places controller poles at the NMP zeros in an attempt to match the frequency response of G_f and $\widetilde{G}_{z\tilde{u}}$. This cancellation causes $\tilde{G}_{zw}$ to be unstable, as shown in Figure 5.7.

Alternatively, consider the FIR target model (4.27) given by

$$G_f(\mathbf{z}) = \frac{\mathbf{z}^2 - 1.68\mathbf{z} + 1.44}{\mathbf{z}^3},$$
(5.93)

which includes the NMP zero of G_{zu}. Figure 5.8 shows the performance of RCAC using the target model (5.93), compares the frequency responses of the ideal controller $\hat{G}_c$, the high-authority LQG controller $G_{c,LQG}$, and the final RCAC controller $G_{c,2000}$, and compares

the frequency response of the target model G_f with the frequency response of the transfer function $\widetilde{G}_{z\tilde{u},2000}$. In this case, the NMP zeros of G_{zu} are included in G_f, and the RCAC controller approximates the frequency response of the high-authority LQG controller as shown in Figure 5.8. Consequently, no unstable pole-zero cancellation occurs as in the case of G_f given by (5.92). $\diamond$
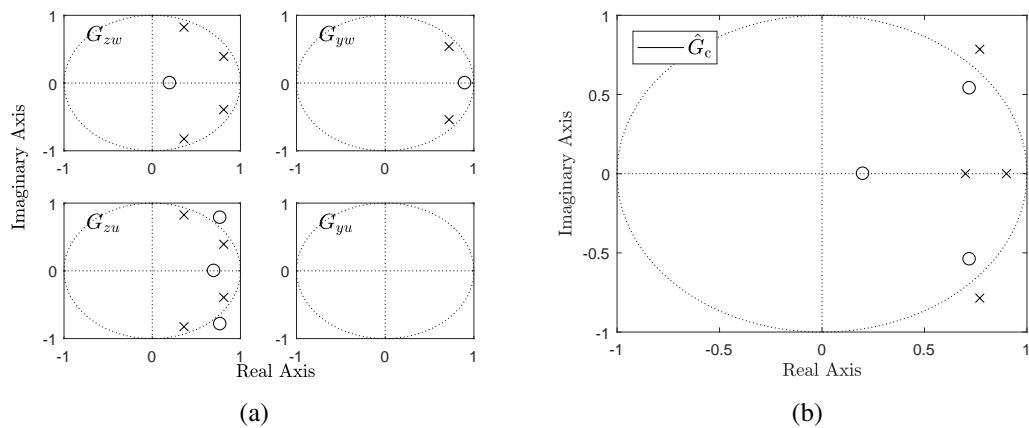
Figure 5.6: Example 5.3: The pole-zero map of (5.90) and (5.91) is shown in (a). The ideal controller is shown in (b). The ideal controller is not strictly proper and unstable, and thus is not implementable.

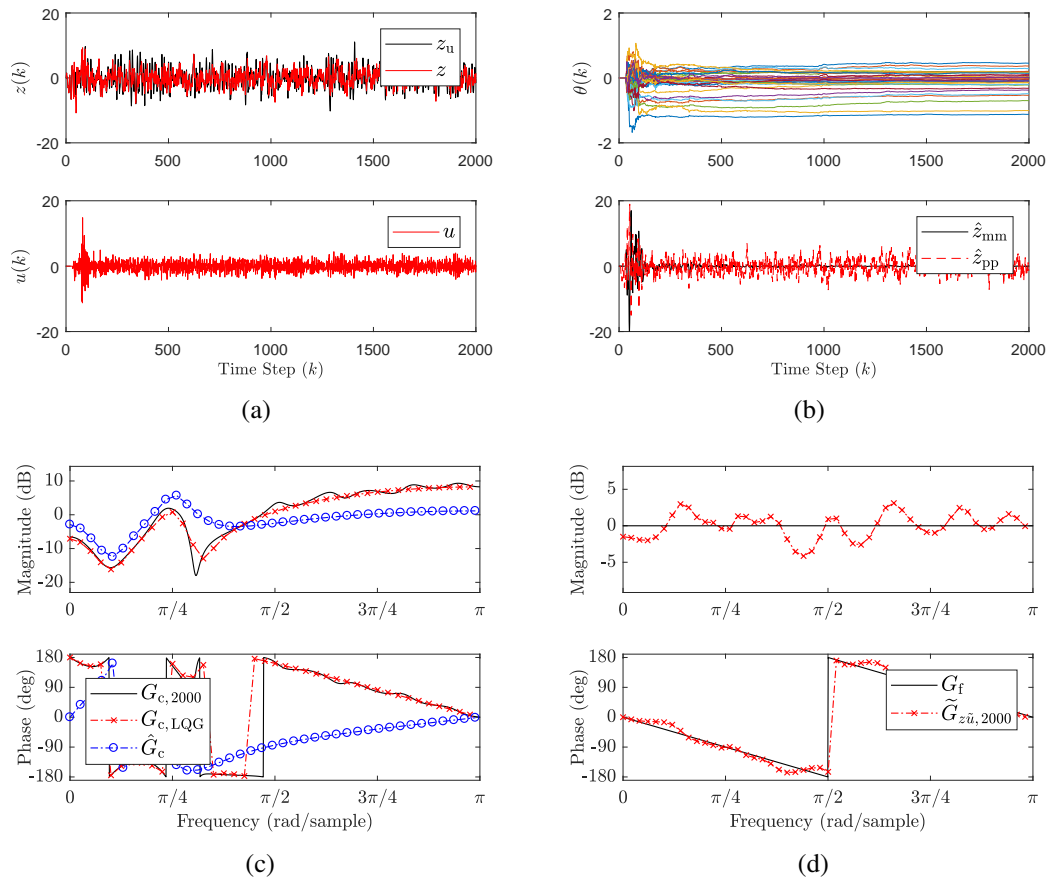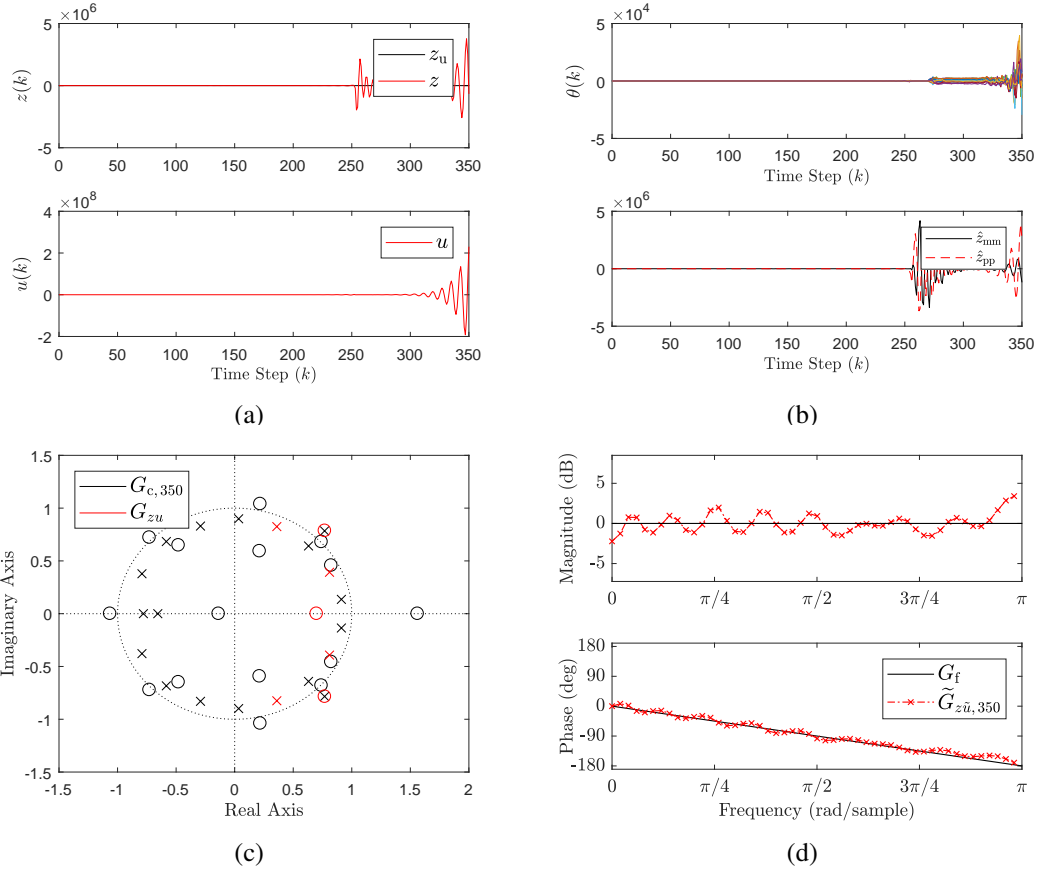Figure 5.7: Example 5.3: RCAC with an IIR controller applied to (5.90) and (5.91) with $n_\mathrm{c} = 16$ and the target model G_f given by (5.92), which does not include the NMP zeros of G_{zu}. The performance and control input are shown in (a), where z_u denotes the uncontrolled performance and z denotes the performance with RCAC. The controller gains and the pseudo-performance and model-matching error of the performance decomposition (4.20) are shown in (b). (c) shows the pole-zero map of G_{zu} and $G_{\mathrm{c},350}$. Note that RCAC places controller poles at the unmodeled NMP zeros of G_f, which produces an unstable controller. (d) compares the frequency response of G_f with the frequency response of $\widetilde{G}_{z\tilde{u},350}$. Note that the frequency response of $\widetilde{G}_{z\tilde{u},350}$ approximates the frequency response of G_f.
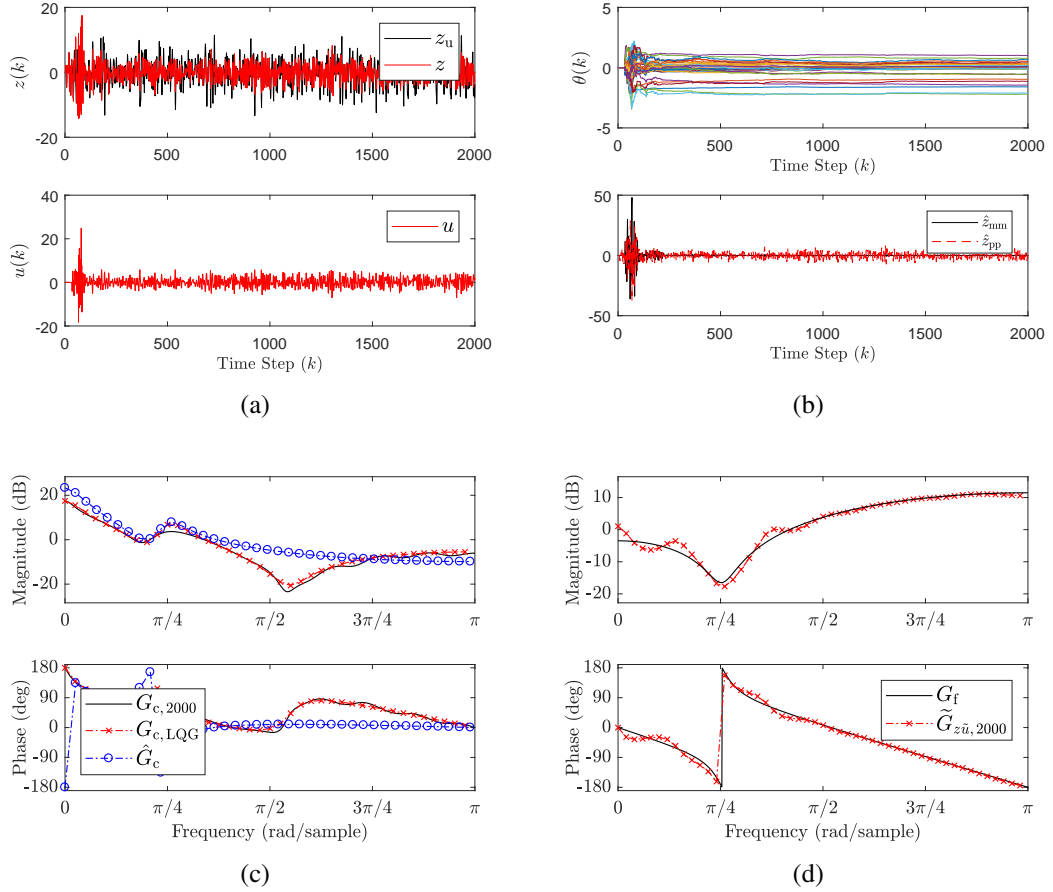
Figure 5.8: Example 5.3: RCAC with an IIR controller applied to (5.90) and (5.91) with $n_\mathrm{c} = 16$ and the target model G_f given by (5.93), which includes the NMP zeros of G_{zu}. The performance and control input are shown in (a), where z_u denotes the uncontrolled performance and z denotes the performance with RCAC. The controller gains and the pseudo-performance and model-matching error of the performance decomposition (4.20) are shown in (b). (c) compares the frequency responses of the final RCAC controller $G_{\mathrm{c},2000}$, $G_{\mathrm{c,LQG}}$, and $\hat{G}_\mathrm{c}$. Note that the frequency response of $G_{\mathrm{c},2000}$ approximates the frequency response of $G_{\mathrm{c,LQG}}$. (d) compares the frequency response of G_f with the frequency response of $\widetilde{G}_{z\tilde{u},2000}$. Note that the frequency response of $\widetilde{G}_{z\tilde{u},2000}$ approximates the frequency response of G_f.

5.8 RCAC and Filtered-x/Filtered-u Feedforward Algorithms

In this section, we compare RCAC with Fx/FuLMS and Fx/FuRLS [4, 5, 24, 25]. This comparison focuses on the recursive controller coefficient updates in the respective algorithms; a numerical comparison is given in the next section.

5.8.1 RCAC and Fx/FuLMS

For $p = 1$, the RCAC sliding-window gradient-based controller update law (3.36) specializes to

$$\theta(k+1) = \theta(k) - \mu(k)[z(k) - (u_{\mathrm{f}}(k) - \Phi_{\mathrm{f}}(k)\theta(k))]^{\mathrm{T}}\Phi_{\mathrm{f}}(k). \tag{5.94}$$

Furthermore, omitting the term $u_{\mathrm{f}}(k) - \Phi_{\mathrm{f}}(k)\theta(k)$, the update equation (5.94) becomes

$$\theta(k+1) = \theta(k) - \mu(k)z^{\mathrm{T}}(k)\Phi_{\mathrm{f}}(k), \tag{5.95}$$

where (5.95) is the update equation for the FuLMS algorithm given in [5,24]. If, in addition, the controller is constrained to be FIR such that $\Phi(k)$ and $\theta(k)$ are given by (3.25), then (5.95) is the update equation for the FxLMS algorithm in [4, 5].

5.8.2 RCAC and FxRLS/FuRLS

Consider the RCAC cumulative-cost RLS-based controller update law (3.43) and (3.45). Let $R_u = 0_{l_u \times l_u}$, $R_{u_{\mathrm{f}}} = 0_{l_z \times l_z}$, $R_\Delta = 0_{l_\theta \times l_\theta}$, and $R_z = I_{l_z}$. If the terms $u_{\mathrm{f}}(k)$ and $\Phi_{\mathrm{f}}(k)\theta(k)$ are omitted from the update equation (3.45), then (3.43) and (3.45) become

$$\theta(k+1) = \theta(k) - P(k)\Phi_{\mathrm{f}}^{\mathrm{T}}(k)\Upsilon^{-1}(k)z(k), \tag{5.96}$$

$$P(k+1) = \frac{1}{\lambda}P(k) - \frac{1}{\lambda}P(k)\Phi_{\mathrm{f}}^{\mathrm{T}}(k)\Upsilon^{-1}(k)\Phi_{\mathrm{f}}(k)P(k), \tag{5.97}$$

where

$$\Upsilon(k) \triangleq \lambda I_{l_z} + \Phi_{\rm f}(k)P(k)\Phi_{\rm f}^{\rm T}(k).\tag{5.98}$$

The equations (5.96), (5.97), and (5.98) are the update equations of the FuRLS algorithm. If the controller is constrained to be FIR such that $\Phi(k)$ and $\theta(k)$ are given by (3.25), then (5.96), (5.97), and (5.98) are the update equations for the FxRLS algorithm given in [5, 25]

Note that $\Phi_{\rm f}$, which is given by (3.29) in terms of the filter $G_{\rm f}$, appears in the Fx/FuLMS update equation (5.95) and the Fx/FuRLS update equations (5.96), (5.97), and (5.98). In the context of Fx/FuLMS and Fx/FuRLS, $G_{\rm f}$ is a model of the secondary path transfer function G_{zu} [5].

5.9   Numerical Comparison of RCAC and FuRLS

In this section, we compare the performance of cumulative-cost, RLS-based RCAC using an IIR controller with FuRLS. We consider direct feedforward disturbance rejection assuming that the ideal controller is implementable.

Two metrics are considered. The *instantaneous controller difference*

$$\Delta G_{{\rm c},k} \triangleq ||G_{{\rm c},k} - \hat{G}_{\rm c}||_2,\tag{5.99}$$

where $|| \cdot ||_2$ denotes the H$_2$ norm, measures the closeness of the controller $G_{{\rm c},k}$ at step k to the ideal controller $\hat{G}_{\rm c}$. Additionally, the *instantaneous performance*

$$\tilde{J}_k \triangleq ||\tilde{G}_{zw,k}||_2\tag{5.100}$$

measures the performance of the controlled system at step k. Note that both metrics are meaningful at step k only if $G_{{\rm c},k}$ is asymptotically stable. All of the RCAC examples in this

section use the tuning parameters $k_c = 1$, $R_u = 0_{l_u \times l_u}$, $k_w = 60$, $\lambda = 1$, and $Q = 0_{l_\theta \times l_\theta}$.

Example 5.4: Comparison of RCAC and FuRLS, where G_f for RCAC is the optimal target model (5.77) and G_f for FuRLS is G_{zu}. Consider

$$G_{zw}(\mathbf{z}) = \frac{\mathbf{z}^2 - 1.71\mathbf{z} + 0.81}{(\mathbf{z}^2 - 1.62\mathbf{z} + 0.81)(\mathbf{z}^2 - 1.52\mathbf{z} + 0.90)}, \tag{5.101}$$

$$G_{zu}(\mathbf{z}) = \frac{(\mathbf{z}^2 - 1.35\mathbf{z} + 0.81)(\mathbf{z} - 0.7)}{(\mathbf{z}^2 - 1.62\mathbf{z} + 0.81)(\mathbf{z}^2 - 1.52\mathbf{z} + 0.90)}. \tag{5.102}$$

Figure 5.9 shows the pole-zero map and the ideal controller $\hat{G}_c$. Note that $\hat{G}_c$ is strictly proper and asymptotically stable, and thus is implementable. We apply RCAC with an IIR
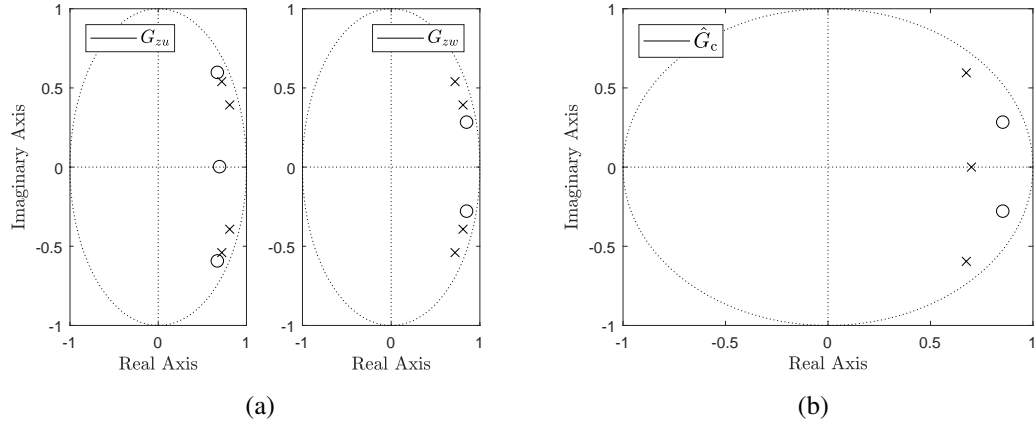
Figure 5.9: Example 5.4: The pole-zero map of (5.101) and (5.102) is shown in (a). The ideal controller is shown in (b). The ideal controller is strictly proper and asymptotically stable, and thus is implementable.

controller and FuRLS with $n_c = n = 4$. For RCAC, the optimal target model (5.77) is given by

$$G_f(\mathbf{z}) = \frac{\mathbf{z}^3}{(\mathbf{z}^2 - 1.62\mathbf{z} + 0.81)(\mathbf{z}^2 - 1.52\mathbf{z} + 0.90)}, \tag{5.103}$$

with $P(0) = R_\theta^{-1} = 10I_{l_\theta}$, and $R_\Delta = 0_{l_\theta \times l_\theta}$. For FuRLS, $G_f = G_{zu}$ given by (5.102). We consider the response of FuRLS for several values of $P(0)$. Figure 5.10 shows the performance of both algorithms and compares the instantaneous performance and the instan-

taneous controller difference. Note that RCAC provides lower values of the instantaneous performance and instantaneous controller difference than FuRLS. ◇

Example 5.5: Comparison of RCAC and FuRLS, where G_f for RCAC is the FIR target model (4.26) *and G_f for FuRLS is G_{zu}.* Consider the system (5.101) and (5.102) defined in Example 5.4. We apply RCAC with an IIR controller and FuRLS. For RCAC, the FIR target model (4.26) is given by

$$G_\mathrm{f}(\mathbf{z}) = \frac{1}{\mathbf{z}}, \tag{5.104}$$

with $P(0) = R_\theta^{-1} = I_{l_\theta}$, and $R_\Delta = 100 I_{l_\theta}$. We consider the response for several values of n_c. For FuRLS, $G_\mathrm{f} = G_{zu}$ is given by (5.102) with $P(0) = 0.1 I_{l_\theta}$ and $n_\mathrm{c} = 10$, which was found to provide the best response.

Figure 5.11 shows the performance of both algorithms and compares the instantaneous performance and instantaneous controller difference. Note that, for sufficiently high controller order, RCAC with the FIR target model (4.26) yields lower values of the instantaneous performance and instantaneous controller difference than FuRLS. ◇
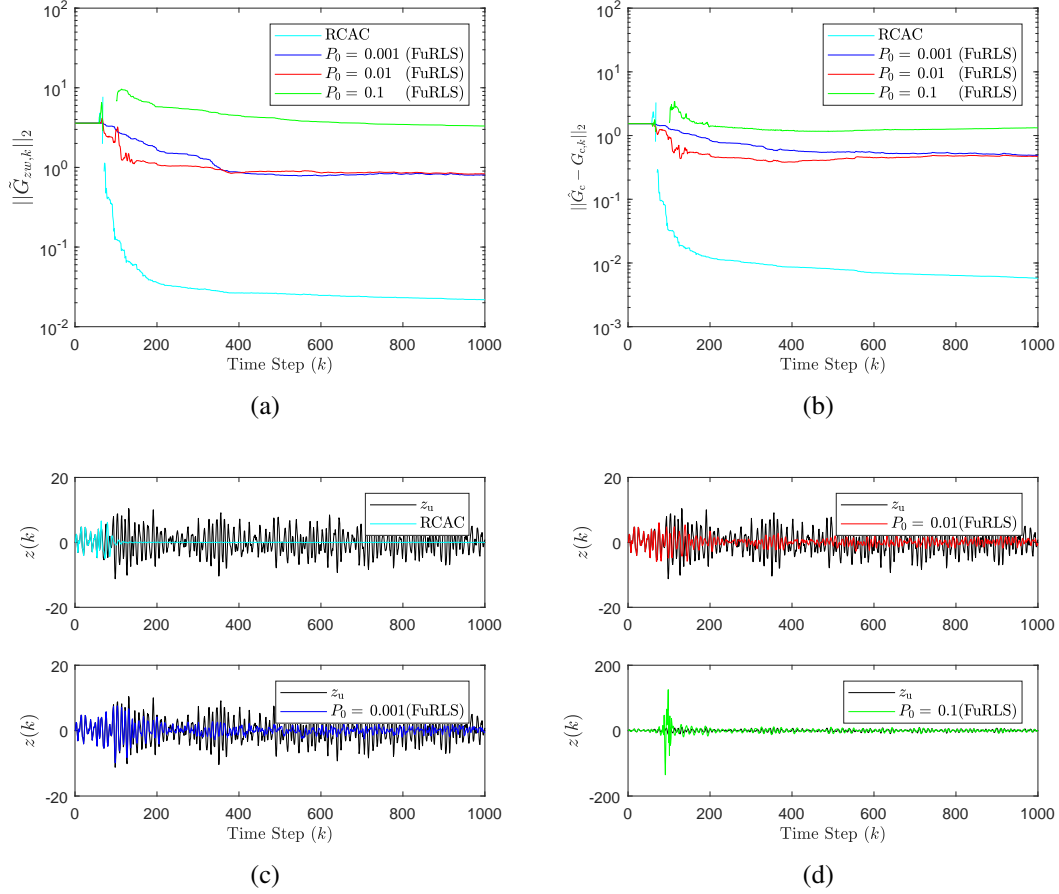
Figure 5.10: Example 5.4: Comparison of RCAC with an IIR controller and FuRLS applied to the system (5.101) and (5.102) with $n_c = n = 4$. For RCAC, the target model G_f is given by (5.103) and $P(0) = 10I_{l_\theta}$ and $R_\Delta = 0_{l_\theta \times l_\theta}$. For FuRLS, $G_f = G_{zu}$, and three values of $P(0)$ are compared. The instantaneous performance is compared in (a). The instantaneous controller difference is compared in (b). Note that, in (a) and (b), $\tilde{J}_k$ and $\Delta G_{c,k}$ are undefined at some steps due to the instability of $G_{c,k}$. (c) and (d) show the time-domain performance. In (a) and (b), the instantaneous performance and instantaneous controller difference of FuRLS improves as $P(0)$ increases to 0.01, but degrades for larger values of $P(0)$. RCAC yields lower values of the instantaneous performance and the instantaneous controller difference than FuRLS.
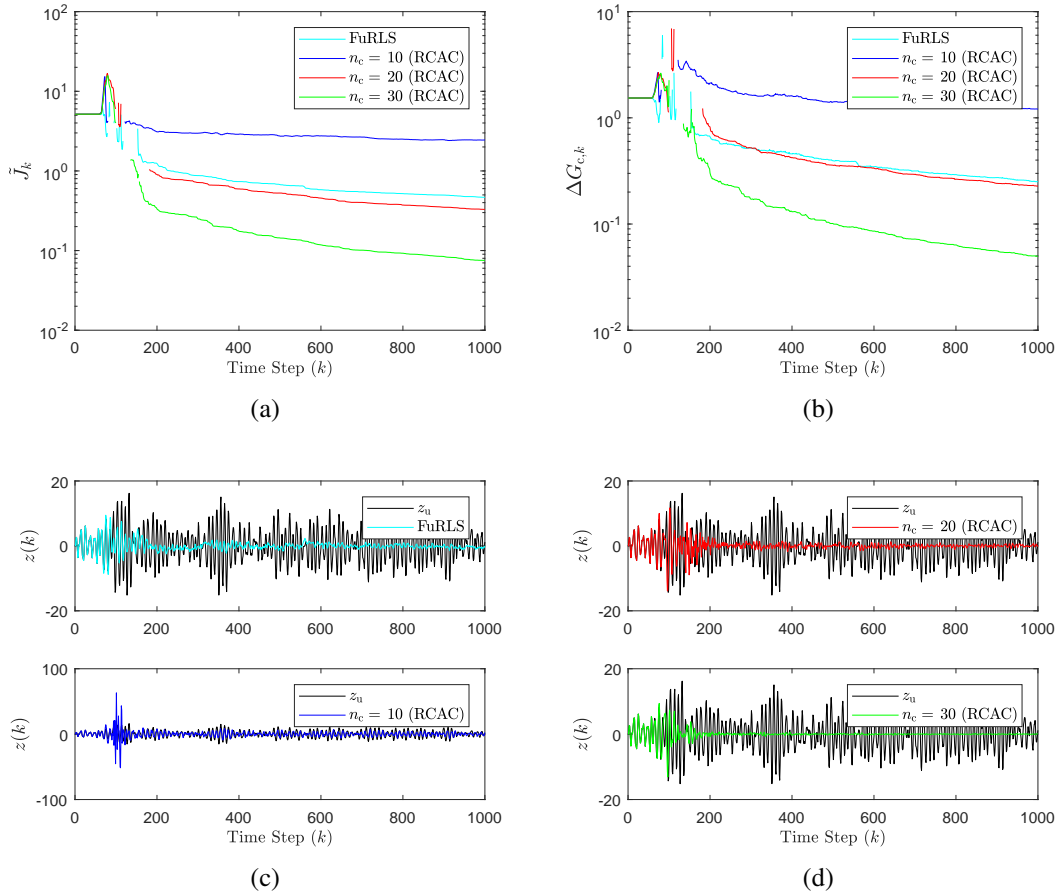
Figure 5.11: Example 5.5: Comparison of RCAC with an IIR controller and FuRLS applied to the system (5.101) and (5.102). For RCAC, the target model G_{f} is given by (5.104) with $P(0) = I_\theta$ and $R_\Delta = 100I_{l_\theta}$. Three values of n_{c} are compared. For FuRLS, $G_{\mathrm{f}} = G_{zu}$, $n_{\mathrm{c}} = 10$, and $P(0) = 0.1I_{l_\theta}$. The instantaneous performance is compared in (a). The instantaneous controller difference is compared in (b). (c) and (d) show the time-domain performance. Note that, in (a) and (b), for sufficiently high controller order, RCAC with the FIR target model (4.26) yields lower values of the instantaneous performance and instantaneous controller difference than FuRLS.

5.10 Experimental Implementation

In this section, we present the implementation of RCAC in an acoustic experiment. Omni-directional microphones are used as sensing, and mid-bass woofers are used as the actuation, both of which are placed in an enclosed space. Additional hardware used in implementation included speaker amplifiers, microphone amplifiers, and low-pass anti-aliasing filters for both the speaker inputs and the microphone outputs. RCAC is implemented in Real Time Workshop (RTW) and MATLAB/Simulink is using a dSPACE DS1104 board. The dSPACE board is also used to generate the digital disturbance signal w, which is zero-mean Gaussian white noise. A diagram of the microphone and speaker placement is shown in Figure 5.12. The approximate dimensions of the acoustic space are
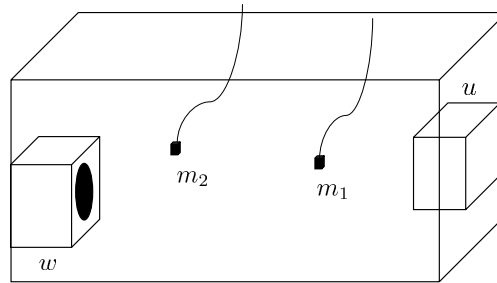
Figure 5.12: Sensor and actuator placement for the experimental implementation of RCAC in direct feedforward disturbance rejection.

6 ft $\times$ 3 ft $\times$ 3 ft. We designate one speaker as the disturbance speaker w and one speaker as the control speaker u. Two locations are considered for the performance microphone z, denoted as m_1 and m_2. We limit the bandwidth of the signals in the system to 250 Hz. The controller and subsequently all data is implemented and sampled at 1kHz. In this study, we consider the direct feedforward disturbance rejection problem and we assume that the disturbance w is measured directly and without delay, that is $y = w$.

5.10.1 Constructing the Target Model

The target model is chosen to be the FIR target model (4.27) for NMP systems. For each location of the z microphone, we obtain the first Markov parameter $H_{d_{zu}}$ and the relative degree d_{zu} from the impulse response as seen in Figure 5.13.

(a)　　　　　　　　　　　(b)
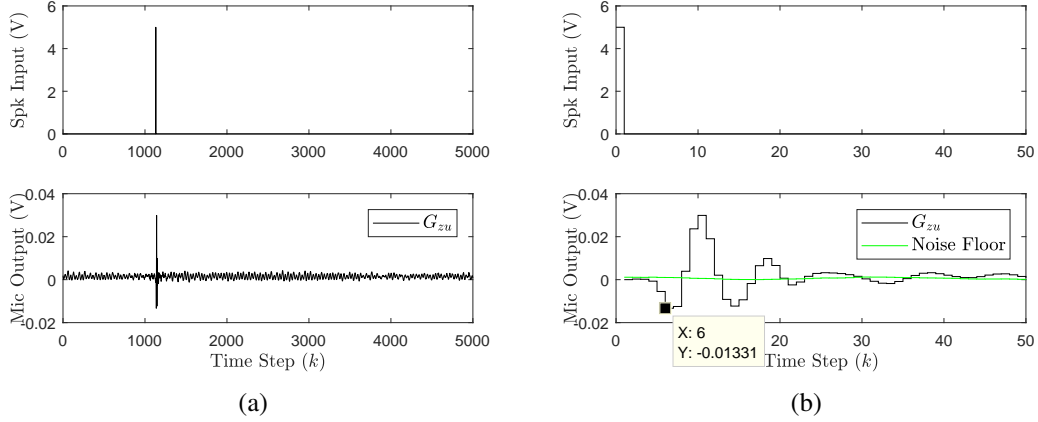
Figure 5.13: The impulse response of the transfer function from u to m_1. In reduce the effect of sensor noise, the discrete-time impulse has amplitude 5 V. (b) shows that $d_{zu} \approx 4$. In fact, $d_{zu} = 6$ with $H_6 \approx -0.01331/5$ yields the best performance.

Two NMP zeros were identified in the system, both of which are attributed to the hardware. We note that both the microphone and the speaker have zero response at DC due to the nature of the acoustics. In discrete-time, this corresponds to a zero on the unit circle at 1. In order to prevent controller poles being placed at DC, we model two zeros at 1 in the target model G_f, one representing the speaker, the other representing the microphone. No other NMP zeros were found for the microphone locations tested. The target model for each example is given by

$$G_f(\mathbf{z}) = \frac{H_{d_{zu}}(\mathbf{z} - 1)^2}{\mathbf{z}^{d_{zu}+2}}. \tag{5.105}$$

5.10.2 The Ideal Controller

In the subsequent experimental examples, we compare the converged RCAC controller to the ideal controller $\hat{G}_\mathrm{c}$ for the direct feedforward disturbance rejection problem (5.8). We use the Blackman-Tukey spectral analysis method [29] with a Hanning window to estimate the frequency response of G_{zw} and G_{zu} and construct an estimate of $\hat{G}_\mathrm{c}$. Despite the fact that G_{zu} is NMP, the NMP zeros at DC are also present in G_{zw}. The ideal controller $\hat{G}_\mathrm{c}$ (5.8) has exact pole-zero cancellation at DC. Since no other NMP zeros of G_{zu} were observed when implementing RCAC we conjecture that the ideal controller is asymptotically stable. Thus, whether or not the ideal controller is implementable depends on the relative degree d_{zu} and d_{zw}.

5.10.3 RCAC Implementation

We first evaluate the signal-to-noise ratio of the experiment without control. Next, two experimental setups are considered, where $d_{zu} < d_{zw}$ in the first case and $d_{zu} > d_{zw}$ in the second case. Figure 5.14 shows the time-domain response and frequency content of the sensor noise and as well as the microphone measurement of the disturbance without control. We note that, below 50 Hz, the sensor noise is dominant.

Example 5.6: Performance of RCAC for $n_\mathrm{c} = 5$ and $n_\mathrm{c} = 10$ with the z microphone placed at m_1 such that $d_{zu} < d_{zw}$. Figure 5.15 shows the impulse response of G_{zu} and G_{zw} as well as the performance of RCAC for $n_\mathrm{c} = 5$ and $n_\mathrm{c} = 10$. Figure 5.15 also shows the frequency content of the performance signal and compares the frequency response of the converged controllers with the estimated frequency response of the ideal controller. In this case, the data suggest that the ideal controller is implementable, and the RCAC controller closely matches the frequency response of the ideal controller, except at low frequencies, where sensor noise is dominant.   ◇

Example 5.7: Performance of RCAC for $n_\mathrm{c} = 5$ and $n_\mathrm{c} = 10$ with the z microphone placed at m_2 such that $d_{zu} > d_{zw}$. Figure 5.16 shows the impulse response of G_{zu} and G_{zw}
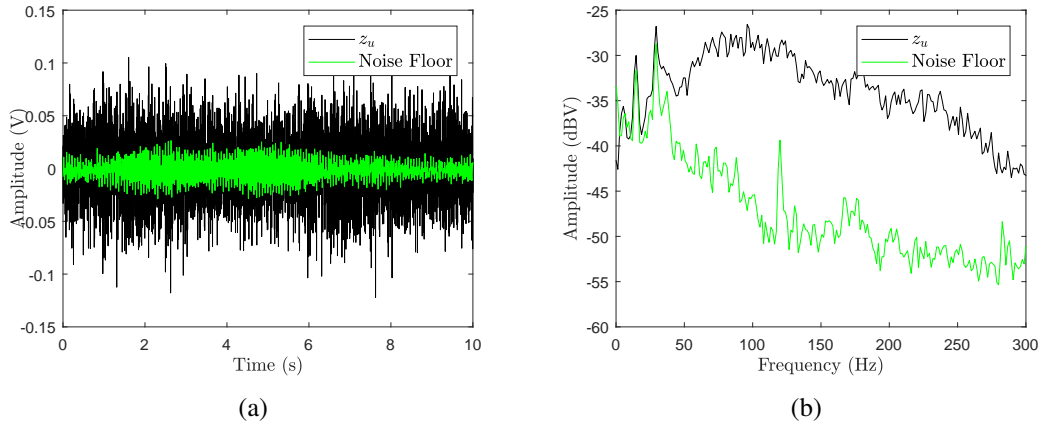
Figure 5.14: Signal-to-noise ratio of the RCAC broadband feedforward disturbance-rejection experiment. The time-domain data is shown in (a), and the frequency content of (a) is shown in (b), which indicates a large amount of sensor noise at low frequencies, particularly below 50 Hz.

as well as the performance of RCAC for $n_c = 5$ and $n_c = 10$ and the frequency content of the performance signal. Figure 5.16 also compares the frequency response of the converged controllers with the estimated frequency response of the ideal controller. In this case, the ideal controller is known to be not implementable. Consequently, the performance is poor relative to Example 5.6, and the frequency response of the ideal controller is not matched.

◇

5.11 Conclusions

The equations of the feedforward disturbance rejection problem are presented which lead to the formulation of an ideal feedforward controller which provides perfect cancellation. The conditions under which the ideal controller is implementable are given. The equations of the LQG control problem and high-authority LQG are applied to the feedforward control problem. In the case when the ideal controller is unstable, and hence not implementable, high-authority LQG reflects the unstable controller poles across the unit circle.
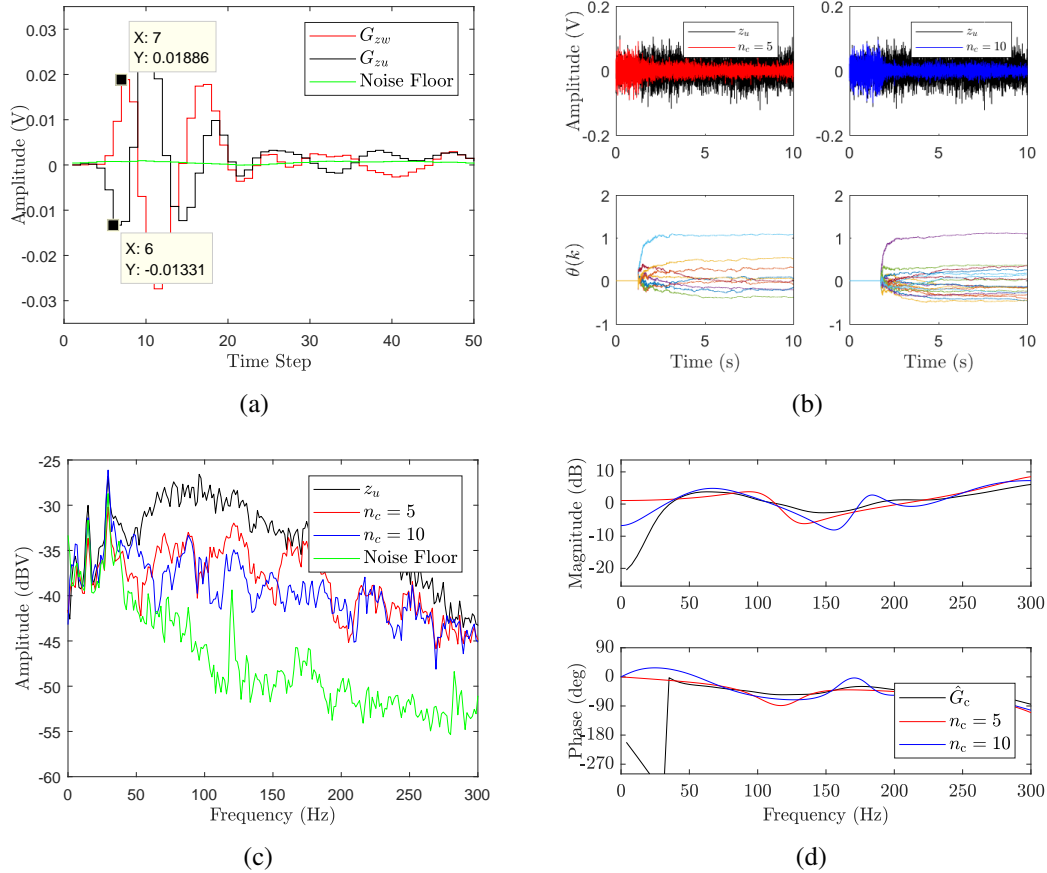
Figure 5.15: Example 5.6: Performance of RCAC for with the z microphone placed at m_1. Controller orders $n_c = 5$ and $n_c = 10$ are considered. (a) shows the impulse response of G_{zu} and G_{zw}. Note that $d_{zu} < d_{zw}$, which suggests that, in this case, the ideal controller is implementable. (b) shows the performance of RCAC for both controller orders. (c) compares the frequency content of the performance between $t = 7.5$ and $t = 10$. (d) compares the frequency response of both controllers at $t = 10$ with the estimated frequency response of the ideal controller. (c) shows improvement in the suppression across several bands due to increasing the controller order from $n_c = 5$ to $n_c = 10$. Further increasing of the controller order (not shown) does not yield noticeable improvement. (d) shows that both RCAC controllers approximate the estimate of the ideal controller above 50 Hz. Below 50 Hz, the matching is poor, likely due to the sensor noise in that range.

(a)

(b)

(c)

(d)
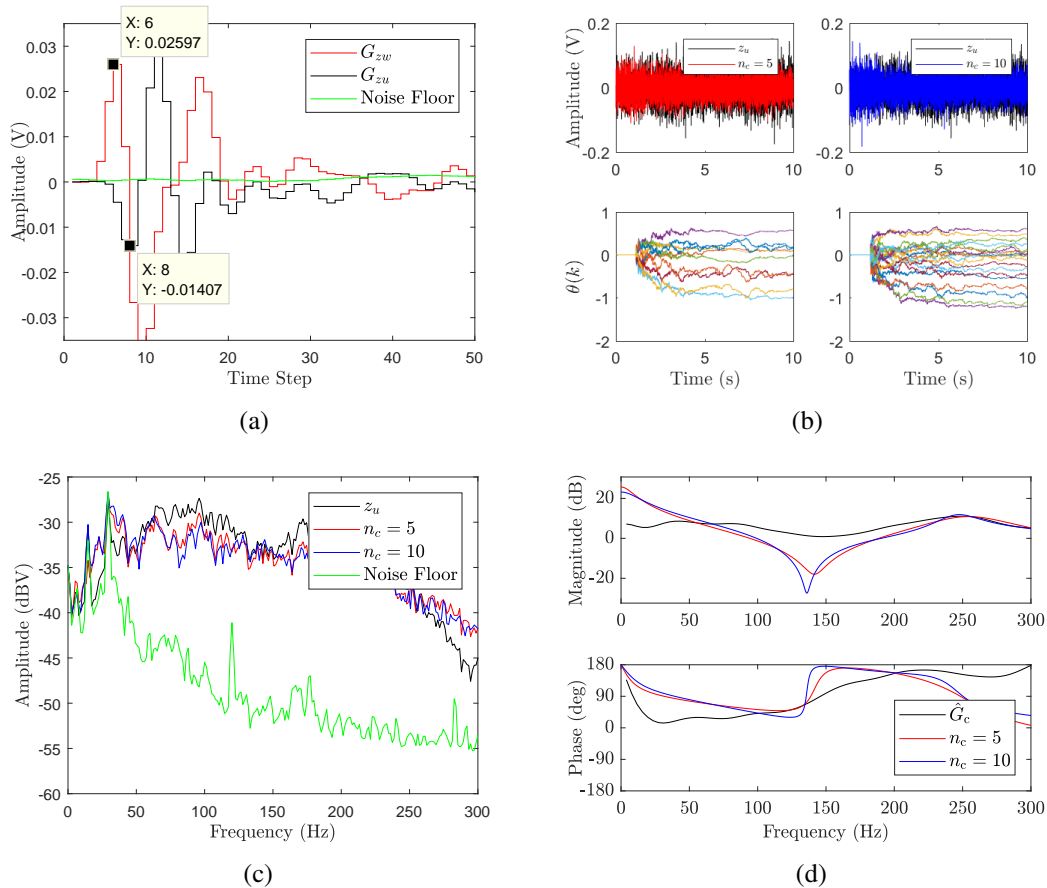
Figure 5.16: Example 5.7: Performance of RCAC with the z microphone placed at m_2. Two controller orders $n_\text{c} = 5$ and $n_\text{c} = 10$ are considered. (a) shows the impulse response of G_{zu} and G_{zw}. Note that $d_{zu} > d_{zw}$, and thus the ideal controller is not implementable. (b) shows the performance of RCAC for both controller orders. (c) shows the frequency content of the performance from $t = 7.5$ to 10. (d) shows the frequency response of the controller at $t = 10$ for both controllers and compares the frequency response of both controllers with the estimated frequency response of the ideal controller. (c) shows that the suppression is significantly worse than in Example 5.6. Increasing the controller order from $n_\text{c} = 5$ to $n_\text{c} = 10$ (not shown) does not improve the performance. (d) shows that the frequency response of the RCAC controllers are approximately the same; however, they do not approximate the estimated frequency response of the ideal controller.

The target model G_{f} for RCAC in feedforward disturbance rejection is analyzed. A target model G_{f}^* which recovers the high-authority LQG performance when $n_{\mathrm{c},RCAC} = n$ is derived and demonstrated numerically. We show numerically that for sufficiently high controller order, RCAC is able to recover the high-authority LQG performance with G_{f}^*.

The RCAC update equations are compared to Fx/FuLMS and Fx/FuRLS. A numerical comparison of RCAC and FuRLS for an example when the ideal controller is implementable showed that RCAC is able to better suppress broadband disturbances.

RCAC is applied to a direct feedforward experimental study. When the ideal controller is believed to be implementable, the RCAC controller was able to approximate the frequency response of the ideal controller. When the ideal controller was known to be not implementable, the performance was poor and the frequency response of the ideal controller was not matched. The experimental study agrees with what was observed in simulation.

CHAPTER 6

Conclusions and Future Work

6.1 Conclusions

The purpose of the present work is to extend both theoretical boundaries and practical applications of retrospective cost adaptive control (RCAC). We extend our understanding of RCAC by developing an alternative interpretation of the retrospective performance $\hat{z}(k, \theta(k+1))$. Previously, it was believed that the retrospective performance represented a residual between a certain closed-loop transfer function $G_{z\tilde{u},\theta(k+1)}$ and the target model G_{f}. In minimizing the retrospective performance, RCAC was attempting to fit $G_{z\tilde{u},\theta(k+1)}$ to G_{f}. This led to a breakthrough in determining the exact role of G_{f}. However, what was lacking in this explanation was how this residual minimization is actually achieving good closed-loop performance. While the closed-loop poles were shared between $\tilde{G}_{zw}$ and $G_{z\tilde{u},\theta(k+1)}$, the transfer functions had inherently different frequency responses in steady-state.

With the formulation of the retrospective performance decomposition, we now know that $\hat{z}(k, \theta(k+1))$ is a combination of a performance-like term $z_{\mathrm{pp}}(k, \theta(k+1))$ and a model-matching residual $z_{\mathrm{mm}}(k, \theta(k + 1))$, where the closed-loop performance is accounted for in $z_{\mathrm{pp}}(k, \theta(k + 1))$. This can potentially be seen as a trade-off. When choosing $\theta(k + 1)$ in order to minimize $\hat{z}(k, \theta(k + 1))$, reducing $z_{\mathrm{pp}}(k, \theta(k + 1))$ may inflate $z_{\mathrm{mm}}(k, \theta(k + 1))$ or vice versa.

The model-matching residual can be seen as one of the key features of RCAC. Since

the model-matching residual is a function of $\theta(k+1)$, this implies that the controller has a certain amount of leeway in "correcting" a poor choice of G_f. There is evidence for this in the RCAC literature. It has been observed that RCAC can match the performance high-authority LQG in both feedback and feedforward control. Sometimes, for minimum-phase systems, this can be done with very little modeling information, specifically, what is needed is an estimate of the first Markov parameter and relative degree of G_{zu}. The caveat is that we need sufficiently high controller order to achieve this, which can typically be 2 or 3 times the order of the plant.

In the context of the retrospective performance decomposition, when a "bad" choice of G_f is chosen, the only way to minimize both $z_\mathrm{pp}(k, \theta(k+1))$ and $z_\mathrm{mm}(k, \theta(k+1))$ is to overparameterize the problem with higher-controller order. The benefit being that very little is needed to be known about the system. Put in another way, RCAC has a certain built-in method to account for the lack of modeling information.

As for extending the applications and improving the practical aspect of RCAC, in this dissertation, we've applied all the framework that we have built with feedback control to feedforward. The two biggest lessons that we have applied are what we know about the target model and the relationship between RCAC and LQG. What we found is that the lessons that we learned in feedback apply directly to feedforward. In some aspects this is not surprising as the feedforward disturbance rejection problem can be viewed as a specialization of the feedback disturbance rejection problem. In a lot of ways, feedback is harder than feedforward, as you need to guarantee close-loop stability and are limited by the bode integral constraint.

The demonstration of RCAC in a real world application such as broadband feedback road noise suppression opened our eyes to a lot the more practical aspects of actually implementing a controller. The limitations of the hardware coupled with the computational complexity of the algorithm made making real-time in an acoustic application a challenge. Furthermore, in such an application when the system is unknown, being able to tell if an

instability was due to unstable-pole zero cancellation due to poorly modeled NMP zeros, closed-loop instability, controller instability, or bias integration and saturation was sometimes difficult. However, we also showed that RCAC does work. Specifically, for all cases considered in the experiment, RCAC was able to suppress the disturbance at the performance microphone. This implies that as long as there is sensing, RCAC can suppress the noise at that location, the caveat being whether this is true in the multiple-input-multiple-output (MIMO) case.

Finally, we develop the spatial spillover function based on the work on the road noise suppression problem. In the case where z, e, and w are scalar signals, we found an operator which relates relative suppression at z to relative suppression at e that was independent of control architecture. In the case where u is also scalar, this operator no longer depends on the controller. While requirement of scalar signals is very limiting, the implication of such an operator could be very useful in determining whether a microphone placement configuration is good without actually having to implement a controller and check the performance experimentally. The work in this dissertation primarily focused on identifying the spatial spillover function experimentally. An attempt was made to try and use the magnitude and phase of the spatial spillover function to predict relative performance in the road noise suppression problem.

6.2 Future Work

In terms of the performance decomposition, the future development, there are some existing questions. We noted that in the model-matching error, $\tilde{u}(k, \theta(k+1))$, is treated as an input, but is not an exogenous signal, hence, persistency is not guaranteed. Another area of research is that we sometimes observe in feedback control that RCAC will at times, during the transient response, be in favor of allowing the closed-loop to go unstable. The transient response of RCAC for a given case can potentially be explained using the performance

decomposition.

In terms of hardware and experimental implementation of RCAC, computational complexity remains a challenge. Recursive-least-squares is a fairly computationally expensive algorithm. There is already an on going effort to attempt to optimize the RCAC code or find hardware that implement the code faster, such as an field-programmable gate array (FPGA). The other aspect would be to explore alternative optimization methods to minimize the retrospective cost that could be computationally cheaper. There may likely be trade-offs on metrics such as convergence speed.

In terms of the spatial spillover function, one of the main priorities is to better understand for a given level of relative suppression at z, what are the conditions under which you can expect either good or poor relative relative suppression at e. Some current work is already being done on being able to identify the spatial spillover function when the disturbance w is unknown and unable to be shut off. Finally, extensions to MIMO where z, e, and w are not assumed to be scalar is untouched.

BIBLIOGRAPHY

[1] Fuller, C. R. and von Flotow, A. H., "Active Control of Sound and Vibration," *IEEE Contr. Sys. Mag.*, Vol. 15, No. 6, 1995, pp. 9–19.

[2] Nelson, P. A. and Elliot, S. J., *Active Control of Sound*, Academic Press, 1992.

[3] Burgess, J. C., "Active adaptive sound control in a duct: A computer simulation," *The Journal of the Acoustical Society of America*, Vol. 70, No. 3, 1981, pp. 715–726.

[4] Widrow, B. and Stearns, S. D., *Adaptive signal processing*, Vol. 15, Prentice-hall Englewood Cliffs, NJ, 1985.

[5] Kuo, S. M. and Morgan, D. R., *Active Noise Control Systems: Algorithms and DSP Implementations*, Wiley, 1995.

[6] Kuo, S. M. and Morgan, D. R., "Active noise control: a tutorial review," *Proceedings of the IEEE*, Vol. 87, No. 6, Jun 1999, pp. 943–973.

[7] Elliot, S., Nelson, P., Stothers, I., and Boucher, C., "In-flight experiments on the active control of propeller-induced cabin noise," *Journal of Sound and Vibration*, Vol. 140, No. 2, 1990, pp. 219–238.

[8] Elliott, S. J. and Nelson, P. A., "Active noise control," *IEEE Signal Processing Magazine*, Vol. 10, No. 4, Oct 1993, pp. 12–35.

[9] Sommerfeldt, S. D., Parkins, J. W., and Park, Y. C., "Global active noise control in rectangular enclosures," *INTER-NOISE and NOISE-CON Congress and Conference Proceedings*, Vol. 1995, Institute of Noise Control Engineering, 1995, pp. 477–488.

[10] Park, Y. C. and Sommerfeldt, S. D., "Global attenuation of broadband noise fields using energy density control," *The Journal of the Acoustical Society of America*, Vol. 101, No. 1, 1997, pp. 350–359.

[11] Xie, A. and Bernstein, D., "On spatial spillover in feedforward and feedback noise control," *Journal of Sound and Vibration*, Vol. 391, 2017, pp. 1 – 19.

[12] Sievers, L. A. and von Flotow, A. H., "Comparison and Extensions of Control Methods for Narrow-Band Disturbance Rejection," *IEEE Trans. Signal Processing*, Vol. 40, 1992, pp. 2377–2391.

[13] Doyle, J. C., Francis, B. A., and Tannenbaum, A. R., *Feedback Control Theory*, Macmillan, 1992.

[14] Hong, J. and Bernstein, D. S., "Bode Integral Constraints, Colocation, and Spillover in Active Noise and Vibration Control," *IEEE Trans. Contr. Sys. Tech.*, Vol. 6, 1998, pp. 111–120.

[15] Freudenberg, J. S., Hollot, C. V., Middleton, R. H., and Toochinda, V., "Fundamental Design Limitations of the General Control Configuration," *IEEE Trans. Autom. Contr.*, Vol. 48, 2003, pp. 1355–1370.

[16] Venugopal, R. and Bernstein, D. S., "Adaptive Disturbance Rejection Using AR-MARKOV/Toeplitz Models," *IEEE Trans. Contr. Sys. Tech.*, Vol. 8, 2000, pp. 257–269.

[17] Hoagg, J. B., Santillo, M. A., and Bernstein, D. S., "Discrete-time Adaptive Command Following and Disturbance Rejection with Unknown Exogenous Dynamics," *IEEE Trans. Autom. Contr.*, Vol. 53, 2008, pp. 912–928.

[18] Santillo, M. A. and Bernstein, D. S., "Adaptive Control Based on Retrospective Cost Optimization," *J. Guid. Contr. Dyn.*, Vol. 33, 2010, pp. 289–304.

[19] Hoagg, J. B. and Bernstein, D. S., "Retrospective Cost Model Reference Adaptive Control for Nonminimum-Phase Systems," *AIAA J. Guid. Contr. Dyn.*, Vol. 35, 2012, pp. 1767–1786.

[20] Rahman, Y., Xie, A., Hoagg, J. B., and Bernstein, D. S., "A Tutorial and Overview of Retrospective-Cost-Based Adaptive Control," *Proc. Amer. Contr. Conf.*, Boston, MA, July 2016, pp. 3386–3409.

[21] Sumer, E. D., Hoagg, J. B., and Bernstein, D. S., "Broadband Disturbance Rejection Using Retrospective Cost Adaptive Control," *Proc. Dyn. Sys. Contr. Conf.*, Fort Lauderdale, FL, October 2012, pp. 1–10.

[22] Rahman, Y., Xie, A., and Bernstein, D. S., "Retrospective Cost Adaptive Control: Pole Placement, Frequency Response, and Connections with LQG Control," *IEEE Contr. Sys. Mag.*, Vol. 37, No. October, 2017, pp. 85–121.

[23] Xie, A. and Bernstein, D. S., "Experimental investigation of spatial spillover in adaptive feedback noise control of broadband disturbances in a 3D acoustic space," *2016 American Control Conference (ACC)*, July 2016, pp. 3410–3415.

[24] Eriksson, L., "Development of the filtered-U algorithm for active noise control," *The Journal of the Acoustical Society of America*, Vol. 89, No. 1, 1991, pp. 257–265.

[25] Bouchard, M. and Quednau, S., "Multichannel recursive-least-square algorithms and fast-transversal-filter algorithms for active noise control and sound reproduction systems," *IEEE Transactions on Speech and Audio Processing*, Vol. 8, No. 5, Sep 2000, pp. 606–618.

[26] Maia, N., Urgueira, A., and Almeida, R., "Whys and Wherefores of Transmissibility, in: F. Beltran-Carbajal (Ed.)," *Vibration Analysis and Control*, 2011, pp. 197–216 (Chapter 10).

[27] Devriendt, C. and Guillaume, P., "Identification of modal parameters from transmissibility measurements," *Journal of Sound & Vibration*, Vol. 314, 2008, pp. 343–356.

[28] Aljanaideh, K. F. and Bernstein, D. S., "Time-domain analysis of motion transmissibilities in force-driven and displacement-driven structures," *Journal of Sound & Vibration*, Vol. 347, 2015, pp. 169–183.

[29] Stoica, P. and Moses, R. L., *Introduction to Spectral Analysis*, Vol. 1, Prentice Hall Upper Saddle River, 1997.

[30] Hoagg, J. and Bernstein, D. S., "Cumulative Retrospective Cost Adaptive Control with RLS-Based Optimization," *Proc. Amer. Contr. Conf.*, Baltimore, MD, June 2010, pp. 4016–4021.

[31] Astrom, K. J. and Wittenmark, B., *Adaptive Control*, Addison-Wesley, 2nd ed., 1995.

[32] Goodwin, G. C. and Sin, K. S., *Adaptive Filtering, Prediction, and Control*, Prentice Hall, 1984.

[33] Teixeira, B., "Kalman Filters," *IEEE Contr. Sys. Mag.*, Vol. 28, No. 2, 2008, pp. 16–18.

[34] Fletcher, H. and Munson, W. A., "Loudness, its definition, measurement and calculation," *Bell Labs Technical Journal*, Vol. 12, No. 4, 1933, pp. 377–430.

[35] Bernstein, D. S., *Matrix Mathematics*, Princeton, 2nd ed., 2009.

[36] Zhou, K., Doyle, J. C., and Glover, K., *Robust and Optimal Control*, Prentice Hall, 1996.

[37] Kwakernaak, H. and Sivan, R., *Linear Optimal Control Systems*, Wiley, 1972.